JSCSEN 80(9)1101–1215(2015)

ISSN 1820-7421(Online)

Journal of the Serbian Chemical Society

Volume 80 : : 2015 : : 85 Years of the Journal

1930 Glasnik Hemijskog Društva Kraljevine Jugoslavije
Journal of the Chemical Society of the Kingdom of Yugoslavia

1947 Glasnik hemijskog društva Beograd
Journal of the Chemical Society of Belgrade

1985 Journal of the Serbian Chemical Society

VOLUME 80

No 9

BELGRADE 2015

Available on line at

www.shd.org.rs/JSCS/

The full search of JSCS
is available through

DOAJ DIRECTORY OF OPEN ACCESS JOURNALS
www.doaj.org

Journal of the Serbian Chemical Society
JSCS-info@shd.org.rs • www.shd.org.rs/JSCS

J. Serb. Chem. Soc. Vol. 80, No. 9 (2015)

CONTENTS

Published by the Serbian Chemical Society
Karnegijeva 4/III, P.O. Box 36, 11120 Belgrade, Serbia
Printed by the Faculty of Technology and Metallurgy
Karnegijeva 4, P.O. Box 35-03, 11120 Belgrade, Serbia

Journal of the Serbian Chemical Society
JSCS-info@shd.org.rs • www.shd.org.rs/JSCS
J. Serb. Chem. Soc. 80 (9) 1101–1111 (2015)
JSCS–4783
UDC 547.822.3'288.4+547.58+542.913:615.281
Original scientific paper

Synthesis, structural characterization and antimicrobial evaluation of some novel piperidin-4-one oxime esters

K. GOKULA KRISHNAN, R. SIVAKUMAR and V. THANIKACHALAM*

Department of Chemistry, Annamalai University, Annamalainagar 608 002, Tamil Nadu, India

(Received 13 November 2014, revised 25 January, accepted 16 April 2015)

Abstract: Fifteen novel biologically active piperidin-4-one oxime esters **8**–**22** were synthesized in good yields. These compounds were prepared in reactions of carboxylic acids, *in situ* activated using $POCl_3$ and pyridine, with piperidin-4-one oximes. The structures of the title compounds were elucidated based on FTIR, NMR (1D and 2D) and mass spectral analyses. Single crystal XRD studies of compounds **12** and **20** provided further unambiguous evidence for the proposed structure. All the synthesized compounds were tested for their *in vitro* antibacterial and antifungal activities. Many of these derivatives exhibited good activity against *Bacillus subtilis*, *Pseudomonas aeruginosa*, *Escherichia coli*, *Trichoderma viride* and *Aspergillus flavus*.

Keywords: piperidin-4-one oxime; aromatic acid; mixed anhydride; *gauche* interaction; conformation; single crystal XRD.

INTRODUCTION

Substituted piperidines and their analogues are basic structural units in numerous naturally occurring alkaloids and drug candidates. A search of piperidines and their derivatives revealed thousands of references to this simple ring system in medicinal and clinical research.[1] In particular, chiral centers at C2 and/or C6 of the piperidine ring were found to be essential for a defined activity, such as CNS,[2] anti-HIV,[3] anti-proliferative,[4] anti-cancer,[5] anti-inflammatory[6] and anti-oxidant[7] activities. Furthermore, the piperidine ring serves as a building block in synthetic and medicinal chemistry as more complex alkaloids include acridone and morphine, which themselves exhibit biological activities.[8]

Oximes[9] and their derivatives represent an important class of organic molecules that attract the interest of both synthetic and medicinal chemists. Oxime esters have showed great potential in biologically active molecules, such as RBPP9 inhibitors,[10] anti-proliferative[11] and anti-convulsant[12] agents, and in

* Corresponding author: E-mail: profvt.chemau@gmail.com
doi: 10.2298/JSC141113037K

agrochemical[13] industries. In addition, oxime esters, such as OXE-1 and OXE-2, were employed as photoinitiators,[14] as they meet the specific requirements desired for color filter displays in LCDs. Recently, oxime esters were reported to exhibit DNA-cleaving[15] ability in a process triggered by UV light.

The formation of the ester is a simple dehydration process, which can be easily catalyzed by strong acids. Previously, numerous methods were documented for the synthesis of esters *via* direct coupling of a carboxylic acid with an alcohol, often involving the use of stoichiometric activators and coupling reagents.[16] In addition, several reports describe the synthesis of esters in good yields using coupling reagents such as dicyclohexylcarbodiimide/4-(*N*,*N*-dimethylamino)pyridine (DCC/DMAP),[17] diethyl azodicarboxylate/triphenylphosphine (DEAD/Ph_3P),[18] *N*,*N*-dimethyl phosphoramidic dichloride[19] and diethyl chlorophosphate.[20] However, some drawbacks still remain due to the formation of byproducts, difficulties in handling and long reaction times. Consequently, a practical and efficient synthesis of oxime esters in good yields under mild conditions is still needed. In this context, an attempt was made with phosphorus oxychloride ($POCl_3$),[21] which is a commercially available and relatively inexpensive superior reagent, and affects carboxylic group activation under mild conditions with excellent yields of the products.

Herein, the synthesis and structural characterization are reported of some novel 3-alkyl-2,6-diphenylpiperidin-4-one oxime esters **8**–**22** through carboxylic acids **7a**–**e**, *in situ*-activated using $POCl_3$ and pyridine as base as well as solvent, with 3-alkyl-2,6-diphenylpiperidin-4-one oximes **4**–**6** in good yields (Scheme 1). The key compounds, 3-alkyl-2,6-diphenylpiperidin-4-ones[22] **1–3** and their oximes[9,23] **4–6** were prepared using literature methods.

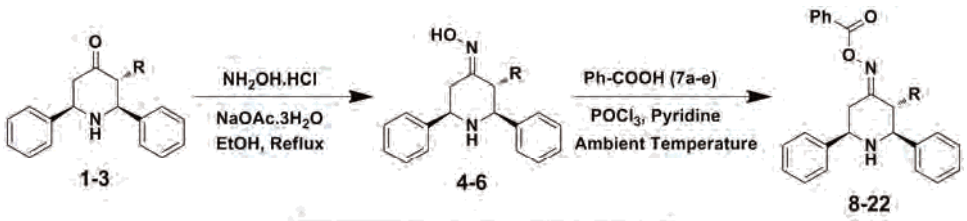

Compound	R	Ph
8, 13, 18	Me, Et, *i*-Pr	C_6H_5
9, 14, 19	Me, Et, *i*-Pr	3-C_5H_4N
10, 15, 20	Me, Et, *i*-Pr	*p*-Cl-C_6H_4
11, 16, 21	Me, Et, *i*-Pr	*p*-NO_2-C_6H_4
12, 17, 22	Me, Et, *i*-Pr	*m*-Me-C_6H_4

Scheme 1. General synthetic route for the synthesis of piperidin-4-one oxime esters **8**–**22**.

EXPERIMENTAL

All the purchased reagents and solvents were of reagent grade and used without further purification. Completion of reactions was monitored by TLC on silica gel-coated aluminum sheets (Type 60 GF254). The melting points were measured in open capillaries and are uncorrected. The FTIR spectra were recorded on Avatar-300 FTIR spectrometer in KBr disks. The NMR (1D and 2D) spectra were recorded on a Bruker 400 MHz spectrometer. The chemical shift values are reported in ppm from TMS.

The analytical and spectral data of the synthesized compounds are given in the Supplementary material to this paper.

*General procedure for the synthesis of piperidin-4-one oxime esters (**8**–**22**)*

A mixture of 3-methyl-2,6-diphenylpiperidin-4-one oxime (0.700 g, 2.5 mmol) and benzoic acid (0.335 g, 2.75 mmol) in dry pyridine (5 mL) was stirred at room temperature (29 °C), $POCl_3$ (0.25 mL, 2.75 mmol) was added dropwise to the mixture and stirring was continued for 15 min. The progress of the reaction was monitored by TLC. After completion of the reaction, the crude product was neutralized with dilute nitric acid and the desired product was regenerated with sodium bicarbonate solution. The crude product was then recrystallized from ethanol to obtain the pure piperidin-4-one oxime ester **8** in good yield (0.6 g, 86 %). The above general method was adopted for the synthesis of compounds **9**–**22** of this series.

RESULTS AND DISCUSSION

Chemistry

In the present investigation, first the reaction of 3-methyl-2,6-diphenyl piperidin-4-one oxime (**4**, 1 equiv.) and benzoic acid (**7a**, 1.1 equiv.) in pyridine as base as well as solvent was studied using various reagents (1.1 equiv.) to examine the feasibility of the reaction. As shown in Table I, a trace amount of product was formed with PCl_5, while moderate yields were obtained with $SOCl_2$ and DCC. Finally, $POCl_3$ gave the corresponding 3-methyl-2,6-diphenyl piperidin-4--one oxime ester **8** in good yield.

TABLE I. Formation of oxime ester from oxime with benzoic acid utilizing various reagents

Entry	Substrate (equiv.)	Reagent (equiv.)	Time, min	Yield[a], %
1	PhCOOH (1.1)	PCl_5 (1.1)	120	Trace
2	PhCOOH (1.1)	$SOCl_2$ (1.1)	80	60
3	PhCOOH (1.1)	DCC (1.1)	90	45
4	PhCOOH (1.1)	$POCl_3$ (1.1)	15	86

[a] Isolated yield

Next, $POCl_3$ was utilized as the reagent in varying amounts, from 0.5 to 2.0 equiv, for the synthesis of 3-methyl-2,6-diphenylpiperidin-4-one oxime ester **8**. Using equimolar quantities of benzoic acid **7a** and $POCl_3$, the desired product was obtained in 86 % yield (Entry 2, Table II). However, 0.5 equiv. of $POCl_3$ resulted in a poor yield of the product (Entry 1, Table II) compared to when 1.1 equiv. of $POCl_3$ was taken, while using 1.5 and 2.0 equiv. of $POCl_3$ resulted in moderate yields (Entries 3 and 4, Table II).

TABLE II. Optimization of reaction conditions with varying amounts of $POCl_3$

Entry	Substrate (equiv.)	$POCl_3$ (equiv.)	Time, min	Yield[a], %
1	PhCOOH (1.1)	0.5	30	trace
2	PhCOOH (1.1)	1.1	15	86
3	PhCOOH (1.1)	1.5	25	80
4	PhCOOH (1.1)	2.0	20	69

[a]Isolated yield

To study the scope and limitation of this protocol, $POCl_3$ and pyridine were used with wide ranges of aromatic/heteroaromatic acids and piperidin-4-one oximes. These methodologies resulted in good yield of products with short reaction times for all the substrates (Table III). The purity of products was high after a single recrystallization; extraction steps and chromatographic separation are thus avoided. The final products were well characterized using FTIR, NMR (1D and 2D) and mass spectrometry. The structures of compounds **12** and **20** were fully established by single crystal XRD analysis.

TABLE III. Substrate scope for piperidin-4-one oxime esters using $POCl_3$/pyridine

Cmpd.	R	Ar	Time, min	Yield[a] %	Cmpd.	R	Ar	Time, min	Yield[a], %
8	Me	C_6H_5	15	86	**16**	Et	*p*-NO_2-C_6H_4	20	95
9	Me	3-C_5H_4N	20	90	**17**	Et	*m*-Me-C_6H_4	25	75
10	Me	*p*-Cl-C_6H_4	20	79	**18**	*i*-Pr	C_6H_5	20	81
11	Me	*p*-NO_2-C_6H_4	15	92	**19**	*i*-Pr	3-C_5H_4N	25	89
12	Me	*m*-Me-C_6H_4	25	77	**20**	*i*-Pr	*p*-Cl-C_6H_4	25	73
13	Et	C_6H_5	20	85	**21**	*i*-Pr	*p*-NO_2-C_6H_4	20	86
14	Et	3-C_5H_4N	20	86	**22**	*i*-Pr	*m*-Me-C_6H_4	35	80
15	Et	*p*-Cl-C_6H_4	25	80					

[a]Isolated yield

FTIR spectral analysis

In general, compounds containing carbonyl group show absorption in the region of 1600–1750 cm^{-1}. In all the compounds **8**–**22**, a strong band appeared in the double bond region of the spectra at 1739–1752 cm^{-1}, which confirmed the formation of oxime ester (C=O). The imino group (C=N) in the piperidine ring gave a band at 1641–1607 cm^{-1}. A collection of bands observed in the region of 3272–3446 cm^{-1} and 2797–3087 cm^{-1} are due to the presence of a secondary amine (N–H) and aromatic and aliphatic C–H stretching.

NMR spectral analysis

For convenience, compound **8** was selected for the NMR spectral discussion. The two sets of signals appearing in the region 7.29–8.05 ppm for 15 protons revealed the presence of two Ph groups at the piperidine ring and one benzene

ring of the *O*-benzoyl group. Of these two sets of signals, one doublet that appeared in the downfield region at 8.03 ppm corresponded to the deshielded *ortho* H-atoms belonging to the *O*-benzoyl group. The remaining protons of Ph groups and the *O*-benzoyl group collectively gave a multiplet at 7.29–7.57 ppm. A doublet appeared in the upfield region of 1.07 ppm (J = 6.4 Hz) with a strong correlation in HSQC with the 11.84 ppm peak and a weak correlation with the 44.86 ppm; the signal at 1.07 ppm is due to Me(C3). A broad singlet appeared at 2.00 ppm, that showed no correlation in HSQC, was unambiguously assigned as the NH proton. In the downfield region, there are three doublets at 3.95, 3.66 and 3.56 ppm. Of these three signals, the two doublets at 3.95 (J = 11.6 Hz) and 3.66 ppm (J = 10 Hz) show strong correlation with 60.94 and 69.02 ppm signals and weak correlation with the 44.36 ppm signal. Obviously, these two signals are due to $H2_{ax}$ and $H6_{ax}$ (benzylic) protons. The latter doublet at 3.56 ppm (J = 13.6 Hz) shows strong correlation with 36.48 ppm signal, which is cross peak with the triplet center at 2.30 ppm, which confirmed that 3.56 and 2.30 ppm are due to $H5_{eq}$ and $H5_{ax}$ protons attached at the C5 carbon. A multiplet appearing at 2.67 ppm showed a strong correlation with the 44.36 ppm signal and a weak correlation with the 69.02 ppm signal, which confirmed the signal be assigned to the $H3_{ax}$ proton.

Akin to compound **8**, the chemical shift and coupling constant of C3 methyl, ethyl, isopropyl substituted analogous compounds **9**–**22** were assigned accordingly. Unlike compound **8**, in compounds **13**–**22**, the $H2_{ax}$ proton is deshielded by 0.14 ppm for the ethyl- and 0.38 ppm for the isopropyl-substituted compounds. Thee deviations indicate that the piperidine ring is flattened or distorted about the C2–C3 bond to decrease the *gauche* interaction. This interaction operates through space irrespective of the equatorial ethyl/isopropyl group at the C3 carbon and the phenyl group at the C2 carbon with an $H2_{ax}$ proton.

In the ^{13}C-NMR spectrum of compound **8**, the aromatic C-atoms appeared in the region of 126.9–129.6 ppm. The signals due to three *ipso* C-atoms were observed at 133.2, 142.0 and 143.0 ppm, respectively. Of these three signals, the one appearing at 133.25 ppm is due to an *ipso* carbon of the *O*-benzoyl group and the rest are due to *ipso* carbons attached to C2 and C6 carbons of piperidine ring. The imino carbon (C4) and *O*-benzoyl carbonyl carbon appear in the downfield region at 164.22 and 169.51 ppm, respectively. In the upfield region, the methyl group attached to the C3 carbon was observed at 11.84 ppm and piperidine ring carbons C2, C3, C5 and C6 appeared at 69.02, 44.36, 36.48, and 60.94 ppm, respectively.

Conformational analysis

The conformation of the piperidine ring and the orientation of the oxime ester group were studied from the values of the NMR coupling constant. Com-

pound **8** exhibited a large coupling constant $J_{6ax,5ax}$ (11.6 Hz) about the C5–C6 bond and about the C2–C3 bond (10 Hz) revealing the equatorial dispositions of the aryl rings at C2 and C6, and the alkyl group at C3. Thus, the synthesized compound **8** existed in a normal chair conformation with equatorial orientation of the Ph ring and Me(C3) substituents. The coupling constant about C2–C3 bond ($J_{2ax,3ax}$) were considerably lower than that about the C5–C6 bond ($J_{6ax,5ax}$), due to the *gauche* interaction between the Ph group and the alkyl group of C2 and C3. Hence, the piperidine ring is flattened/distorted about the C2–C3 bond and hence the lower magnitude of $J_{2ax,3ax}$ relative to $J_{6ax,5ax}$. The chemical shift difference between the C5 carbon (33.88 ppm) and C3 carbon (49.51 ppm) arises due to $A^{1,3}$ interactions between the N–O and C5–H bonds. Thus, the C5 carbon signal was more shielded compared to C3 carbon. It was concluded that *O*-benzoyl group was *syn* to the C5 carbon.

*Single crystal XRD analysis of compounds **12** and **20***

The crystal data and refinement parameters for compounds **12**[24] and **20** are summarized in Table S-I of the Supplementary material. The ORTEP view of compounds **12** and **20** are shown in Figs. 1 and 2, respectively. In compound **12**, the piperidine ring (N1/C7–C11) adopts a chair conformation (the N1 and C9 atoms deviate from the best plane of C7/C8 and C10/C11 by 54.9(2)° and –47.7(2)°, respectively) with an equatorial orientation of the Ph rings and Me group substituted on the heterocyclic. The C–C=N bond angles are different (C8–C9=N2 = 126.54(19)° and C10–C9=N2 = 117.50(18)°) and the dihedral angle between the atoms C10–C9=N2–O1 is –177.16(19)°, showing that the molecule exists as the *E*-isomer.

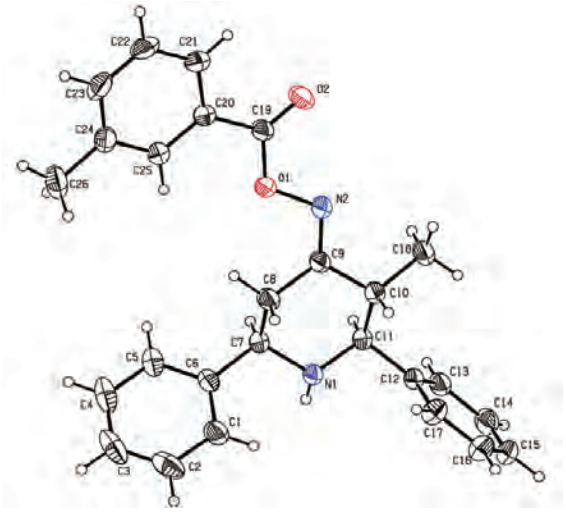

Fig. 1. The ORTEP view of compound **12** showing 30 % probability displacement ellipsoids.

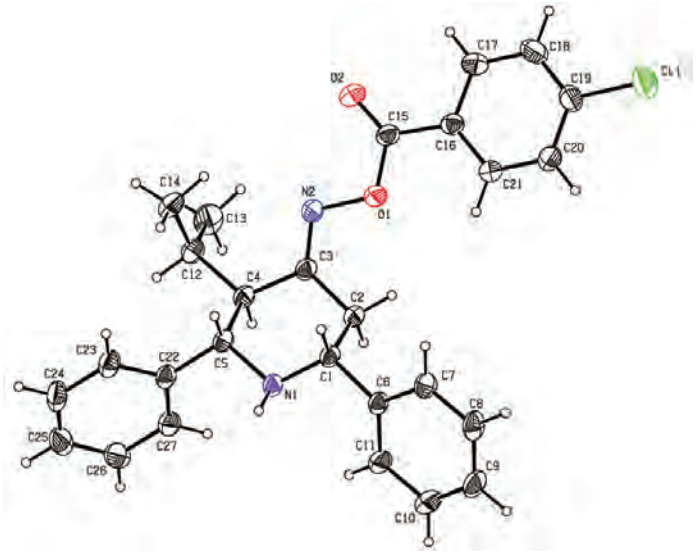

Fig. 2. The ORTEP view of compound **20** showing 50 % probability displacement ellipsoids.

In compound **20**, the piperidine ring (N1/C1–C5) also exists in a chair conformation with the ring atoms N1 and C3 deviating from the best plane of C1/C2 and C4/C5 by 66.77 and –62.22°, respectively. The Ph rings and the isopropyl group substituted on the heterocyclic ring are equatorially orientated. The bond angles of the C–C=N are different (C2–C3=N2 is 126.45° and C4–C3=N2 is 118.97°) and the molecule is found to exist in *E*-isomeric form as evidenced by the C2–C3=N2–O1 dihedral angle of 179.08°.

Antimicrobial screening

All the synthesized compounds **8**–**22** were screened for their *in vitro* antimicrobial activity in nutrient broth (NB) for bacteria and Sabouraud dextrose broth (SDB) for fungi by the twofold serial dilution method. A standard procedure was adopted for the preparation of all test samples.[25] The minimum inhibitory concentration (MIC) values of the synthesized compounds **8**–**22** against bacterial strains *viz*. *Bacillus subtilis*, *Staphylococcus aureus*, *Pseudomonas aeruginosa* and *Escherichia coli* are compared with the those of ampicillin in Table IV and against fungal strains *viz*. *Penicillim chrysogenum*, *Trichoderma viride*, *Aspergillus niger* and *A. flavus* are compared with those of amphotericin-B in Table V.

Antibacterial activity

All the synthesized piperidin-4-one oxime esters exhibited a wide range of *in vitro* antibacterial activity from the highest concentration (200 μg mL^{-1}) to the lowest concentration (6.25 μg mL^{-1}) against all the tested organisms, except **8** that

TABLE IV. Antibacterial activity (*MIC* / μg mL^{-1}) of compounds **8**–**22**; –: no inhibition at 200 μg mL^{-1}

Cmpd.	Bacteria			
	B. subtilis	*S. aureus*	*P. aeruginosa*	*E. coli*
8	100	–	200	200
9	25	50	25	50
10	25	100	50	50
11	50	100	50	50
12	100	200	100	100
13	50	200	100	200
14	12.5	25	12.5	12.5
15	25	50	50	25
16	25	50	25	25
17	50	100	50	50
18	50	100	50	50
19	6.25	12.5	6.25	6.25
20	12.5	25	6.25	12.5
21	6.25	25	25	12.5
22	25	50	25	25
Ampicillin	12.5	50	25	25

TABLE V. Antifungal activity (*MIC* / μg mL^{-1}) of compounds **8**–**22**; – no inhibition at 200 μg mL^{-1}

Cmpd.	Fungi			
	P. chrysogenum	*T. viride*	*A. niger*	*A. flavus*
8	–	200	–	–
9	200	100	100	200
10	200	200	200	200
11	–	–	200	200
12	–	200	–	200
13	200	100	100	100
14	50	50	50	25
15	100	50	50	50
16	100	100	50	25
17	100	100	100	50
18	50	25	50	50
19	25	12.5	12.5	12.5
20	25	12.5	25	25
21	50	25	25	25
22	50	25	25	25
Amphotericin B	25	25	50	50

failed to inhibit the growth of *S. aureus* at the highest concentration (200 μg mL^{-1}). Compounds **9**–**11** recorded moderate activity against *S. aureus* (100 μg mL^{-1}) and improved activity against *B. subtilis*, *P. aeruginosa* and *E. coli*. However, compounds **8** and **12** showed weaker activity against *S. aureus*, *P. aeruginosa*

and *E. coli* at 200 μg mL^{-1}. On introducing an ethyl and/or isopropyl group at the 3rd position of the piperidine ring instead of a methyl group and replacing of *O*-benzoyl group in the oxime part of all the compounds registered better activity against all the strains. Several authors also documented that the 3-ethyl and/or 3-isopropyl substituted piperidin-4-one oxime derivatives exhibited outstanding antibacterial and antifungal activities.[26,27] The 3-ethyl substituted oxime esters **13**–**17** showed better activity against all the tested organisms compared to compounds **8**–**12**. Among these compounds, **14** registered greater activity (12.5–25 μg mL^{-1}) against all the tested organisms and compounds **15** and **16** recorded good activity against *B. subtilis* and *E. coli* at 25 μg mL^{-1}. Compound **17** showed moderate activity against *B. subtilis*, *P. aeruginosa* and *E. coli* at 50 μg mL^{-1} and compound **13** did not show any significant activity against *S. aureus* and *E. coli* even at the highest concentration (200 μg mL^{-1}). The presence of an isopropyl group at the 3rd position in compounds **18**–**22** showed better activity with *MIC* values of 6.25–12.5 μg mL^{-1} when compared with the other substituents (methyl or ethyl). Especially compound **19** registered greater activity against all the tested strains at lower concentrations (6.25–12.5 μg mL^{-1}) and compounds **20** and **21** also registered better activity (12.5–50.0 μg mL^{-1}) against all the tested organisms compared with **18** and **22** (25–100 μg mL^{-1}). From the above observations, it is obvious that the nicotinoyl-substituted oxime esters **14** and **19** recorded excellent activity among the substituted oxime esters. The chloro- and nitro-substituted oximes esters **15**, **16**, **20** and **21** also registered good activity.

Antifungal activity

The synthesized compounds **8**–**22** were also screened for their *in vitro* antifungal activity against the tested organisms. Compounds **8** and **12** showed no significant inhibition of *P. chrysogenum*, *A. niger* and *A. flavus* even at the highest concentration of 200 μg mL^{-1}, nor did compound **11** against *P. chrysogenum* and *T. viride*. Compounds **9**, **10** and **13** showed weak activity against *A. flavus* and *P. chrysogenum* at 200 μg mL^{-1}. Replacement of the methyl group by ethyl and/or isopropyl led to significant activity against all the tested organisms. Compound **14** registered better activity against *T. viride*, *P. chrysogenum* and *A. niger* at 50 μg mL^{-1} and compound **15** also showed better activity against *T. viride*, *A. flavus* and *A. niger*. Compounds **16** and **17** exhibited moderate activity against *P. chrysogenum*, *T. viride* with *MIC* value of 100 μg mL^{-1}. Compound **18** showed good activity against *P. chrysogenum*, *A. flavus* and *A. niger* and improved activity against *T. viride* at 25 μg mL^{-1}. Introduction of nicotinoyl and/or an electron-withdrawing group (chloro or nitro) at the oxime part increased the activity of compounds **19** and **20** against *T. viride*, *A. niger* and *A. flavus* at 12.5–25 μg mL^{-1}, of compounds **21** and **22** against *P. chrysogenum*, *T. viride* and *A. niger* at 25–50 μg mL^{-1}. An isopropyl group at the 3rd position of the piperidine ring

resulted in greater activity against all the tested organisms (12.5–50 μg mL^{-1}), when compared with the other compounds.

CONCLUSIONS

In summary, the $POCl_3$ and pyridine system was described as an *in situ* activating agent for direct piperidin-4-one oxime ester formation in the reaction between aromatic acids and piperidin-4-one oximes. The present method is practically efficient, involves shorter reaction times, simple purification procedures and is economic for the synthesis of piperidin-4-one oxime esters. From XRD crystallographic results, it was shown that the piperidine rings of compounds **12** and **20** adopt chair confirmations with equatorial orientation of the aryl groups. Based on the antimicrobial studies, it was proved that piperidin-4-one oxime esters show better activities against standard strains than ampicillin and amphotericin-B. In particular, nicotinoyl oximes **14** and **19** showed excellent antibacterial as well as antifungal activities in comparison with the other oxime esters.

SUPPLEMENTARY MATERIAL

Analytical and spectral data of the synthesized compounds and the crystal data and structural refinement of compounds **12** and **20** are available electronically from http://www.shd.org.rs/JSCS/, or from the corresponding author on request.

ИЗВОД

СИНТЕЗА, СТРУКТУРНА КАРАКТЕРИЗАЦИЈА И ИСПИТИВАЊЕ АНТИМИКРОБНЕ АКТИВНОСТИ НОВИХ ЕСТАРА ПИПЕРИДИН-4-ОН-ОКСИМА

K. GOKULA KRISHNAN, R. SIVAKUMAR и V. THANIKACHALAM

Department of Chemistry, Annamalai University, Annamalainagar 608 002, Tamil Nadu, India

Синтетисано је петнаест нових, биолошки активних, естара пиперидин-4-он-оксима естара **8**–**22** у добром приносу. Једињења су добијена реакцијом непосредно припремљених алканоил-хлорида, добијених из одговарајућих карбоксилних киселина и $POCl_3$, са пиперидин-4-он-оксимима. Структура добијених деривата утврђена је FTIR, NMR (1D и 2D) и масеном спектралном анализом. Структура деривата недвосмислено је потврђена XRD анализом монокристала једињења **12** и **20**. Испитана је *in vitro* антибактеријска и антифунгална активност свих синтетисаних деривата. Значајан број ових једињења показује добру активност према *Bacillus subtilis*, *Pseudomonas aeruginosa*, *Escherichia coli*, *Trichoderma viride* и *Aspergillus flavus*.

(Примљено 13. новембра 2014, ревидирано 25. јануара, прихваћено 16. априла 2015)

REFERENCES

1. a) S. Jegham, G. DeFoase, T. Purcell, J. Sehoernaker, US Patent 5,280,030 (1994); b) M. J. Schneider, *Alkaloids: Chemical and Biological Perspectives*; S. W. Pelletier, Ed., Pergamon, Oxford, 1996; c) A. P. Kozikowski, G. L. Araldi, J. Boja, W. M. Meil, K. M. Johnson, J. L. Flippen-Anderson, C. George, E. Saiah, *J. Med. Chem.* **41** (1998) 1962; d) S. S. Hadida-Ruah, H. M. Binch, M. P. DeNinno, L. T. D. Fanning, B. A. Frieman, P. D. J. Grootenhuis, N. Hilgraf, P. Joshi, E. A. Kallel, M. T. Miller, J. Pontillo, A. Silina, U. J. Sheth, D. J. Hurley, V. Arumugam, US Patent 2012/0264749 A1 (2012)

2. S. O. Thorberg, S. Berg, J. Lundstrom, B. Pettersson, A. Wijkstrom, D. Sanchez, P. Lindberg, J. L. G. Nilsson, *J. Med. Chem.* **30** (1987) 2008
3. G. Xu, A. Kannan, T. L. Hartman, H. Wargo, K. Watson, J. A. Turpin, R. W. Buckheit Jr., A. A. Johnson, Y. Pommier, M. Cushman, *Bioorg. Med. Chem.* **10** (2002) 2807
4. P. Lagisetty, P. Vilekar, K. Sahoo, S. Anant, V. Awasthi, *Bioorg. Med. Chem*. **18** (2010) 6109
5. D. Cheng, S. Valente, S. Castellano, G. Sbardella, R. D. Santo, R. Costi, M. T. Bedford, A. Mai, *J. Med. Chem*. **54** (2011) 4928
6. A. M. Katsori, M. Chatzopoulou, K. Dimas, C. Kontogiorgis, A. Patsilinakos, T. Trangas, D. Hadjipavlou-Litina, *Eur. J. Med. Chem.* **46** (2011) 2722
7. S. T. Harini, H. V. Kumar, J. Rangaswamy, N. Naik, *Bioorg. Med. Chem. Lett*. **22** (2012) 7588
8. J. P. Michael, *Nat. Prod. Rep*. **5** (2003) 476
9. a) D. J. Lauffer, M. R. Pavia, H. Tecle, A. J. Thomas, European Patent 445,731, A1 (1991); b) I. Damljanovic, M. Vukicevic, R. D. Vukicevic, *Monatsh. Chem*. **137** (2006) 301; c) P. Politzer, J. S. Murray, *The Chemistry of Hydroxylamines, Oximes and Hydroxamic Acids*, Wiley, Chichester, 2009
10. D. A. Bachovchin, M. R. Wolfe, K. Masuda, S. J. Brown, T. P. Spicer, V. Fernandez-Vega, P. Chase, P. S. Hodder, H. Rosen, B. F. Cravatt, *Bioorg. Med. Chem. Lett*. **20** (2010) 2254
11. G. Surkau, K. J. Bohm, K. Muller, H. Prinz, *Eur. J. Med. Chem*. **45** (2010) 3354
12. A. Karakurt, M. A. Alagoz, B. Sayoglu, U. Calis, S. Dalkara, *Eur. J. Med. Chem*. **57** (2012) 275
13. X. H. Liu, L. Pan, C. X. Tan, J. Q. Weng, B. L. Wang, Z. M. Li, *Pest. Biochem. Physiol*. **101** (2011) 143
14. K. Kunimoto, J. Tanabe, H. Kura, H. Oka, M. Ohwa, US Patent 7 189 489 B2 (2007)
15. R. R. Hwu, S. C. Tsay, S. C. Hong, M. H. Hsu, C. F. Liu, S. S. P. Chou, *Bioconjugate Chem*. **24** (2013) 1778
16. J. Otera, J. Nishikido, *Esterification: Methods, Reactions and Applications*, 2nd ed., Wiley-VCH, Weinheim, 2010
17. B. Neises, W. Steglich, *Angew. Chem. Int. Ed. Engl*. **17** (1978) 522
18. O. Mitsunobu, M. Eguchi, *Bull. Chem. Soc. Jpn.* **44** (1971) 3427
19. A. K. Adak, *Synlett* (2004) 1651
20. J. McNulty, R. Vemula, V. Krishnamoorthy, A. Robertson, *Tetrahedron* **68** (2012) 5415
21. F. Effenberger, G. Konig, H. Klenk, *Angew. Chem., Int. Ed. Engl.* **17** (1978) 695
22. a) C. R. Noller, V. Baliah, *J. Am. Chem. Soc.* **70** (1948) 3853; b) K. Gokula Krishnan, R. Sivakumar, V. Thanikachalam, *Can. Chem. Trans*. **2** (2014) 353
23. a) K. Pandiarajan, R. T. Sabapathy Mohan, M. U. Hasan, *Magn. Reson. Chem*. **24** (1986) 312; b) E. Abele, R. Abele, O. Dzenitis, E. Lukevics, *Chem. Heterocycl. Compd. (N.Y., NY, U.S.)* **39** (2003) 3
24. V. Kathiravan, K. Gokula Krishnan, T. Mohandas, V. Thanikachalam, P. Sakthivel, *Acta Crystallogr*., *E* **70** (2014) o883
25. M. L. Dhar, M. M. Dhar, B. N. Dhawan, B. N. Mehrotra, C. Ray, *Indian J. Exp. Biol*. **6** (1968) 232
26. P. Parthiban, S. Balasubramanian, G. Aridoss, S. Kabilan, *Med. Chem. Res*. **14** (2005) 523
27. P. Parthiban, G. Aridoss, P. Rathika, V. Ramkumar, S. Kabilan, *Bioorg. Med. Chem. Lett*. **19** (2009) 2981.

Journal of the Serbian Chemical Society
JSCS@tmf.bg.ac.rs • www.shd.org.rs/JSCS
J. Serb. Chem. Soc. 80 (9) S286–S291 (2015) *Supplementary material*

SUPPLEMENTARY MATERIAL TO

Synthesis, structural characterization and antimicrobial evaluation of some novel piperidin-4-one oxime esters

K. GOKULA KRISHNAN, R. SIVAKUMAR and V. THANIKACHALAM*

Department of Chemistry, Annamalai University, Annamalainagar 608 002, Tamil Nadu, India

J. Serb. Chem. Soc. 80 (9) (2015) 1101–1111

ANALYTICAL AND SPECTRAL DATA OF THE SYNTHESIZED COMPOUNDS

*(*E*)-3-Methyl-2,6-diphenylpiperidin-4-one* O-*benzoyloxime* (**8**). Colorless solid; m.p.: 116–118 °C; FTIR (KBr, cm^{-1}): 3446 (N–H stretching), 2786–3064 (C–H stretching), 1745 (C=O stretching), 1629 (C=N stretching), 1456 (C=C stretching), 735 (N–O stretching); ^{1}H-NMR (400 MHz, $CDCl_3$, δ / ppm): 8.03 (2H, *d*, *J* = 7.2 Hz, Ar), 7.29–7.57 (13H, *m*, Ar), 3.95 (2H, *d*, *J* = 11.6 Hz, 1H, H6), 3.66 (2H, *d*, *J* = 10 Hz, 1H, H2), 3.56 (2H, *d*, *J* = 13.6, Hz, 1H, $H5_{eq}$), 2.67 (2H, *m*, 1H, H3), 2.30 (2H, *t*, *J* = 12.6 Hz, 1H, $H5_{ax}$), 2.00 (1H, *br s*, N–H), 1.07 (3H, *d*, *J* = 6.4 Hz, CH_3 at C3); ^{13}C-NMR (100 MHz, $CDCl_3$, δ / ppm): 69.02 (C2), 44.36 (C3), 164.22 (C4), 36.48 (C5), 60.94 (C6), 11.84 (CH_3 at C3), 169.51 (–O–C=O), 143.03, 141.98, 133.25, 129.63, 129.41, 128.77, 128.62, 128.15, 128.06, 127.98, 126.89 (aryl carbons); ESI-HRMS (*m/z*): Calcd. for $C_{25}H_{24}N_2O_2$: 384.1838. Found: 385.1916 (M+1).

*(*E*)-3-Methyl-2,6-diphenylpiperidin-4-one* O-*nicotinoyloxime* (**9**). Colorless solid; m.p.: 130–132 °C; FTIR (KBr, cm^{-1}): 3318 (N–H stretching), 2832–3036 (C–H stretching), 1746 (C=O stretching), 1631 (C=N stretching), 1453 (C=C, stretching), 755 (N–O stretching); ^{1}H-NMR (400 MHz, $CDCl_3$, δ / ppm): 9.22 (1H *s*), 8.77 (1H, *d*, *J* = 2.8 Hz), 8.30 (1H, *d*, *J* = 8.0 Hz), 7.25–7.48 (11H, *m*, Ar), 3.97 (1H, *d*, *J* = 11.2 Hz, H6), 3.67 (1H, *d*, *J* = 10 Hz, H2), 3.54 (1H, *d*, *J* = = 13.6 Hz, $H5_{eq}$), 2.71 (1H, *m*, H3), 2.32 (1H, *t*, *J* = 12.6 Hz, $H5_{ax}$), 2.08 (1H, *s*, N–H), 1.07 (3H, *d*, *J* = 6.4 Hz, CH_3 at C3); ^{13}C-NMR (100 MHz, $CDCl_3$, δ / / ppm): 68.99 (C2), 44.37 (C3), 162.89 (C4), 36.59 (C5), 60.90 (C6), 11.75 (CH_3 at C3), 170.16 (–O–C=O), 153.67, 150.64, 142.78, 141.81, 137.17, 128.79, 128.61, 128.41, 128.17, 128.11, 127.94, 127.05, 126.78, 125.51, 123.57 (aryl carbons); GC–MS (*m/z*): Calcd. for $C_{24}H_{23}N_3O_2$: 385.18. Found: 386.13 (M+1).

* Corresponding author: E-mail: profvt.chemau@gmail.com

*(*E*)-3-Methyl-2,6-diphenylpiperidin-4-one* O-*(4-chlorobenzoyl)oxime* ***(10)***. Colorless solid; m.p.: 126–130 °C; FTIR (KBr, cm^{-1}): 3312 (N–H stretching), 2831–3084 (C–H stretching), 1746 (C=O stretching), 1641 (C=N stretching), 1447 (C=C stretching), 753 (N–O stretching); ^{1}H-NMR (400 MHz, $CDCl_3$, δ / / ppm): 7.95 (2H, *d*, *J* = 7.6 Hz, Ar), 7.29–7.47 (12H, *m*, Ar), 3.94 (1H, *d*, *J* = = 11.6 Hz, H6), 3.64 (1H, *d*, *J* = 10 Hz, H2), 3.52 (1H, *d*, *J* = 13.6 Hz, $H5_{eq}$), 2.67 (1H, *m*, H3), 2.30 (1H, *t*, *J* =12.6 Hz, $H5_{ax}$), 2.03 (1H, *s*, N–H), 1.06 (3H, *d*, *J* = 6.4 Hz, CH_3 at C3); ^{13}C-NMR (100 MHz, $CDCl_3$, δ / ppm): 68.99 (C2), 44.37 (C3), 163.36 (C4), 36.51 (C5), 60.93 (C6), 11.82 (CH_3 at C3), 169.73 (–O–C=O), 142.96, 141.91, 139.70, 131.01, 130.73, 128.99, 128.80, 128.62, 128.17, 128.11, 127.97, 127.83, 127.15, 126.88 (aryl carbons); GC–MS (*m/z*): Calcd. for $C_{25}H_{23}ClN_2O_2$: 418.14. Found: 419.07 (M+1).

*(*E*)-3-Methyl-2,6-diphenylpiperidin-4-one* O-*(4-nitrobenzoyl)oxime* ***(11)***. Pale yellow solid; m.p.: 138–142 °C; FTIR (KBr, cm^{-1}): 3309 (N–H stretching), 2830–3106 (C–H stretching), 1745 (C=O stretching), 1607 (C=N stretching), 1453 (C=C stretching), 755 (N–O stretching); ^{1}H-NMR (400 MHz, $CDCl_3$, δ / / ppm): 8.28 (2H, *d*, *J* = 7.2 Hz), 8.19 (2H, *d*, *J* = 7.2 Hz), 7.31–7.48 (10H, *m*, Ar), 3.98 (1H, *d*, *J* = 11.2 Hz, H6), 3.67 (1H, *d*, *J* = 9.6 Hz, H2), 3.52 (1H, *d*, *J* = = 13.6 Hz, $H5_{eq}$), 2.74 (1H, *m*, H3), 2.35 (1H, *t*, *J* = 12.6 Hz, $H5_{ax}$), 1.97 (1H, *s*, N–H), 1.07 (3H, *d*, *J* = 5.6 Hz, CH_3 at C3); ^{13}C-NMR (100 MHz, $CDCl_3$, δ / / ppm): 68.97 (C2), 44.40 (C3), 162.38 (C4), 36.57 (C5), 60.92 (C6), 11.73 (CH_3 at C3), 170.47 (–O–C=O), 150.64, 149.74, 142.75, 141.71, 134.84, 130.72, 128.82, 128.63, 128.23, 128.20, 127.92, 126.83, 123.78 (aryl carbons); GC–MS (*m/z*): Calcd. for $C_{25}H_{23}N_3O_4$: 429.16. Found: 430.13 (M+1).

*(*E*)-3-Methyl-2,6-diphenylpiperidin-4-one* O-*(3-methylbenzoyl)oxime* ***(12)***. Colorless solid; m.p.: 122–124 °C; FTIR (KBr, cm^{-1}): 3320 (N–H stretching), 2790–3064 (C–H stretching), 1746 (C=O stretching), 1628 (C=N stretching), 1454 (C=C stretching), 758 (N–O stretching); ^{1}H-NMR (400 MHz, $CDCl_3$, δ / ppm): 7.86 (1H, *s*, Ar), 7.82 (1H, *d*, *J* = 7.6 Hz, Ar), 7.24–7.47 (12H, *m*, Ar), 3.97 (1H, *d*, *J* = 11.2 Hz, H6), 3.67 (1H, *d*, *J* = 10 Hz, H2), 3.57 (1H, *d*, *J* = 13.6 Hz, $H5_{eq}$), 2.70 (1H, *m*, H3), 2.39 (3H, *s*, *m*-CH_3), 2.30 (1H, *t*, *J* = 12.8 Hz, $H5_{ax}$), 2.05 (1H, *br s*, N–H), 1.07 (3H, *d*, *J* = 6.4 Hz, CH_3 at C3); ^{13}C-NMR (100 MHz, $CDCl_3$, δ / ppm): 69.01 (C2), 44.36 (C3), 164.43 (C4), 36.50 (C5), 60.93 (C6), 21.38 (*m*-CH_3), 11.82 (CH_3 at C3), 169.51 (–O–C=O), 143.07, 141.99, 138.43, 134.02, 130.18, 129.32, 128.74, 128.59, 128.45, 128.12, 128.02, 127.96, 126.86, 126.68 (aryl carbons); GC–MS (*m/z*): Calcd. for $C_{26}H_{26}N_2O_2$: 398.19. Found: 399.13 (M+1).

*(*E*)-3-Ethyl-2,6-diphenylpiperidin-4-one O-benzoyloxime* ***(13)***. Colorless solid; m.p.: 130–134 °C; FTIR (KBr, cm^{-1}): 3311 (N–H stretching), 2866–3068 (C–H stretching), 1739 (C=O stretching), 1631 (C=N stretching), 1450 (C=C stretching), 750 (N–O stretching); ^{1}H-NMR (400 MHz, $CDCl_3$, δ / ppm): 8.03

(2H, *d*, *J* = 7.6 Hz), 7.26–7.57 (13H, *m*), 3.96 (1H, *d*, *J* = 11.2 Hz, H6), 3.79 (1H, *d*, *J* = 10 Hz, H2), 3.54 (1H, *d*, *J* = 13.6 Hz, $H5_{eq}$), 2.59 (1H, *m*, H3), 2.29 (1H, *t*, *J* = 12.6 Hz, $H5_{ax}$), 1.95 (1H, *br s*, N–H), 1.74 (1H, *m*, C**H**$_2$CH$_3$ at C3), 1.39 (1H, *q*, C**H**$_2$CH$_3$ at C3), 0.95 (3H, *t*, *J* = 7.2 Hz, CH$_2$C**H**$_3$ at C3); ^{13}C-NMR (100 MHz, $CDCl_3$, δ / ppm): 67.40 (C2), 51.16 (C3), 164.22 (C4), 36.81 (C5), 61.00 (C6), 19.14 (CH$_2$CH$_3$ at C3), 12.06 (CH$_2$CH$_3$ at C3), 168.15 (–O–C=O), 143.08, 142.04, 133.22, 129.62, 129.45, 128.76, 128.64, 128.61, 128.12, 128.09, 128.03, 126.87 (aryl carbons); ESI-HRMS (*m/z*): Calcd. for $C_{26}H_{26}N_2O_2$: 398.1994. Found: 399.2076 (M+1).

*(*E*)-3-Ethyl-2,6-diphenylpiperidin-4-one* O-*nicotinoyloxime* ***(14)***. Colorless solid; m.p.: 126–128 °C; FTIR (KBr, cm^{-1}): 3275 (N–H stretching), 2813–3034 (C–H stretching), 1751 (C=O stretching), 1629 (C=N stretching), 1456 (C=C stretching), 761 (N–O stretching); ^{1}H-NMR (400 MHz, $CDCl_3$, δ / ppm): 9.22 (1H, *s*), 8.77 (1H, *d*, *J* = 4 Hz), 8.30 (1H, *d*, *J* = 8 Hz), 7.29–7.48 (11H, *m*, Ar), 3.97 (1H, *d*, *J* = 11.2 Hz, H6), 3.80 (1H, *d*, *J* = 10 Hz, H2), 3.52 (1H, *d*, *J* = 13.2 Hz, $H5_{eq}$), 2.60 (1H, *m*, H3), 2.31 (1H, *t*, *J* = 12.6 Hz, $H5_{ax}$), 2.02 (1H, *s*, N–H), 1.74 (1H, *m*, C**H**$_2$CH$_3$ at C3), 1.39 (1H, *q*, C**H**$_2$CH$_3$ at C3), 0.95 (3H, *t*, *J* = 7.2 Hz, CH$_2$C**H**$_3$ at C3); ^{13}C-NMR (100 MHz, $CDCl_3$, δ / ppm): 67.38 (C2), 51.19 (C3), 162.88 (C4), 36.90 (C5), 60.95 (C6), 19.08 (CH$_2$CH$_3$ at C3), 11.97 (CH$_2$CH$_3$ at C3), 168.81 (–O–C=O), 153.63, 150.64, 142.83, 141.88, 137.15, 128.77, 128.63, 128.14, 128.08, 128.04, 126.75, 125.55, 123.56 (aryl carbons); GC–MS (*m/z*): Calcd. for $C_{25}H_{25}N_3O_2$: 399.1. Found: 399.6 (M+).

*(*E*)-3-Ethyl-2,6-diphenylpiperidin-4-one* O-*(4-chlorobenzoyl)oxime* ***(15)***. Colorless solid; m.p.: 130–132 °C; FTIR (KBr, cm^{-1}): 3294 (N–H stretching), 2874–3064 (C–H stretching), 1741 (C=O stretching), 1638 (C=N stretching), 1454 (C=C stretching), 747 (N–O stretching); ^{1}H-NMR (400 MHz, $CDCl_3$, δ / ppm): 7.96 (2H, *d*, *J* = 8 Hz, Ar), 7.28–7.47 (12H, *m*, Ar), 3.95 (1H, *d*, *J* = 11.2 Hz, H6), 3.79 (1H, *d*, *J* = 10 Hz, H2), 3.49 (1H, *d*, *J* = 13.6 Hz, $H5_{eq}$), 2.59 (1H, *m*, H3), 2.29 (1H, *t*, *J* = 12.2 Hz, $H5_{ax}$), 1.96 (1H, *br s*, N–H), 1.74 (1H, *m*, C**H**$_2$CH$_3$ at C3), 1.38 (1H, *t*, C**H**$_2$CH$_3$ at C3), 0.94 (3H, *t*, *J* = 7.2 Hz, CH$_2$C**H**$_3$ at C3); ^{13}C-NMR (100 MHz, $CDCl_3$, δ / ppm): 67.36 (C2), 51.15 (C3), 163.36 (C4), 36.80 (C5), 60.97 (C6), 19.11 (CH$_2$CH$_3$ at C3), 12.00 (CH$_2$CH$_3$ at C3), 168.38 (–O–C=O), 142.98, 141.94, 139.66, 130.98, 128.97, 128.77, 128.64, 128.14, 128.06, 127.87, 126.83 (aryl carbons); GC–MS (*m/z*): Calcd. for $C_{26}H_{25}ClN_2O_2$: 432.16. Found: 433.07 (M+1).

*(*E*)-3-Ethyl-2,6-diphenylpiperidin-4-one* O-*(4-nitrobenzoyl)oxime* ***(16)***. Pale yellow solid; m.p.: 124–128 °C; FTIR (KBr, cm^{-1}): 3295 (N–H stretching), 2816–3065 (C–H stretching), 1743 (C=O stretching), 1640 (C=N stretching), 1454 (C=C stretching), 755 (N–O stretching); ^{1}H-NMR (400 MHz, $CDCl_3$, δ / / ppm): 8.26 (2H, *d*, *J* = 8.4 Hz), 8.18 (2H, *d*, *J* = 8.4 Hz), 7.28–7.47 (10H, *m*, Ar), 3.97 (1H, *d*, *J* = 10.8 Hz, H6), 3.80 (1H, *d*, *J* = 10 Hz, H2), 3.50 (1H, *d*, *J* =

= 13.2 Hz, $H5_{eq}$), 2.61 (1H, *m*, H3), 2.34 (1H, *t*, *J* = 12.6 Hz, $H5_{ax}$), 1.99 (1H, *s*, N–H), 1.73 (1H, *m*, C**H**$_2$CH$_3$ at C3), 1.38 (1H, *q*, C**H**$_2$CH$_3$ at C3), 0.95 (3H, *t*, *J* = 7.2 Hz, CH$_2$C**H**$_3$ at C3); ^{13}C-NMR (100 MHz, $CDCl_3$, *δ* / ppm): 67.32 (C2), 51.19 (C3), 162.36 (C4), 36.86 (C5), 60.96 (C6), 19.11 (CH$_2$CH$_3$ at C3), 11.98 (CH$_2$CH$_3$ at C3), 169.11 (–O–C=O), 150.62, 142.85, 141.83, 134.92, 130.72, 128.82, 128.68, 128.20, 128.16, 128.06, 126.83, 123.78 (aryl carbons); GC–MS (*m/z*): Calcd. for $C_{26}H_{25}N_3O_4$: 443.1. Found: 444.6 (M+1).

*(*E*)-3-Ethyl-2,6-diphenylpiperidin-4-one* O-*(3-methylbenzoyl)oxime* ***(17)***. Colorless solid; m.p.: 114–116 °C; FTIR (KBr, cm^{-1}): 3323 (N–H stretching), 2802–3029 (C–H stretching), 1748 (C=O stretching), 1625 (C=N stretching), 1454 (C=C stretching), 741 (N–O stretching); ^{1}H-NMR (400 MHz, $CDCl_3$, *δ* / ppm): 7.86 (1H, *s*, Ar), 7.82 (1H, *d*, *J* = 7.2 Hz, Ar), 7.26–7.45 (12H, *m*, Ar), 3.95 (1H, *d*, *J* = 11.2 Hz, H6), 3.79 (1H, *d*, *J* = 10 Hz, H2), 3.53 (1H, *d*, *J* = 13.2 Hz, $H5_{eq}$), 2.58 (1H, *m*, H3), 2.37 (3H, *s*, *m*-CH$_3$), 2.28 (1H, *t*, *J* = 12.6 Hz, $H5_{ax}$), 1.98 (1H, *br s*, N–H), 1.76 (1H, *m*, C**H**$_2$CH$_3$ at C3), 1.39 (1H, C**H**$_2$CH$_3$ at C3), 0.95 (3H, *t*, *J* = 7 Hz, CH$_2$C**H**$_3$ at C3); ^{13}C-NMR (100 MHz, $CDCl_3$, *δ* / ppm): 67.42 (C2), 51.18 (C3), 164.42 (C4), 36.83 (C5), 61.00 (C6), 21.42 (*m*-CH$_3$), 19.15 (CH$_2$CH$_3$ at C3), 12.08 (CH$_2$CH$_3$ at C3), 168.17 (–O–C=O), 143.12, 142.07, 138.43, 134.02, 130.19, 129.40, 128.76, 128.64, 128.50, 128.11, 128.02, 126.87, 126.72 (aryl carbons); ESI-HRMS (*m/z*): Calcd. for $C_{27}H_{28}N_2O_2$: 412.2151. Found: 413.2225 (M+1).

*(*E*)-3-Isopropyl-2,6-diphenylpiperidin-4-one* O-*benzoyloxime* ***(18)***. Colorless solid; m.p.: 124–126 °C; FTIR (KBr, cm^{-1}): 3321 (N–H stretching), 2822––3087 (C–H stretching), 1747 (C=O stretching), 1635 (C=N stretching), 1456 (C=C stretching), 759 (N–O stretching); ^{1}H-NMR (400 MHz, $CDCl_3$, *δ* / ppm): 8.00 (2H, *d*, *J* = 7.6 Hz, Ar), 7.26–7.54 (13H, *m*, Ar), 4.03 (2H, *t*, *J* = 7.2 Hz), 3.33 (1H, *d*, *J* = 14.8 Hz, $H5_{eq}$), 2.76 (1H, *t*, *J* = 3.4 Hz, H3), 2.55 (1H, *t*, *J* = 12.6 Hz, $H5_{ax}$), 1.90 (1H, *t*, *J* = 6.4, Hz, C**H**(CH$_3$)$_2$ at C3),1.86 (1H, *br s*, N–H), 1.17 (3H, *d*, *J* = 6.8 Hz, CH–(Me)C**H**$_3$), 1.02 (3H, *d*, *J* = 6.4 Hz, CH–(Me)C**H**$_3$); ^{13}C-NMR (100 MHz, $CDCl_3$, *δ* / ppm): 64.95 (C2), 54.16 (C3), 164.05 (C4), 36.16 (C5), 59.64 (C6), 28.48 (CH(CH$_3$)$_2$ at C3), 21.08, 18.75 (CH(CH$_3$)$_2$ at C3 carbon), 167.51 (–O–C=O), 143.45, 143.03, 133.16, 129.63, 129.45, 128.76, 128.64, 128.57, 128.01, 127.96, 126.82 (aryl carbons); ESI-HRMS (*m/z*): Calcd. for $C_{27}H_{28}N_2O_2$: 412.1151. Found: 413.1329 (M+1).

*(*E*)-3-Isopropyl-2,6-diphenylpiperidin-4-one* O-*nicotinoyloxime* ***(19)***. Colorless solid; m.p.: 128–132 °C; FTIR (KBr, cm^{-1}): 3272 (N–H stretching), 2819––3035 (C–H stretching), 1752 (C=O stretching), 1628 (C=N stretching), 1456 (C=C stretching), 761 (N–O stretching); ^{1}H-NMR (400 MHz, $CDCl_3$, *δ* / ppm): 9.18 (1H, *s*), 8.72 (1H, *d*, *J* = 2 Hz), 8.25 (1H, *d*, *J* = 7.6 Hz), 7.26–7.50 (11H, *m*, Ar), 4.05 (2H, *d*, *J* = 8.8 Hz), 3.31 (1H, *d*, *J* = 14.4 Hz, $H5_{eq}$), 2.77 (1H, *m*, H3), 2.56 (1H, *t*, *J* =12.6 Hz, $H5_{ax}$), 1.91 (2H, *br s*, C**H**(CH$_3$)$_2$ at C3 merged with

N–H), 1.16 (3H, *d*, *J* = 6.4 Hz, CH–(Me)C**H**$_3$), 1.02 (3H, *d*, *J* = 6.4 Hz, CH–Me)C**H**$_3$); ^{13}C-NMR (100 MHz, $CDCl_3$, δ / ppm): 64.89 (C2), 54.25 (C3), 162.69 (C4), 36.25 (C5), 59.54 (C6), 28.42 ($CH(CH_3)_2$ at C3), 21.11, 18.69 ($CH(CH_3)_2$ at C3 carbon), 168.20 (–O–C=O), 153.59, 150.66, 143.26, 142.90, 137.12, 128.79, 128.64, 128.02, 127.97, 126.72, 125.53, 123.54 (aryl carbons); ESI-HRMS (*m/z*): Calcd. for $C_{26}H_{27}N_3O_2$: 413.2103. Found: 414.2180 (M+1).

*(*E*)-3-Isopropyl-2,6-diphenylpiperidin-4-one* O-*(4-chlorobenzoyl)oxime* ***(20)***. Colorless solid; m.p.: 134–136 °C; FTIR (KBr, cm^{-1}): 3315 (N–H stretching), 2803–3073 (C–H stretching), 1745 (C=O stretching), 1631 (C=N stretching), 1454 (C=C stretching), 753 (N–O stretching); ^{1}H-NMR (400 MHz, $CDCl_3$, δ / ppm): 7.91 (*d*, *J* = 8 Hz), 7.25–7.48 (12H, *m*, Ar), 4.03 (2H, *d*, *J* = 7.6 Hz), 3.29 (1H, *d*, *J* = 14.8 Hz, $H5_{eq}$), 2.75 (1H, *m*, H3), 2.54 (1H, *t*, *J* =12.6 Hz, $H5_{ax}$), 1.89 (1H, *t*, *J* = 6, Hz, C**H**$(CH_3)_2$ at C3),1.85 (1H, *br s*, N–H), 1.16 (3H, *d*, *J* = 6.4 Hz, CH–(Me)C**H**$_3$), 1.02 (3H, *d*, *J* = 6.8 Hz, CH–(Me)C**H**$_3$); ^{13}C-NMR (100 MHz, $CDCl_3$, δ / ppm): 64.96 (C2), 54.29 (C3), 163.17 (C4), 36.20 (C5), 59.64 (C6), 28.46 ($CH(CH_3)_2$ at C3), 21.16, 18.78 ($CH(CH_3)_2$ at C3 carbon), 167.79 (–O–C=O), 143.46, 143.00, 139.57, 131.03, 128.96, 128.82, 128.69, 128.04, 127.97, 127.83 (aryl carbons); GC–MS (*m/z*): Calcd. for $C_{27}H_{27}ClN_2O_2$: 446.1. Found: 446.0 (M+).

*(*E*)-3-Isopropyl-2,6-diphenylpiperidin-4-one* O-*(4-nitrobenzoyl)oxime* ***(21)***. Pale yellow solid; m.p.: 140–142 °C; FTIR (KBr, cm^{-1}): 3318 (N–H stretching), 2816–3087 (C–H stretching), 1752 (C=O stretching), 1635 (C=N stretching), 1456 (C=C stretching), 777 (N–O stretching); ^{1}H-NMR (400 MHz, $CDCl_3$, δ / ppm): 8.23 (2H, *d*, *J* = 8 Hz), 8.14 (2H, *d*, *J* = 8 Hz), 7.27–7.50 (10H, *m*, Ar), 4.07 (2H, *d*, *J* = 8 Hz), 3.31 (1H, *d*, *J* = 14.4 Hz, $H5_{eq}$), 2.79 (1H, *m*, H3), 2.59 (1H, *t*, *J* =12.4 Hz, $H5_{ax}$), 1.92 (2H, *br s*, C**H**$(CH_3)_2$ at C3 merged with N–H), 1.16 (3H, *d*, *J* = 6 Hz, CH–(Me)C**H**$_3$), 1.02 (3H, *d*, *J* = 6 Hz, CH–(Me)C**H**$_3$); ^{13}C-NMR (100 MHz, $CDCl_3$, δ / ppm): 64.89 (C2), 54.32 (C3), 162.20 (C4), 36.21 (C5), 59.55 (C6), 28.44 ($CH(CH_3)_2$ at C3), 21.11, 18.67 ($CH(CH_3)_2$ at C3 carbon), 168.55 (–O–C=O), 150.57, 143.28, 142.81, 134.93, 130.72, 128.82, 128.68, 128.08, 127.96, 126.76, 123.73 (aryl carbons); GC–MS (*m/z*): Calcd. for $C_{27}H_{27}N_3O_4$: 457.2. Found: 458.9 (M+1).

*(*E*)-3-Isopropyl-2,6-diphenylpiperidin-4-one* O-*(3-methylbenzoyl)oxime* ***(22)***. Colorless solid; m.p.: 136–138 °C; FTIR (KBr, cm^{-1}): 3313 (N–H stretching), 2797–3030 (C–H stretching), 1749 (C=O stretching), 1632 (C=N stretching), 1455 (C=C stretching), 757 (N–O stretching); ^{1}H-NMR (400 MHz, $CDCl_3$, δ / ppm): 7.83 (1H, *s*, Ar), 7.79 (1H, d, *J* = 7.6 Hz, Ar), 7.26–7.50 (12H, *m*, Ar), 4.05 (2H, *d*, *J* = 8 Hz), 3.32 (1H, *dd*, *J* = 14.4 Hz, $H5_{eq}$), 2.77 (1H, *m*, H3), 2.56 (1H, *q*, *J* =11.2 Hz, $H5_{ax}$), 2.37 (3H, *s*, *m*-CH_3), 1.91 (1H, *t*, *J* = 5.8 Hz, C**H**$(CH_3)_2$ at C3),1.83 (1H, *br s*, N–H), 1.16 (3H, *d*, *J* = 6.8 Hz, CH–(Me)C**H**$_3$), 1.01 (3H, *d*, *J* = 6.8 Hz, CH–(Me)C**H**$_3$); ^{13}C-NMR (100 MHz,

$CDCl_3$, δ / ppm): 64.94 (C2), 54.18 (C3), 164.27 (C4), 36.10 (C5), 59.63 (C6), 28.49 ($CH(CH_3)_2$ at C3), 21.39 (*m*-CH_3), 21.05, 18.78 ($CH(CH_3)_2$ at C3 carbon), 167.54 (–O–C=O), 143.49, 143.05, 138.35, 133.93, 130.18, 129.38, 128.74, 128.62, 128.42, 128.01, 127.97, 127.93, 126.81, 126.72 (aryl carbons); GC–MS (*m/z*): Calcd. for $C_{28}H_{30}N_2O_2$: 426.2. Found: 426.9 (M+).

TABLE S-I. Crystal data and structural refinement for compounds **12** and **20**

Parameter	Compound	
	(*E*)-3-Methyl-2,6-diphenyl-piperidin-4-one *O*-(3-methyl-benzoyl)oxime (**12**)	(E)-3-Isopropyl-2,6-diphenyl-piperidin-4-one *O*-(4-chloro-benzoyl)oxime (**20**)
CCDC No.	CCDC 1005453	CCDC 951598
Empirical formula	$C_{26}H_{26}N_2O_2$	$C_{27}H_{27}N_2O_2Cl$
Formula weight	398.49	446.96
Color/Shape	Colorless	Colorless
Crystal dimensions, mm	0.20×0.25×0.30	0.20×0.25×0.30
Temperature, K	293(2)	293(2)
Wavelength, Å	0.71073	0.71073
Crystal system, space group	Monoclinic; $P\ 2_1/n$	Monoclinic; $P\ 2_1/n$
Unit cell dimensions	a = 10.6265(6) Å α = 90.00° b = 12.7146(7)Å β = 99.52(2)° c = 16.4031(8) Å γ = 90.00°	a = 11.2010(3) Å α = 90.00° b = 13.3924(4) Å β = 100.87(2)° c = 16.3108(5) Å γ = 90.00°
Z, volume, Å^3	4, 2185.7(2)	4, 2402.8(12)
Calculated density, g cm^{-1}	1.21	1.24
Absorption coefficient	0.077	0.185
F(000)	848	944
Reflections Collected	5367 (3097 unique reflections)	22941 (5982 unique reflections)
θ range	2.04 – 28.26	1.98 – 28.40
Index ranges	h = –14 – 14; k = –16 – 16; l = –21 – 19	h = –14 – 14; k = –15 – 17; l = –21 – 20
Final R, R_W (obs., data)	$R2$ = 0.057; w$R2$ = 0.151	$R2$ = 0.052; w$R2$ = 0.137
Final R, R_w (all data)	$R2$ = 0.112; w$R2$ = 0.195	$R2$ = 0.087; w$R2$ = 0.159
Goodness of fit	1.045	1.022

Journal of the Serbian Chemical Society
JSCS-info@shd.org.rs • www.shd.org.rs/JSCS
J. Serb. Chem. Soc. 80 (9) 1113–1125 (2015)
JSCS–4784
UDC 661.183.8+577.115:541.183
Original scientific paper

Adsorption of *Candida rugosa* lipase onto alumina: effect of surface charge

LIDIJA T. IZRAEL ŽIVKOVIĆ[1]*#, LJILJANA S. ŽIVKOVIĆ[2#], BOJAN M. JOKIĆ[3], ANDRIJA B. SAVIĆ[2] and IVANKA M. KARADŽIĆ[1]

[1]*University of Belgrade, School of Medicine, Institute of Chemistry in Medicine, Visegradska 26, 11000 Belgrade, Serbia,* [2]*University of Belgrade, The Vinča Institute of Nuclear Sciences, 11000 Belgrade, Serbia and* [3]*University of Belgrade, Faculty of Technology and Metallurgy, Karnegijeva 4, 11001 Belgrade, Serbia*

(Received 22 February, revised 16 April, accepted 30 April 2015)

Abstract: The impact of the surface charge of alumina supports on the adsorption of *Candida rugosa* lipase was investigated in terms of the zeta potentials of the adsorption partners. The lipase adhered onto alumina with similar efficiency under both repulsive and attractive electrostatic conditions, shifting the zeta potential of the support towards that of the enzyme. The behavior was explained by a heterogeneous distribution of the surface charge of the lipase molecule. Special emphasis in this study was placed on the effect of immobilization on the enzyme kinetics and principal reasons for enzyme immobilization: improvement in stability and potential for reuse. The enzyme affinity was not altered by its adsorption onto alumina, while the V_{max} value of the lipase decreased. The thermostability of the adsorbed lipase was improved. A significant potential for reuse was found.

Keywords: alumina; lipase; adsorption; immobilization; *Candida rugosa*.

INTRODUCTION

Increasing environmental concerns have led to the replacement of conventional chemical methods with enzyme-based strategies. The utilization of enzymes as biocatalysts has become an integral part of different processes in the oil, pharmaceutical, detergent, and food industries. During the last decade, the potential of different techniques for immobilization has been studied in order to overcome instability, enhance enzyme reuse, as well as easier separation.[1] Among them, the most commonly used methods for enzyme immobilization are cross-linking or covalent binding, entrapment and adsorption. One of the simplest methods, with high commercial potential and wide applicability, is adsorption.[2] Adsorption

* Corresponding author. E-mail: lidija.izrael-zivkovic@mfub.bg.ac.rs
# These authors contributed equally to this article.
doi: 10.2298/JSC150222035I

causes little or no conformational changes of the enzyme but the linkages established between the enzyme and support are weak, so the enzyme could be easily desorbed (leaking of the enzyme from the support). The frequently used supports are inert polymers and inorganic materials.[3] Alumina exhibits high mechanical strength, excellent corrosion and wear resistance and good biocompatibility[4] and it is among the mostly used ceramics.[5]

Lipases are an important group of biocatalysts as they improve a variety of reactions with high specificity and selectivity.[6,7] *Candida rugosa* lipase has been widely used in stereoselective synthesis of pharmaceuticals, production of carbohydrate esters of fatty acids, biodiesel, biosensors, food and flavor making.[8,9] Considering the fact that *C. rugosa* is one of the most important enzymes in biotransformations, different protocols for its immobilization have been developed but novel and efficient methods are still required. Even though common and simple for performing, adsorption is a very complex phenomenon.[10]

Research teams have identified numerous factors that strongly influence enzyme loading and biocatalyst activity, such as support surface area, pore size distribution, pore volume, particle size, ionic strength as well as surface charge of both support and enzyme.[11] In a few studies, electrokinetic measurements were conducted, yielding different results. Although there is no doubt that electrostatic interactions influence the adsorption process, some authors claim that the maximal affinity of a protein towards a support surface occurs when the adsorption partners exhibit opposite surface charges,[11,12] while others suggest the highest adsorption efficiency under repulsive electrostatic conditions (same surface charge),[13,14] or at pHs close to the isoelectric point of the protein,[15] thus creating contradictory approaches.

In this regard, a previous study dealt with effect of the surface charge on the adsorption of *C. rugosa* lipase. Two inorganic supports, mesoporous silica SBA--15 and macroporous zirconia were used.[16] The electrostatic nature of the process was estimated based on the electrokinetic (zeta) potentials of the interacting partners. However, no direct correlation between adsorption efficiency and immobilization pH was hitherto established; the enzyme adhered similarly under both attractive and repulsive electrostatic conditions. Aimed at obtaining better insight into the impact of electrostatics on the adsorption of enzymes onto supports, the idea of the current study was to minimize the influence of the support morphology. For this purpose, nonporous submicron-sized alumina was selected as the model support. The same methodology was used, *i.e.*, changes in zeta (ζ) potential of the adsorption partners were monitored at different pH values and correlated with the amount of adsorbed lipase. The second part of the study focused on the effect of immobilization on the enzyme kinetics and the principal reasons for enzyme immobilization: improvement in stability and potential for reuse.

EXPERIMENTAL

Materials

Lipase from *C. rugosa* (lyophilized powder, Type VII, nominal activity 746 U mg^{-1}) and *p*-nitrophenyl palmitate (*p*-NPP) were purchased from Sigma Chemical Co. (St. Louis, MO, USA). The support material, alumina (Al_2O_3, AKP-30 Sumitomo, Japan), was a high purity (>99.99 %) α-phase, with an average particle size of 0.32 μm (size distribution: d_{90}, d_{50} and d_{10} of 0.61, 0.35 and 0.2 μm, respectively, Sedigraph 5100, Micrometrics)[17] and a specific surface area, Sp = 7 m^2 g^{-1}. All other chemicals were of analytical grade.

Enzyme assay

The activity of free lipase was measured spectrophotometrically using an assay based on the hydrolysis of *p*-NPP. The *p*-NPP solution was prepared as follows: 30 mg of *p*-NPP in 10 mL of 2-propanol was added to 90 mL of 0.05 M phosphate buffer (pH 8.0) supplemented with 200 mg of Na deoxycholate and 100 mg of gum arabic, (the final *p*-NPP concentration was 0.8 mM). The absorbance was measured at 410 nm for the first 3 min of the reaction at 25 °C. One unit (1 U) was defined as the quantity of enzyme that under the test conditions liberated 1 μmol of *p*-nitrophenol per min (ε = 18.5 mM^{-1} cm^{-1}). The reaction mixture was composed of 900 μL of *p*-NPP solution and 100 μl of lipase solution (lipase concentration 0.05 mg mL^{-1}).[18]

Activity of immobilized lipase was determined using 10 mg of immobilized preparation supplemented with 2 mL of *p*-NPP solution (the *p*-NPP of concentration was 0.8 mM, in phosphate buffer of pH 8.0) The reaction was performed at 25 °C for 3 min when it was stopped by the addition of 0.5 M sodium carbonate solution. The precipitate was removed by centrifugation at 10,000 rpm for 10 min. The supernatant was diluted 10-fold with deionized water and the absorbance was measured at 410 nm. One unit of enzyme activity (1 U) was defined as explained in the previous paragraph. The activity of the immobilized enzyme was calculated as U per g of support material.

Lipase immobilization

The effect of pH on the adsorption of lipase was investigated in the pH range 5 to 9, using the following 10 mM buffer solutions: acetate buffer (pH 5.0), phosphate buffer (pH 6.0, 7.0 and 8.0) and Tris-buffer (pH 7.6 and 9.0).

Alumina was prepared for immobilization as follows: 8 mg support mL^{-1} in the selected buffer was de-agglomerated for 10 min by sonication. Then, a lipase solution (2 mg mL^{-1} in the selected buffer) was added, the resulting suspension sonicated for 10 min and immobilization realized at room temperature under mild stirring (90 rpm). After 60 min, the immobilized lipase was precipitated by centrifugation at 10,000 rpm for 10 min using a microcentrifuge (Denver Instruments, USA). The immobilized enzyme was washed twice to remove the excess of unbound enzyme, dried for 1 h at room temperature and used for the assay.

The efficiency of immobilization was evaluated as the percent of the lipase adsorbed, which was calculated as:

$$\text{Lipase adsorbed (\%)} = \frac{100P_1}{P_0} \quad (1)$$

where P_0 is the initial concentration of lipase and P_1 is the concentration of immobilized lipase. The concentration of immobilized lipase was calculated as a difference between initial lipase concentration and lipase concentration in the supernatant after immobilization.[19]

The concentration of lipase was determined by the Bradford method using bovine serum albumin as the standard.[20]

Zeta potential measurements

Electrokinetic (zeta) potential measurements were performed by means of a Zetasizer Nano ZS instrument (Malvern, UK). The instrument uses the electrophoretic light scattering and laser Doppler velocimetry methods for determination of particle velocity, and from it, the zeta (*ζ*) potential. The integrated software calculates the *ζ*-potential from mobility values by the Henry equation, using the Smoluchowski approximation.[21,22] The measurements were performed at least in triplicate and the average values are presented. Each measurement comprised of minimum 10 runs. Only the results that met quality criteria were taken into account.

Aimed at determining of the isoelectric point (IEP) of support, the *ζ*-potential of the alumina particles was measured over a wide range of pH values (4–10), using aqueous solution of NaCl (0.01 M) as the inert background electrolyte.[23] Prior to titration, powder dispersion (1 mg mL^{-1}) was equilibrated for 24 h under mild shaking at room temperature. The *ζ*-potential measurements of lipase and that of the support particles (before and after enzyme adsorption) were then performed in the selected buffers adjusted to different pH values (5–9).

Field emission scanning electron microscopy (FESEM)

Field emission scanning electron microscopy (FESEM), using a Tescan Mira3 XMU (Czech Republic) at 20 kV, was employed to study the morphology of the support before and after the adsorption of lipase. Prior to analysis, the samples were coated with Au–Pd alloy using a sputter coater.

Determination of the kinetic parameters

Michaelis–Menten kinetics were used to describe the dependence of enzyme activity on substrate concentration for free and immobilized lipase. The kinetic parameters, V_{max} and K_m were determined for free and adsorbed lipase using solutions of *p*-NPP of the following concentrations: 0.1, 0.2, 0.4, 0.8, 1.2, 1.6 and 2.0 mM, according to the above-described methods for the determination of lipase activity.

V_{max} – units of activity per milligram of protein (U mg^{-1}) and K_m – substrate concentration that gives a reaction rate of $V_{max}/2$ (mM) were estimated from the experimental data using the Lineweaver–Burk equation:

$$\frac{1}{v} = \frac{1}{V_{max}} + \frac{K_m}{V_{max}}\left(\frac{1}{[S]}\right) \tag{2}$$

The *y*-axis intercept is $1/V_{max}$ and the slope is K_m/V_{max}.

Thermal stability

Reaction mixtures containing free or immobilized enzyme were incubated at 50 and 60 °C for various periods (20–120 min) and quickly cooled. Enzyme activity was measured according to the standard protocol for free and immobilized enzyme with *p*-NPP as the substrate. The half-life ($t_{1/2}$) of the enzyme with k_d as the decay constant was calculated as:

$$t_{1/2} = (\ln 2)/k_d \tag{3}$$

Reuse stability

The potential for reuse was determined using 25 mg of immobilized enzyme packed in a small filter paper bag soaked into 3 mL of *p*-NPP solution for 30 min at room temperature,

under mild stirring. After each batch reaction, the immobilized lipase was washed three times with deionized water and then reused. Into 2 mL of removed supernatant solution, 2 mL of 0.5 M sodium carbonate was added to stop the reaction. The absorbance was measured at 410 nm after centrifugation at 10,000 rpm for 10 min and 10-fold dilutions.

RESULTS AND DISCUSSION

Zeta (ζ) potential and immobilization pH study

There are close analogies between protein adsorption and particle deposition[24,25] both being governed by short-range interactions between charged surfaces at the solid–liquid interface. The DLVO (Derjuangin–Landau–Verbey––Overbeek) theory[26] plays an essential role in the quantification of the processes. Although based on simple additivity of electrostatic and van der Waals forces, it is successful in predicting the basic features of colloidal stability and adsorption or deposition processes. Since the electrostatic forces are dominant for attachment, the relative charges of the surfaces dictate whether the interaction is repulsive or attractive. The isoelectric points (*IEP*) of the partners indicate the pH where the ζ potential equals zero and the range over which the interactions are favored. Thus, a prediction of the process requires knowledge of the *IEP* values for both materials.

The reactions occurring at the solid–liquid interface were the subject of numerous experimental and theoretical investigations. To better understand the adsorption of proteins onto the surface of a support (*e.g.*, the mechanism of binding, the build-up of layers, *etc.*), the electrokinetic ζ potential changes *vs.* pH were often collected.[22,27–29] However, the aim of this study was not to elucidate the mechanism of *C. rugosa* lipase adsorption onto alumina surface by means of electrokinetic measurements, but to test the zeta potential of the adsorption partners as a diagnostic tool for the efficiency of binding of the protein to the support.

The variation in zeta potential of alumina, used as support, as a function of pH is presented in Fig. 1. As is evident, the isoelectric point was located at pH

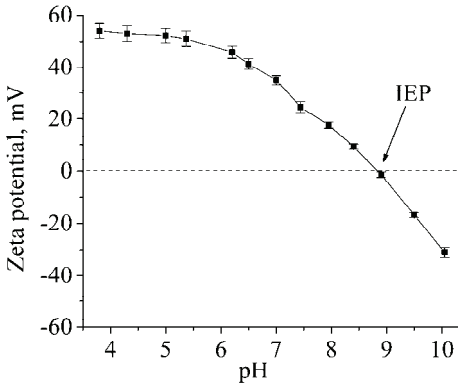

Fig. 1. Titration curve: zeta potential *vs.* pH for alumina powder in NaCl (0.01 M).

8.8, in good accordance with the literature.[17] Thus, the alumina develops positive and negative surface charges below and above this pH by protonation–deprotonation of the hydroxide groups present on the surface.[30]

Lipase from *C. rugosa* is a globular glycoprotein with molecular mass of 57 kDa. Its basic structural characteristics are summarized in Table I. With 31 acidic and 18 basic amino acids exposed on the surface,[16] its IEP is located at pH 4.65. Above this pH, the lipase acquires a negative charge and hence the enzyme should always be negative in this study.

TABLE I. Protein parameters of *C. rugosa* lipase, P20261 (UniprotKB)

Parameter	Value
Molecular mass, kDa	57
Dimensions, mm	5×4.2×3.3
Isoelectric point (IEP)	4.65
Total number of amino acids	534
Number of acidic amino acids	52
Number of basic amino acids	39
Non-polar surface, %	63
Surface acidic amino acids	31
Surface basic amino acids	18
α-Helical structure, %	38
β-Sheet structure, %	18
Post-translational modifications, PTM	Disulfide bonds: 75–112, 283–292 Glycosilation (*N*-acetyl-D-glucosamine): 329, 366
E.C. (Brenda)	3.1.1.3.1139.
3D structure in PDB	1CRL

To evaluate the effect of the surface charge of the adsorption partners on the adsorption efficiency, experiments were performed below and around the *IEP* of alumina (pH 8.8), where 2 different electrostatic scenarios were expected. The first one (pH < $IEP_{alumina}$) includes favorable adsorption conditions, *i.e.*, negatively charged lipase in the presence of positively charged alumina particles. The second adsorption scenario (pH ≈ $IEP_{alumina}$) is related to the interaction of negatively charged lipase with uncharged alumina, thus being much less favorable.

Different buffers were used over the investigated pH range 5–9. The ζ-potentials of enzyme and support, before and after adsorption, were monitored in parallel, and the percent of adsorbed lipase (η_{enz}) related to the values of the ζ-potential are summarized in Table II.

Indeed, in agreement with theoretical calculations, the lipase was negatively charged in the investigated pH range, reaching the highest absolute magnitude of ζ-potential at pH values 7–9. On the other hand, the alumina particles were positive in the acetic buffer adjusted to pH 5, as expected (Fig. 1). Surprisingly, in the presence of phosphate buffer, a charge reversal occurred: the alumina

turned highly negative even at pH 6. This result was confirmed for pH values 7–8, indicating specific adsorption of phosphates onto alumina surface occurred. A significant shift in the *IEP* towards acidic pH upon addition of PO_4^{3-} was also reported by Zheng.[31] To avoid preferential adsorption of phosphates, tris buffer was introduced, in which alumina behaved analogously as in NaCl. Likewise, at pH 7.6, the particles developed a positive charge, whilst at pH 9, a negative ζ-value was recorded.

TABLE II. ζ-potentials of free lipase and alumina, before and after adsorption of lipase, and the amount of lipase adsorbed at pH values 5–9

Buffer	ζ-potential, mV			η_{enz} / %
	Lipase	Alumina	Alumina–lipase	
pH 5 (acetic)	–4.3±0.5	+40.2±1.6	–9.4±1.1	30
pH 6 (phosphate)	–9.8±1.2	–35.9±2.1	–13.7±1.4	32
pH 7 (phosphate)	–12.4±0.4	–36.7±0.4	–25.0±2.3	33
pH 8 (phosphate)	–14.3±1.3	–30.7±1.3	–17.3±1.4	30
pH 7.6 (tris)	–14.3±0.6	+22.1±0.9	–25.4±2.2	38
pH 9 (tris)	–16.7±0.8	–12±0.5	–16.4±0.8	5

Albeit two electrostatic scenarios were expected, the phosphate buffer actually created the third repulsive electrostatic conditions, in which both alumina and lipase carried a negative surface charge.

As presented in Table II, the percent of adsorbed lipase was comparable under both attractive and repulsive electrostatic conditions. Whatever the charges of the immobilization partners were (like or dislike, as a function of the buffer used), the amount of adsorbed enzyme was moderate (around 30 %). Contrarily, at pH 9 (*i.e.*, when the pH ≈ IEP of alumina), only a small percentage (5 %) of adsorbed lipase was registered. This result is logical, since a pH value in the close vicinity of the IEP of alumina, when the particles carry only a negligible surface charge, strongly promoted their aggregation and sedimentation. Such adsorption condition was inconvenient for the lipase to reach the surfaces of the particles and adhere. On the contrary, the alumina particles were quite well dispersed at the other investigated pH values. A ζ-potential of *ca*. 30 mV (positive or negative) is normally required to achieve a reasonably stable dispersion.[30]

An anomalous adsorption of lipase molecules onto alumina bearing the same surface charge contradicts the classical DLVO theory. However, adsorption–deposition of protein–particles under repulsive electrostatic conditions is not an unusual phenomenon.[13,32,33] Although the overall charge of the lipase was negative in the selected pH range, the enzyme surface consists of positively (Lys, Arg, His) or negatively (Glu, Asp) charged, and non-polar residues dispensed into a patchwork which leads to localized interactions (Table I). The hetero-

geneous surface charge of an enzyme always establishes attractive electrostatic conditions, whatever is the charge on the support particles.

Therefore, the adsorption efficiency of enzyme depends on the dispersion state of support particles, *i.e.*, on the magnitude of the ζ-potential, not its sign, increasing enzyme availability to approach and adhere onto the surfaces of the particle. The presented results suggest that the zeta potential is a useful indicator of an adsorption process. An obvious change in the ζ-potential of the support was always registered after enzyme immobilization, indicating that the surfaces of the alumina particle were altered. Negatively charged lipase shifted the ζ-potential of support towards negative values, sometimes even more negative than its own.

The highest adsorption was achieved in the tris buffer of pH 7.6, therefore this buffer was chosen as suitable for lipase immobilization. Lipolytic activity of immobilized enzyme in chosen system was determined to be 58 U g^{-1} of alumina.

Field emission scanning electron microscopy (FESEM)

Adsorption of lipase onto support was also characterized by FESEM (Fig. 2). The powder was composed of differently sized sub-micrometer particles of irregular shapes. Their surfaces appeared smooth and nonporous, corroborating well the small value of specific surface area (7 m^2 g^{-1}). At high magnification (inset), a certain number of small, differently sized piles (20–80 nm), can be randomly spotted on the particle surfaces. They could be associated with lipase aggregates, composed of several lipase molecules (5 nm×4.2 nm×3.3 nm).

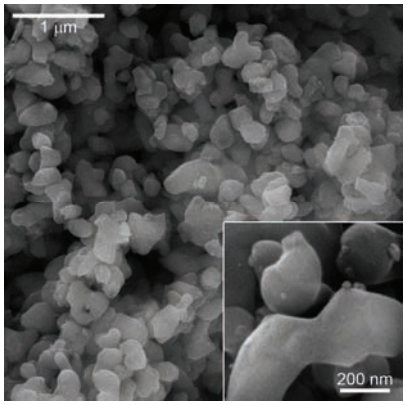

Fig. 2. FESEM micrographs of alumina before and after (inset) lipase adsorption.

The rather moderate adsorption of enzyme achieved (*ca*. 30 %) could be related to the poorly developed surface geometry of the alumina particles, not favorable for lipase adhesion. A much higher percent adsorption of *C. rugosa* lipase was reported in a previous work (*ca*. 80 % onto silica), which was due to mesoporous and fibrous morphology of SBA-15.[16]

Therefore, besides electrostatics, the morphology of the support seems to plays an important role in the adsorption and should also be considered. It could be a determining factor of the efficiency of enzyme adsorption, once the optimum dispersion conditions were provided.

Effect of immobilization on the catalytic properties of the enzyme

Catalytic properties of an enzyme can be modified by immobilization. These changes may be due to conformational alterations within the enzyme. The kinetic behavior of an immobilized enzyme could differ significantly from that of the same enzyme in free solution. Immobilization can also greatly affect the stability of an enzyme. This is primarily due to the physical prevention of large conformational changes within the protein structure.

The catalytic action of the lipase depends on the interfacial activation that occurs when the lipase binds to a lipid interface *via* the opening of the *α*-helical lid that covers the active site. There are several kinetic models for lipase activity, ranging from Michaelis–Menten kinetics and the first order Ping Pong Bi Bi mechanism[34] to more complicated ones taking into consideration the differences between the interfacial and bulk concentration[35] and also the time of solution penetration into support with immobilized lipase.[36] Although Michaelis–Menten mechanism assumes enzyme reaction in the medium where enzyme and substrate must be part of the same phase and does not take into account the activation of the lipase, it is still commonly used as a simplified model for explanations and the determination of the kinetic parameters.

Free lipase and lipase immobilized onto alumina obeyed Michaelis–Menten kinetics. Two parameters, V_{max} and K_m, for the free and immobilized *C. rugosa* lipase were determined and compared. The V_{max}, defined as the highest possible rate of enzyme activity, occurs when the enzyme is saturated with the substrate, and reflects the intrinsic catalytic character of the enzyme. K_m is defined as the substrate concentration that gives a reaction rate of $0.5V_{max}$, implying an affinity between enzyme and substrate. Values of kinetic parameters could not be directly compared with those previously reported for free and immobilized enzyme if the assay conditions (temperature, reaction system used) were not the same, but the trend of the modification of the catalytic property is comparable.

V_{max} and K_m were calculated from the experimental data using the Lineweaver–Burk equation. In this study, the K_m value of the immobilized lipase was similar to that of free lipase, 0.264 *vs*. 0.241 mM, suggesting that enzyme affinity towards the substrate was not altered by its adsorption onto alumina. Similar results were reported for *C. rugosa* lipase immobilized on zirconia, magnetized dacron and niobium oxide,[16,37,38] since adsorption causes little or no conformational change of the enzyme or destruction of its active site.[39] The V_{max} value for the free lipase was 172.0 U mg^{-1} that decreased after immobilization onto

alumina to 28.8 U mg^{-1}, which might be a consequence of increased rigidity of the enzyme. A reduced maximal velocity of immobilized enzymes was reported for *C. rugosa* lipase adsorbed onto silica, zirconia and niobium oxide.[16,38]

Thermal stability

One of the advantages of enzyme immobilization is its improved stability. Thermal stability of the immobilized lipase was evaluated, as shown in Fig. 3. Immobilized lipase was incubated for 2 h at 50 and 60 °C and the lipase activities were measured at 20 min intervals.

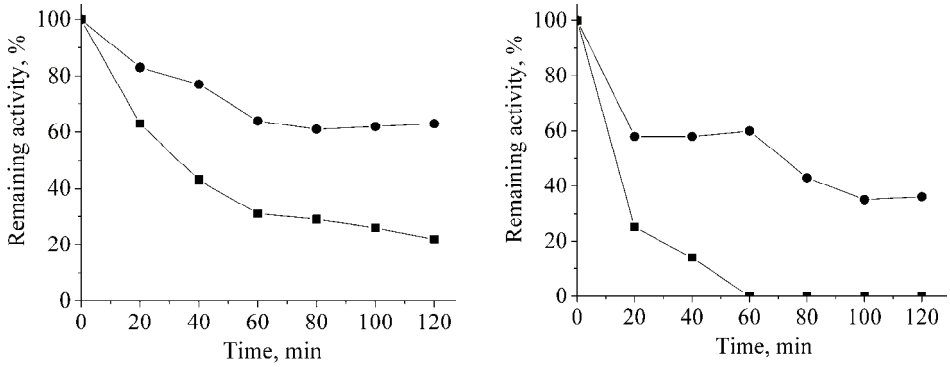

Fig. 3. Thermal stability of free (■) and immobilized lipase (●) at: a) 50 and b) 60 °C.

After 2 h of incubation at 50 °C, the remaining activity of free lipase was 31 %, but the remaining activity of immobilized lipase was 73 % (Fig. 3a). In terms of the half-life at 50 °C, the $t_{1/2}$ of lipase increased after immobilization onto alumina 5.6 times (from 32 min to 180 min).

After 1 h of incubation at 60 °C, the free lipase was not active at all while 60 % of its activity remained when immobilized (Fig. 3b). Even after 2 h, the activity of the lipase immobilized onto alumina was significantly preserved (nearly 40 %). In terms of half-life at 60 °C, the $t_{1/2}$ of the lipase increased after adsorption 5.8 times (from 14 to 81 min).

Thermal stability of lipase on support was significantly improved. Improvement in thermal stability seems to be a result of restricted movement of the protein after adsorption, which prevents conformation changes and unfolding.

Reuse stability

One of the most useful advantages of immobilization of an enzyme is its reusability. Adsorption on a matrix as an immobilization method is usually considered a method with poor reuse potential. However, the remaining activity of the enzyme on alumina was higher than 80 % after seven reuses and almost 50 %

after 11 cycles of use (Fig. 4). As the strength of protein–support interactions can be rated from the ability of the enzyme to resist removal – leaching, this result suggests a significant potential of lipase immobilized on alumina to be reused in biotechnological processes.

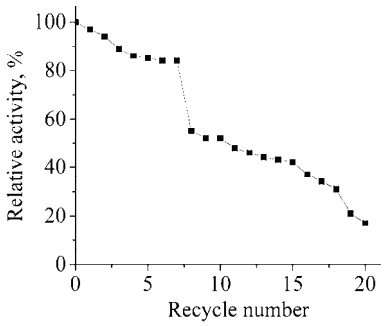

Fig. 4. Effect of reuse on the activity of immobilized lipase.

CONCLUSIONS

In this study, *C. rugosa* lipase was successfully adsorbed onto alumina as a support. The lipase adhered under both repulsive and attractive electrostatic conditions with comparable efficiency. Patchwork surface with mixed positive and negative charges was supposed to be responsible for this behavior. The zeta potential was proven an indicator of protein binding, *i.e.*, a shift in the zeta potential of the support towards that of enzyme was always registered. The morphology of the support also seems to play an important role in the adsorption process. Kinetic constants provided clear evidence that the enzyme affinity was not altered by its adsorption onto alumina, while V_{max} of the lipase decreased 6-fold after immobilization. The thermostability of the adsorbed lipase was improved more than 5 times at 50 and 60 °C. The results suggest a significant potential for reuse of the lipase immobilized onto alumina.

Acknowledgment. This research was financed by the Ministry of Education, Science and Technological Development of the Republic of Serbia (Projects Nos. III 43004 and III 45012).

ИЗВОД

АДСОРПЦИЈА ЛИПАЗЕ ИЗ *Candida rugosa* НА ГЛИНИЦИ: УТИЦАЈ ПОВРШИНСКОГ НАЕЛЕКТРИСАЊА

ЛИДИЈА Т ИЗРАЕЛ ЖИВКОВИЋ[1], ЉИЉАНА С ЖИВКОВИЋ[2], БОЈАН М. ЈОКИЋ[3], АНДРИЈА Б. САВИЋ[2] и ИВАНКА М. КАРАЦИЋ[1]

[1]*Универзитет у Београду, Медицински факултет, Институт за хемију у медицини, Вишеградска 26, 11000 Београд,* [2]*Универзитет у Београду, Институт за нуклеарне науке Винча, 11000 Београд и* [3]*Универзитет у Београду, Технолошко–металуршки факултет, Карнегијева 4, 11000 Београд*

У овом раду испитиван је утицај површинског наелектрисања глинице на адсорпцију *Candida rugosa* липазе на основу зета потенцијала оба учесника процеса. Липаза се адсорбује у условима и електростатичког привлачења и одбијања, при чему се вредност зета потенцијала носача помера ка вредности истог ензима. Овакво понашање је објаш-

њено хетерогеном расподелом површинског наелектрисања молекула липазе. Посебна пажња је посвећена проучавању утицаја имобилизације на кинетичке параметре липазе. Афинитет ензима није промењен након адсорпције, али је максимална брзина смањена. Термостабилност адсорбоване липазе је побољшана. Потврђена је и могућност вишеструке употребе имобилизоване липазе.

(Примљено 22. фебруара, ревидирано 16. априла, прихваћено 30. априла 2015)

REFERENCES

1. S. Roger, S. Van Pelt, *Chem. Soc. Rev*. **42** (2013) 6223
2. H. Ghamgui, N. Miled, M. Karra-Chaabouni, Y. Gargouri, *Biochem. Eng. J*. **37 (**2007) 34
3. S. Datta, L. R. Christena, Y. R. S. Rajaram, *Biotech* **3** (2013) 1
4. L. L. Hench, *J. Am. Ceram. Soc.* **74** (1991) 1487
5. A. Marti, *Injury* **31** (2000) 33
6. B. Andualem, A. Gessesse, *Biotechnology* **11** (2012) 100
7. H. Fariha, A. S. Aamer, H. Abdul, *Enzyme Microb. Techol*. **39** (2006) 235
8. A. Pandey, S. Benjamin, C. R. Soccol, P. Nigam, N. Krieger, V. Soccol, *Biotechnol. Appl. Biochem*. **29** (1999) 119
9. A. Rajendran, A. Palanisamy, V. Thangavelu, *Braz. Arch. Biol. Technol*. **52** (2009) 207
10. M. Rabe, D. Verdes, S. Seeger, *Adv. Colloid Interface Sci*. **162** (2011) 87
11. S. Hudson, E. Magner, J. Cooney, B. K. Hodnett, *J. Phys. Chem., B* **109** (2005) 19496
12. N. Schultz, G. Metreveli, M. Franzreb, F. H. Frimmel, C. Syldatk, *Colloids Surfaces, B* **66** (2008) 39
13. P. Zeliszewska, A. Bratek-Skicki, Z. Adamczyk, M. Ciesla, *Langmuir* **30** (2014) 11165
14. K. Rezwan, A. R. Studart, J. Voros, L. J. Gauckler, *J. Phys. Chem., B* **109** (2005) 14469
15. M. E. Aubin-Tam, K. Hamad-Schifferli, *Langmuir* **21** (2005) 12080
16. L. Izrael Živković, Lj. Živković, B. Babić, M Kokunešoski, B. Jokić, I. Karadžić, *Biochem. Eng. J*. **93** (2015) 73
17. R. Laucournet, C. Pagnoux, T. Chartier, J. F. Baumard, *J. Am. Ceram. Soc.* **83** (2000) 2661
18. I. Karadžić, A. Masui, L. Izrael Živković, N. Fujiwara, *J. Biosci. Bioeng.* **102** (2006) 309
19. Z. Knežević, N. Milosavić, D. Bezbradica, Z. Jakovljević, R. Prodanović, *Biochem. Eng. J*. **30** (2006) 269
20. M. M. Bradford, *Anal. Biochem*. **72** (1976) 248
21. S. Fazio, J. Guzman, M. T. Colomer, A. Salomoni, R. Moreno, *J. Eur. Ceram. Soc.* **28** (2008) 2171
22. B. Jachimska, M. Wasilewska, Z. Adamczyk, *Langmuir* **24 (**2008) 6866
23. M. Kosmulski, *Chemical Properties of Materials Surfaces*, Marcel Dekker Inc., New York, 2001, pp. 223–265
24. Z. Adamczyk, *Adv. Colloid Interfac*e *Sci*. **100**–**102** (2003) 263
25. Z. Adamczyk, M. Nattich, M. Wasilewska, M. Zaucha, *Adv. Colloid Interface Sci*. **168** (2011) 3
26. J. N. Israelachvili, *Intermolecular and Surface Forces*, Academic Press, London, 1992
27. D. Kovačevic, D. Mazur, T. Preočanin, N. Kallay, *Adsorption* **16** (2010) 405
28. I. Đapić, D. Kovačević, *Croat. Chem. Acta* **84** (2011) 185
29. J. Lutzenkirchen, T. Preočanin, D. Kovačević, V. Tomišić, L. Lovgren, N. Kallay, *Croat. Chem. Acta* **85** (2012) 391
30. R. J. Pugh, *Dispersion and Stability of Ceramic Powders in Liquids,* in *Surface and Colloid Chemistry in Advanced Ceramics Processing,* R. J. Pugh, L. Bergstrom, Eds., Marcel Dekker Inc., New York, 1994, pp. 127–192

31. T. Zheng, *M.Sc. Thesis*, Luleå University of Technology, Luleå, 2008
32. Lj. Čerović, G. Lefèvre, A. Jaubertie, M. Fédoroff, S. Milonjić, *J. Colloid Interface Sci*. **330** (2009) 284
33. B. D. Bowen, N. Epstein, *J. Colloid Interface Sci.* **206** (1998) 314
34. S. Al-Zuhair, K. B. Ramachandran, M. Hasan, *Biochem. Eng. J.* **19** (2004) 81
35. S. Al-Zuhair, K. B. Ramachandran, M. Hasan, *Process Biochem. (Oxford, U.K.)* **38** (2003) 1155
36. A. E. Wiacek, *Powder Technol.* **212** (2011) 332
37. M. C. Pimentel, A. B. Leao, E. H. Melo, W. M. Ledingham, J. L. Lima Filho, M. Sivewright, J. F. Kennedy, *Artif. Cells, Blood Substituents Immobilization Biotechnol*. **35** (2007) 221
38. M. Michele, D. Urioste, L. T. Andrade Souya, A. A. Mendes, H. F. De Castro, *Enzyme Res.* (2011) 216435
39. S. C. Wu, Y. K. Li, *J. Mol. Catal., B* **54** (2008) 103.

Journal of the Serbian Chemical Society
JSCS-info@shd.org.rs • www.shd.org.rs/JSCS
J. Serb. Chem. Soc. 80 (9) 1127–1137 (2015)
JSCS–4785
UDC 504.53.054:577.15–188:577.153+
66.094.258:544.032.4
Original scientific paper

Temperature dependent effect of difenoconazole on enzymatic activity from soil

MARIOARA NICOLETA FILIMON[1,2], SORIN OCTAVIAN VOIA[3]*, DIANA LARISA VLADOIU[1,2], ADRIANA ISVORAN[1,2] and VASILE OSTAFE[1,2]

[1]*West University of Timişoara, Faculty of Chemistry–Biology–Geography, Department of Biology–Chemistry, Pestalozzi, 16, Timisoara, 300115, Romania,* [2]*West University of Timisoara, Laboratory of Advanced Research in Environmental Protection, Oituz 4, Timisoara 300086, Romania,* [3]*Banat's University of Agricultural Sciences and Veterinary Medicine, Faculty of Animal Science and Biotechnologies, Calea Aradului, 119, Timisoara, 300645, Romania*

(Received 18 December 2014, revised 24 March, accepted 25 March 2015)

Abstract: The purpose of this study was to quantify the effect of difenoconazole (DFC) on the activity of a few enzymes commonly found in soil: dehydrogenase, urease, phosphatase and protease. Three experimental variants were established: under field conditions with variable temperature (10–21 °C, variants A1–A3), under laboratory conditions with constant temperature (30 °C, variants B1–B3) and untreated soil (C variant). The commercial product "Score 250EC" with 250 g DFC L^{-1} was used at the following concentrations: 0.037 mg DFC g^{-1} soil (variants A1 and B1), 0.075 mg DFC g^{-1} soil (variants A2 and B2) and 0.150 mg DFC g^{-1} soil (variants A3 and B3). The dehydrogenase, phosphatase and urease activities decreased significantly ($p < 0.05$) under both field (variants A1–A3) and laboratory (variants B1–B3) conditions compared to untreated soil (variant C). The protease activity was reduced in variants A1––A3 compared to variant C and increased at the dose of 0.150 mg DFC g^{-1} soil in the variant B3.

Keywords: fungicide; soil; dehydrogenase; phosphatase; urease; protease.

INTRODUCTION

Widespread and intense application of a large number of fungicides for controlling fungal pathogens of crops promotes high productivity in the modern agriculture. The fungicides used to inhibit the growth and developments of pathogenic fungi of crops have a negative effect on soil quality through quantitative and qualitative changes in the communities of microorganisms.[1–3]

* Corresponding author. E-mail: voia@animalsci-tm.ro
doi: 10.2298/JSC141218030F

Soil microorganisms produce a variety of exo-enzymes: ureases, invertases, dehydrogenases, cellulases, amylases, phosphatases, proteases, *etc*. Enzyme activity can be used as a biomarker of soil fertility and an indicator of many biological processes manifested in the soil.[4] Fungicides applied directly to plants were also found in the soil.[5,6] Literature data concerning the effects of fungicides on soil reveal stimulation or inhibition of enzyme activities depending on the fungicide dose, incubation temperature and time of application,[7,8] and the inorganic and organic matter content of soil, the soil type, soil tillage, content of heavy metals and other environmental factors.[9–11]

The fungicides captan and trifloxystrobin applied for a short-term did not affect the phosphorous cycle in soil, but their application in large doses caused inhibition of enzymes involved in the nitrogen cycle.[12] Chen and Edwards[13] emphasized the toxic effect of benomyl, captan and chlorothalonil upon the microorganisms from soil and on the nitrogen cycle: reduction of fungi and nitrifying bacteria populations and inhibition of several enzyme found in soil (nitrogenase, dehydrogenase, cellulase, phosphatase urease and protease). Other fungicides, such as propiconazole and chlorothalonil, applied in the recommended doses to crops did not show inhibitory effects on urease and protease activities from soil.[14]

Published data concerning the effect of difenoconazole on communities of microorganisms in soil and on enzyme activities showed different aspects. Thus, depending on the soil type, short term application of difenoconazole had an inhibitory effect on microbial activity in unfertilized soils, but not in fertilized soils.[15] Another study concerning the effects of difenoconazole on the activity of microorganism community in soil based on enzymatic activities (urease, arylsulfatase, β-glucosidase, alkaline phosphatase and dehydrogenase) was conducted under laboratory conditions using different concentrations of fungicide. It reflected dose dependent effects of difenoconazole on the microbial population of the soil.[16]

The purpose of this study was to determine the effects of different doses of difenoconazole on soil quality during 21 days of contact with the fungicide, based on enzymatic activities (dehydrogenase, urease, phosphatase, protease), under variable (10–30 °C, in experimental fields) and constant (30 °C, in laboratory conditions) temperatures. To the best of our knowledge, this is the first study comparing the effects of difenoconazole upon some enzymes from soil at variable temperatures and a constant temperature, *i.e.*, under field and laboratory conditions.

EXPERIMENTAL

Materials

Difenoconazole (DFC, 1-[[2-[2-chloro-4-(4-chlorophenoxy)phenyl]-4-methyl-1,3-doxolan-2-yl]methyl]-1*H*-1,2,4-triazole) is a fungicide that inhibits sterol demethylation and is widely used against Ascomycetes, Basidiomycetes and Deuteromycetes. The experiments

were performed using a product sold on a local market under the trade name "Score 250 EC", that contains 250 g L^{-1} DFC.

Soil sampling

The soil samples were collected from an experimental field located nearby Timisoara city, in an area where insecticides, fungicides, herbicides or chemical fertilizers were never used. Chernozem soil samples were collected from the top layer of soil (0–20 cm) from five different spots in quantities varying between 1 and 2 kg. The material was ground, sieved (2 mm) and spooned by random sampling, giving sub-samples of 20 g per polyethylene bag. The samples were preserved in a refrigerator and processed as soon as possible during the following 30 days.

Treatment of soil samples with fungicide

Three doses of DFC were prepared using distilled water: half dose HD – 0.037 mg DFC g^{-1} soil, normal dose ND – 0.075 mg DFC g^{-1} soil and double dose DD – 0.150 mg DFC g^{-1} soil. The three DFC doses were prepared in distilled water and then applied to the soil samples to obtain 40 % humidity. The plastic bags containing the samples were homogenized on a rotary homogenizer for 2 h in order to achieve a uniform distribution in the sample.[17]

The following variants were obtained: Variant A with three sub-variants depending on the DFC concentration (A1 – HD, A2 – ND and A3 – DD), with soil pH 6.20, storage for 21 days under field conditions, at 10–21 °C (mean temperature 17.19 °C); Variant B (B1 – HD, B2 – ND and B3 – DD), with soil pH 6.44, incubated for 21 days at 30 °C (laboratory conditions); Variant C was untreated soil, with a soil pH of 6.14.

Biochemical analyses

The following enzymatic activities were assayed: dehydrogenase, urease, acid phosphatase and protease. The enzymatic activities were determined using a T90 UV/Vis spectrophotometer (PG Instruments, UK).

The dehydrogenase activity (*DA*) was measured using 2,3,5-triphenyltetrazolium chloride (TTC) as substrate, monitoring the reaction product (triphenylformazane, TPF) at 485 nm. The reaction mixture containing 3 g soil sample, 0.5 mL of 3% solution of TTC, 1.2 mL Tris buffer (0.1 M, pH 7.6) was kept at 37 °C for 48 h. TPF was extracted with 20 mL acetone and the absorbance of the supernatant was measured at 485 nm. The *DA* is expressed as mg TPF g^{-1} soil during 48 h.[18]

The urease activity (*UA*) was determined in accordance with the method described by Alef and Nannipieri.[19] The reaction mixture consisted of 3 g soil, 5 mL phosphate buffer (0.6 M, pH 6.8) and 2 mL toluene. After homogenization (2 min on vortex), 5 mL 3 % urea was added and the mixture was vortexed for a further 2 min. Finally, the reaction mixture was incubated at 37 °C for 24 h. In the collected supernatant, the quantity of produced NH_4^+ was determined using Nessler's reagent. The absorbance was measured at 445 nm and the *UA* is expressed as mg NH_4^+ g^{-1} soil during 24 h.

The phosphatase activity (*PhA*) was estimated measuring the phenol resulting from the hydrolytic separation of phenyl phosphate into disodium phosphate and phenol catalyzed by phosphomonoesterases. For each sample, about 3 g of soil were mixed into a test tube with 10 mL of 0.5 % phenyl phosphate and incubated for 48 h at 37 °C. Next, 50 mL of 0.3 % ammonium aluminum sulfate were added to each test tube and the mixture was then filtered through ash-free filter paper. From each test tube, 1 mL filtrate was transferred to an empty test tube together with 5 mL borax solution (0.1 M, pH 9.4). The mixture was brought to a

volume of 25 mL with distilled water and the absorbance was measured at 597 nm. *PhA* was defined[20] as mg phenol g^{-1} soil during 48 h.

The protease activity (*PA*) was estimated by reaction of ninhydrin with the amino acids resulting from the hydrolysis of gelatin used as substrate. For each sample, about 3 g soil was mixed with 7 mL of 2 % gelatin and 0.5 mL toluene. The mixture was homogenized (2 min on vortex) and incubated at 37 °C for 24 h. Next, 25 mL of distilled water was added and the mixture was filtered through ash-free filter paper. From each test tube, 2 mL of filtrate was transferred to an empty test tube together with 5 mL of 0.2 % ninhydrin solution and the absorbance was measured at 578 nm. The *PA* was defined[20] as mg amino-N g^{-1} soil during 24 h.

Statistical data interpretation

Statistical analysis of the recorded data was performed using variance analysis and the software MINITAB 17.[21] All data are presented as average values with standard deviation (*X*±*SD*). In order to establish the correlation coefficient, the Spearman test was used. Significant differences in variables were tested using Mann–Whitney at the 0.05 level of probability.

RESULTS AND DISCUSSIONS

The enzymatic activities *DA*, *UA*, *PhA* and *PA* were assayed in 6 experimental variants during 21 days. The results revealed increases of enzymatic activities for some enzymes and decreases for other during the monitoring period, in relation with the incubation temperature and DFC concentration.

The average values and standard deviations for *DA* during the 21 days of experiment were determined (Fig. 1). The recorded values ranged between 0.462±0.375 mg TPF g^{-1} soil in 48 h (variant B3) and 1.734±0.601 mg TPF g^{-1} soil in48 h (variant A1). As the values of *DA* obtained in the soil samples containing DFC were lower than that registered for the control soil sample (5.847±0.501 mg TPF g^{-1} soil in 48 h), it could be concluded that DFC had a toxic effect on the respiration process of microorganisms from soil. The higher was the DFC concentration, the higher was the percent of reduction of *DA* in the soil samples. For example, in variant B3, the *DA* activity was decreased with 90.16 % in comparison with the control sample (variant C).

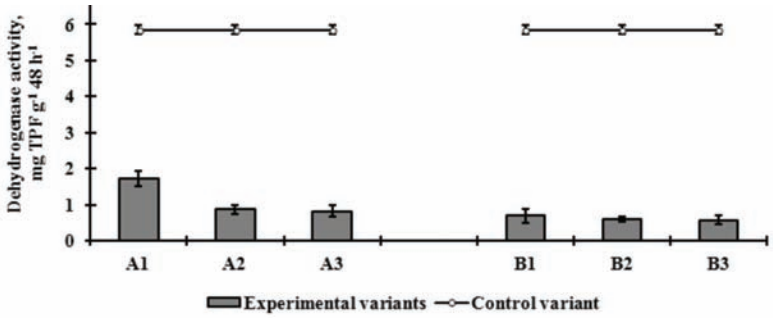

Fig. 1. Average values of the dehydrogenase activity in the soil samples.

The decrease of *DA* for the experimental variants A and B during the 21 days of the monitoring was roughly linear with the increase of the concentration of DFC. There are significant differences between variant A and B, during the 21 days of experiment ($p < 0.05$).

Among all the enzymatic activities assayed, *DA* was the most sensitive to the variation of the DFC concentration in the soil samples. *DA* is considered as an ecotoxicological test for an estimation of the toxicant effects on soil microorganisms as *DA* reflects the intensity of the respiration processes of these germs.[22]

The results of the present study were in good agreement with other published data. The studies conducted by Muñoz-Leoz *et al.*[23] revealed that small concentrations of DFC cannot show a clear effect on *DA*, but high concentrations of DFC applied on soil lead to significant decreases in the *DA*. Srinivasulu and Rangaswamy[24] reported inhibition of *DA* of soil microorganisms due to the treatment of soil with high doses of metalaxyl and mancozeb during a period of 35 days. There are reports mentioning that at low doses some fungicides increase *DA* when applied to soil,[7,25] but when large doses were applied, the *DA* of the soil microorganisms was reduced.[26,27]

Beside the concentration of DFC, other factors may also affect the enzymatic activities of soil microorganisms. There are reports mentioning that the water content from soil and the temperature influence the *DA* indirectly by interfering with the redox status of the soil.[28] In the present study under field conditions (variant A), *DA* presented a negative correlation with temperature ($r = –0.243$).

The values of urease activity (*UA*) registered during the 21 days of the monitoring ranged between 318.127±16.124 mg NH_4^+ g^{-1} soil in 24 h (variant A2)[1] and 169.502±27.980 mg NH_4^+ g^{-1} soil in 24 h^{-1} (variant A3). The average values of *UA* are presented in Fig. 2.

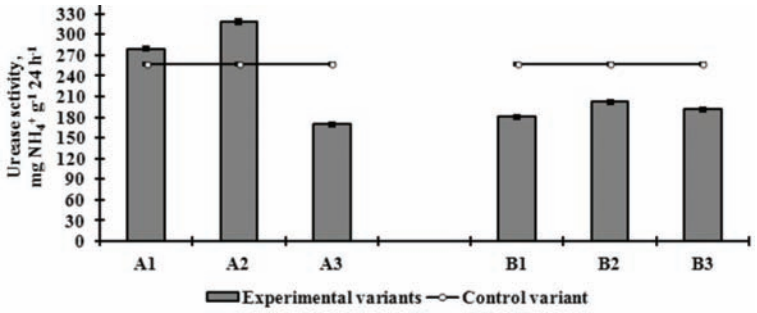

Fig. 2 Average values of the urease activity in the soil samples.

The highest values of *UA* were obtained in variants A1 and A2, an indication of the possible utilization of DFC as a carbon and nitrogen source by some microorganisms from the soil, at temperatures varying between 10 and 21 °C. Using

DFC as a substrate determines urease activity growth. Thus, the values of UA obtained in variants A1 and A2 were higher with 23.23 and 61.92 mg NH_4^+ g^{-1} soil than the value of UA in the control soil (256.204±11.971 mg NH_4^+ g^{-1} soil in 24 h).

Nevertheless, at high concentrations of DFC in the soil, the *UA* decreased significantly ($p < 0.05$): by 33.84 % in variant A3 and by 29.63 % in variant B3, in comparison to the value of *UA* in the untreated soil. Based on the differences of the values of *UA* in variant A and variant B during the 21-day period of monitoring, it could be concluded that temperature has a significant impact on the influence of DFC on the *UA* of microorganisms from the treated soil.

Other chemicals, such as profenofos, deltamethrin and thiram, seemed to increase *UA* in soil at low concentrations and to reduce it when applied at high doses.[29] At high concentrations, pyrimorph reduces significantly the *UA*.[7] Qian *et al*.[30] hypothesized that validamycin may be toxic for some species as several enzymatic activities were reduced, but the obtained higher values of *UA* and *PhA* may indicate the possible use of validamycin as a carbon source by some species of microorganisms. The biomass of the microbes that can use validamycin as a carbon source increased until this source was exhausted, subsequently, the number of microorganisms from the soil would return to the normal level. As the reduction of the *UA* by captan and trifloxystrobin can be as high as 70 % of that of control untreated soil, it was assumed that these chemicals could modify the nitrogen cycle in the soil. This kind of modification has to be considered as repeated applications of fungicides could lead to their accumulation in the treated soil.

As the negative effects on the populations of microorganism are stronger at high concentrations of DFC in soil, the importance of the optimal dose of fungicide that should be applied on soil becomes more obvious. The potential non-target side effects of pesticides against microbial communities from soil and the reduced rates of degradation of these chemicals should be considered principally when repeated treatment of soil is performed.[23]

As for the *DA*, the *UA* of organisms from soil treated with DFC was influenced by factors other than the DFC concentration. The correlation between *UA* and temperature (range 10–21 °C, variant A) was positive, although with a moderately low value for the correlation coefficient ($r = +0.439$). Similar studies confirmed a small increase in *UA* at moderate temperatures.[25] The time a pesticide acted on the microorganisms also affected the *UA* of germs from treated soils.[29]

The values of phosphatase activity (*PhA*) registered during the 21 days of the experiments ranged between 2.427±0.753 (variant A3) and 4.004±1.516 mg phenol g^{-1} soil in 48 h (variant B3). DFC applied on soil caused a reduction of the *PhA* of microorganisms, as all the values of the *PhA* from the experimental variants were lower than the *PhA* found in the control untreated soil (4.828±

±0.751 mg phenol g^{-1} soil in 48 h). For variant A, the decrease in *PhA* correlated almost linearly with the increase in the DFC concentration ($p < 0.05$). The average values of *PhA* are presented in Fig. 3.

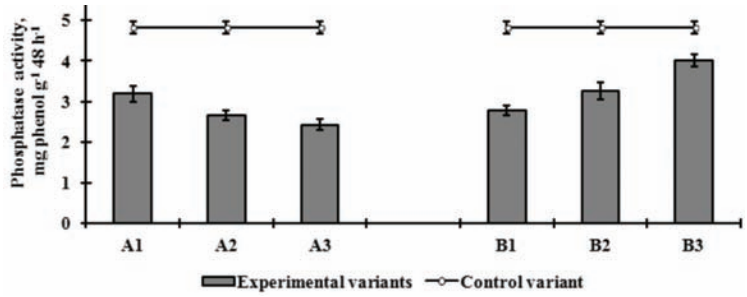

Fig. 3. Average values of the phosphatase activity in the soil samples.

In comparison to the control sample, the lowest value of *PhA* (49.73 %) was obtained for variant A3, when the highest DFC dose was used and the temperature ranged between 10–21 °C. The lower temperature (average = 17.19 °C) and higher dose of DFC provided the conditions for a significant decrease in the *PhA* of the microorganisms from the treated soil.

Under laboratory conditions at high and constant incubation temperature (30 °C), the *PhA* from variant B1 (the lowest applied concentration of DFC) decreased by 42.56 % compared with the control sample. In variant B3 (the highest concentration of DFC), although the *PhA* decreased, the extent of diminution was smaller.

Phosphatases are the enzymes responsible for releasing of orthophosphoric acid from organic combinations with metaphosphates and pyrophosphate. In soil ecosystems, phosphatases play a critical role in the phosphate cycle, being good indicators of soil fertility.[31] When phosphate is deficient in the soil, the amount of acidic phosphatase released by plant roots is increased to augment the solubilization and remobilization of phosphate, influencing the resistance of plants to stress conditions.[32,33]

In the short term, the phosphate cycle was not influenced by moderate doses of captan and trifloxystrobin applied on the soil.[12] In small concentrations, validamycin did not influence significantly *PhA* during the incubation period, but at high doses, an increase (29.8 %) of acidic *PhA* was observed.[30] For variant A (field conditions), a weak positive correlation ($r = +0.147$) between the variation of temperature and *PhA* was detected.

The values for the protease activity (*PA*) recorded during the 21 days of the experiments ranged between 5.948±3.843 (variant A3) and 19.824±7.354 mg amino-N g^{-1} soil in 24 h (variant B3). In comparison with the control, untreated soil (13.289±1.751 mg amino-N g^{-1} soil in 24 h), almost all other samples pre-

sented lower values for *PA*. The only exception was observed in variant B3, when the *PA* increased by 40.24 % comparing with the control sample. The most important decrease was observed in variant A3, when the *PA* was reduced by 56.98 %. The average values of *PA* are shown in Fig. 4.

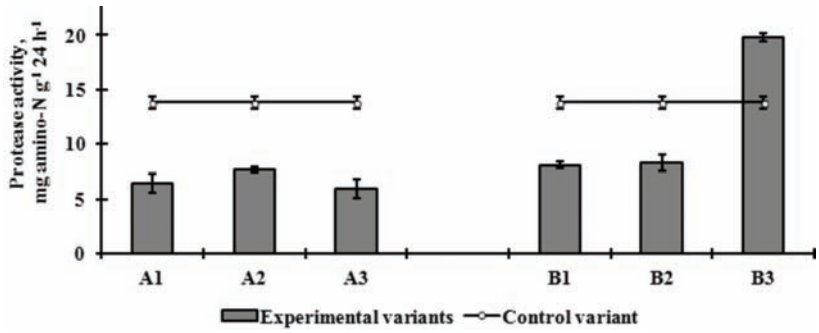

Fig. 4. Average values of the protease activity in the soil samples.

The values of *PA* obtained for variants A have similar values for all concentrations of DFC applied to the soil, but when the soil was incubated at a high temperature (variant B), there was a significant increase of *PA* at the highest dose of DFC. The fact that between variant A and B there was a difference of 5.38 mg amino-N g^{-1} soil during the 21 days of the experiments, this could be considered as evidence for the influence of temperature on the *PA*. A constant incubation temperature of 30 °C seems to stimulate an increase of *PA*, perhaps by stimulating the overall metabolism. Under field conditions, the variation of temperature had a negative influence on *PA* ($r = –0.170$).

Proteases play an important role in the nitrogen cycle in soil, performing the hydrolysis of large peptides with production of amino acids and small peptides.[34] Fungicides, such as chlorothalonil and propiconazol, have a positive influence on urease and protease activities of soil microorganisms at low and moderate doses. Application of these chemicals in the recommended doses does not influence the metabolism of soil germs.[14] At high doses, chlorothalonil produces a reduction of *PA*, in comparison with untreated soil.[35] Similar results were obtained in case of mancozeb[10] and carbendazim.[36]

The increase in temperature has had a significant influence on the metabolic reactions of organisms from soil by promoting the development of communities of microorganisms resistant to DFC and supporting the use of the fungicide as a source of carbon and nitrogen. At high doses of DFC, these positive effects are overcome by the inhibition of the metabolism of organisms present in soil. As similar results were obtained in the case of other fungicides, it may be concluded that most of these types of chemicals at high and repeated doses may produce an inhibition of the metabolism of communities of microorganisms present in soil.[7]

The present study confirms that soil enzymes behave differently when exposed to DFC that can stimulate or inhibit some enzymatic activities depending on the dose and temperature. Several factors may influence the enzyme activity besides the concentration of DFC, such as temperature and time of exposure to the toxicant. The degree of absorbency of fungicide in soil could reduce the contact time between some pesticides and microorganisms. Biodegradation seems to be the most important mechanism for reduction the concentration of DFC in soil. At least at low doses, the microorganisms from soil can degrade chemicals from soil, including pesticides, progressively reducing their toxicity. Some degradation products may act as growth factors for certain microorganisms in the soil. Although the assay of the activities of enzymes from soil could be considered a good indication of soil quality and health, the levels of enzymes activities cannot be correlated with the quantities of pesticides in soil.

CONCLUSIONS

The results indicated that DFC inhibited the enzymatic activities of dehydrogenase, urease, phosphatase and protease in the treated soil samples. Depending on the dose of DFC and incubation temperature, with rare exceptions, the recorded values of enzymatic activities were significantly lower ($p < 0.05$) than those in untreated soil. Above average increases were recorded for soil with urease at HD and ND of DFC applied to the soil sample and variable temperature (variants A1 and A2) and for protease at DD of DFC at constant temperature (variant B3). It could be concluded that the metabolism of the communities of microorganisms from DFC treated soil was affected by the DFC dose and incubation temperature.

Acknowledgments. This work was supported by a grant of the Romanian Ministry of Education, CNCS-UEFISCDI, Project No. PN-II-RU-PD-2012-3-0220, "Metabolization of difenoconazole by crop plants and fungi communities from soil".

ИЗВОД

УТИЦАЈ ДИФЕНОКОНАЗОЛА НА АКТИВНОСТ ЕНЗИМА ИЗ ЗЕМЉИШТА

MARIOARA NICOLETA FILIMON[1,2], SORIN OCTAVIAN VOIA[3], DIANA LARISA VLADOIU[1,2], ADRIANA ISVORAN[1,2] и VASILE OSTAFE[1,2]

[1]West University of Timişoara, Faculty of Chemistry–Biology–Geography, Department of Biology–Chemistry, Timisoara, [2]West University of Timisoara, Laboratory of Advanced Research in Environmental Protection, Timisoara, [3]Banat University of Agricultural Sciences and Veterinary Medicine, Faculty of Animal Science and Biotechnology, Timisoara, Romania

Циљ овог рада је био да се квантификује ефекат фунгицида дифеноконазола (DFC) на активности ензима (дехидрогеназе, уреазе, фосфатазе и протеазе), који се налазе у земљишту. Успостављене су три експерименталне варијанте: у теренским условима са променљивом температуром (10–21 °C, варијанте А1–А3), у лабораторијским условима са константном температуром (30 °C, варијанте Б1–Б3) и контролна варијанта (нетретирано земљиште, Ц). Комерцијални производ „Score 250 EC" *са*. 250 g L^{-1} DFC је коришћен у следећим концентрацијама: 0,037 mg g^{-1} DFC/маса земљишта (променљиве

А1 и Б1), 0,075 mg g^{-1} (променљиве А2 и Б2) и 0,150 mg g^{-1} (променљиве А3 и Б3). Активности дехидрогеназе, фосфатазе и уреазе су биле значајно смањене у теренским и лабораторијским условима применом DFC ($p < 0,05$) у односу на нетретиране узорке. Протеазна активност је била смањена у варијантама А1–А3 у односу на варијанту Ц, а повећала се у варијанти Б3, када је примењена доза DFC 0,150 mg g^{-1} земљишта.

(Примљено 18. децембра 2014, ревидирано 24. марта, прихваћено 25. марта 2015)

REFERENCES

1. A. Monkiedje, M. O. Ilori, M. Spiteller, *Soil Biol. Biochem*. **34** (2002) 1939
2. R. M. Niemi, I. Heiskanen, J. H. Ahtiainen, A. Rahkonen, K. Mäntykoski, L. Welling, P. Laitinen, P. Ruuttunen, *Appl. Soil Ecol*. **41** (2009) 293
3. M. Cycon, Z. Piotrowska-Seget, J. Kozdroj, *Int. Biodeter. Biodegr*. **64** (2010) 316
4. C. Garbisu, I. Alkorta, L. Epelde, *Appl. Soil Ecol*. **49** (2011) 1
5. Z. H. Wang, T. Yang, D. M. Qin, G. Yong, J. Ying, *Chin. Chem. Lett.* **19** (2008) 969
6. A. Bermúdez-Couso, M. Arias-Estévez, J. C. Nóvoa-Muñoz, E. López-Periago, B. Soto-González, J. Simal-Gándara, *Water Res.* **41** (2007) 4515
7. D. Xiong, Z. Gao, B. Fu, H. Sun, S. Tian, Y. Xiao, Z. Qin, *Eur. J. Soil Biol.* **56** (2013) 44
8. H. Guo, G. F. Chen, Z. P. Lu, H. Zhao, H. Yang, *J. Environ. Sci*. **21** (2008) 494
9. M. Srinivasulu, G. J. Mohiddin, M. Madakka, V. Rangaswamy, *Asian J Microbiol. Biotech. Env. Sci.* **12** (2010) 141
10. N. Rasool, Z. A. Reshi, *Trop. Ecol. India* **51** (2010) 199
11. Z. Yang, S. Liu, D. Zheng, S. Feng, *J. Environ. Sci*. **18** (2006) 1135
12. A. M. Wightwick, S. M. Reichman, N. W. Menzies, G. Allinson, *Water Air Soil Pollut.* **224** (2013) 1703
13. S. K. Chen, C. A. Edwards, *Soil Biol. Biochem.* **33** (2001) 1981
14. A. C. Ramudu, M. Srinivasulu, G. Jaffer Mohiddin, V. Rangaswamy, *Int. J. Environ. Protection*, **2** (2012) 23
15. B. Muñoz-Leoz, C. Garbisu, I. Antigüedad, E. Ruiz-Romera, *Soil Biol. Biochem*. **48 (**2012) 125
16. M. Madakka, M. Srinivasulu, G. J. Mohiddin, V. Rangaswamy, *Dyn. Soil Dyn. Plant* **5** (2011) 75
17. R. M. Atlas, D. Parmer, R. Partha, *Soil Biol. Biochem.* **10** (1978) 231
18. F. Schinner, R. Öhlinger, E. Kandeler, R. Margesin, *Methods in Soil Biology*, Springer, Berlin, 1996, p. 241
19. K. Alef, P. Nannipieri, *Methods in Applied Soil Microbiology and Biochemistry*, Academic Press, London, 1995, p. 316
20. M. Dragan-Bularda, *Microbiologie generala-Lucrari practice*, Editura Universitatii Babes-Bolyai, Cluj-Napoca, 2000, pp. 178–180, 189–191 (in Romanian)
21. Softonic, http://en.softonic.com/s/minitab-14-free-download-full-version (accessed in Sep, 2015)
22. P. Nannipieri, E. Kandeler, P. Ruggiero, in *Enzymes in the Environment*, R. G. Burns, R. Dick, CRC Press, Marcel Dekker, New York, 2002, p. 1
23. B. Muñoz-Leoz, C. Garbisu, J.-Y. Charcosset, J. M. Sanchez-Pérez, I. Antigüedad, Estilita Ruiz-Romera, *Sci. Total Environ.* **449** (2013) 345
24. M. Srinivasulu, V. Rangaswamy, *Int. J. Environ. Sci. Technol.* **10** (2013) 341
25. D. S. Kumar, V. Ajit, *Soil Enzymology, Soil Biology*, Series 22, Springer, Berlin, 2011, p. 25
26. O. Crouzet, I. Batisson, P. Besse-Hoggan, F. Bonnemoy, C. Bardot, F. Poly, *Soil Biol. Biochem*. **42** (2010) 193

27. B. Muñoz-Leoz, Estilita Ruiz-Romera, I. Antigüedad, C. Garbisu, *Soil Biol. Biochem.* **43** (2011) 2176
28. M. Brzezinska, Z. Stepniewska, W. Stepniewski, *Soil Biol. Biochem.* **30** (1998) 1783
29. M. Madakka, G. J. Mohiddin, M. Srinivasulu, V. Rangaswamy, *Dyn. Soil Dyn. Plant* **5** (2011) 70
30. H. Qian, B. Hu, Z. Wang, X. Xu, T. Hong, *Environ. Monit. Assess.* **125** (2007) 1
31. W. A. Dick, L. Cheng, P. Wang, *Soil Biol. Biochem.* **32** (2000) 1915
32. A. S. Karthikeyan, D. K. Varadarajan, U. T. Mukatira, M. P. D'Urzo, B. Damaz, K. G. Raghothama, *Plant Physiol.* **130** (2002) 221
33. W. K. Versaw, M. J. Harrison, *Plant Cell* **14** (2002) 1751
34. P. Nannipieri, P. Sequi, P. Fusi, in *Humic substances in terrestrial ecosystems*, A. Piccolo, Ed., Elsevier, Amsterdam, 1996, p. 293
35. B. K. Singh, W. Allan, J. W. Denis, *Environ. Toxicol. Chem.* **21** (2002) 2600
36. M. Srinivasulu, G. Jaffer Mohiddin, M. Madakka, P. Vasundhara, V. Rangaswamy, *IJESDM* **1** (2010) 19.

Journal of the Serbian Chemical Society
JSCS-info@shd.org.rs • www.shd.org.rs/JSCS
J. Serb. Chem. Soc. 80 (9) 1139–1148 (2015)
JSCS–4786
UDC 546.14'11+547.81+519.677+
541.124:66.095.252.091.7:543.637
Original scientific paper

Theoretical study on the Diels–Alder reaction of bromo-substituted 2*H*-pyran-2-ones and some substituent vinyls

MINA HAGHDADI*, HAMED AMANI and NASIM NAB

Department of Chemistry, Islamic Azad University, P. O. Box 755, Babol branch, Babol, Iran

(Received 5 December 2014, revised 8 February, accepted 8 February 2015)

Abstract: A DFT study of the reactivity, regio- and stereoselectivity of Diels–Alder reactions between 3-bromo, 5-bromo, and 3,5-dibromo-2*H*-pyran-2-ones and some weakly activated and unactivated alkenes was performed using the density functional theory (DFT). Four possible reaction channels, which are related to the formation of *meta*- and *para*- and *endo*- and *exo*-cycloadducts, were explored and characterized. The energy and natural bond orbital analysis showed that the *meta*-regioselectivity on the *exo* pathway was preferred and followed an asynchronous concerted mechanism with a polar nature in all Diels–Alder cycloadditions. Moreover, the activation free energies of the Diels–Alder cycloadditions of 3,5-dibromo-2*H*-pyran-2-one were lower than those for 3-bromo-2*H*-pyran-2-one and 5-bromo-2*H*-pyran-2-one, which is in line with experimental observations. DFT-based reactivity indices clearly predicted the regiochemistry of the isolated cycloadducts.

Keywords: bromo-2*H*-pyran-2-ones; DFT study; reaction mechanism; reactivity indices; regio- and stereoselectivity.

INTRODUCTION

During investigations on the role of substituents on the cycloaddition reaction of 2*H*-pyran-2-ones, it was found that 3-bromo and 5-bromo-2*H*-pyran-2-ones are the most interesting and unique, and have useful features.[1–5] These two 2*H*-pyran-2-ones are ambident dienes[3] and react with electron-rich, electron-poor and electron-neutral dienophiles with good regio- and stereoselectivity.[4,6,7] The cycloadditions of 2*H*-pyran-2-one itself are not selective.[5] Moreover, in contrast to the bromo-pyrones, 4-chloro-2*H*-pyran-2-one, in line with 2*H*-pyran-2-one itself, is neither ambident diene nor undergoes regioselective cycloadditions.[8] It undergoes cycloadditions only with electron-deficient dienophiles that were stereoselective, but not regioselective.[3a] During the course of a study of 2*H*-

* Corresponding author. E-mail: mhaghdadi2@gmail.com
doi: 10.2298/JSC141205014H

-pyran-2-ones, Cho and co-workers investigated 3,5-dibromo-2*H*-pyran-2-one in Diels–Alder (DA) reactions with a series of electronically and sterically distinct dienophiles.[3b] Their results showed that it is a highly potent ambident diene, being more reactive and stereoselective than monobromo-2*H*-pyran-2-ones, and thus capable of generating a variety of bicycloadducts in much higher chemical yields and *endo*/*exo* rations than monobromo-2*H*-pyran-2-ones.[3]

Afarinkia and co-workers studied the Diels–Alder reactions of 3- and 5-halo--substituted 2*H*-pyran-2-ones with poor electron-rich, electron-rich and deficient dienophiles.[7–9] Their experimental results showed that these cycloadditions proceed with excellent regioselectivity and very good stereoselectivity. In contrast, the 4-halo-substituted-2*H*-pyran-2-ones reactions proceed with only moderate regio- and stereoselectivity.[9] Furthermore, their results showed that the nature of halogen substituent had only a small, sometimes negligible, influence on the cycloaddition of 2*H*-pyran-2-ones, and also, in both the 3- and 5-substituted series, the distribution of the products did not appear to be significantly different.[8] Therefore, changing the halogen substituent did not significantly change the electronic demand of the 3- and 5-halo-substituted 2*H*-pyran-2-one, although it may influence their reactivity. Furthermore, they performed a range of calculations on substituted 2*H*-pyran-2-one cyclo-additions, at the B3LYP/6-31G level of theory, to demonstrate the advantage of 3- and 5-halo-substituted 2*H*-pyran-2--ones over 4-halo-substituted 2*H*-pyran-2-ones.[8,9]

Although there are many reports about the alternative synthetic routs,[3–9] there are no theoretical investigations about the detailed molecular mechanism and electronic parameters. As a part of a program directed toward the investigation of related DA cycloadditions, herein the results of a theoretical study on the mechanism of cycloaddition reactions between 3-bromo, 5-bromo and 3,5-dibromo-2*H*-pyran-2-ones **1a**–**c**, with a range of vinyl derivatives: vinyl acetate (**2a**), vinyl benzoate (**2b**), 2-ethenyl-1*H*-isoindole-1,3(2*H*)-dione (*N*-vinylphthalimide) (**2c**) and 2-propenenitrile (**2d**), to give the bridged bicyclic lactones **3**–**13** are presented (Scheme 1). The purpose of the present study was to provide a better understanding the mechanistic features of these processes, especially by localization and characterization of all stationary points involved in these formally [2+4]cycloadditions. A density functional theory (DFT) analysis was performed to explain both the *exo*/*endo* stereocontrol and regioselectivity of these processes in order to find a possible mechanism that may explain the different reactivity observed in each case.

Although DA cycloadditions of 5-bromo and 3,5-dibromo-2*H*-pyran-2-ones with poor electron-rich dienophiles **2a**–**c** were not prepared as part of experimental studies, the calculations based on them provided a better understanding of the trends, differences, and similarities between halogen substituted 2*H*-pyran--2-ones.

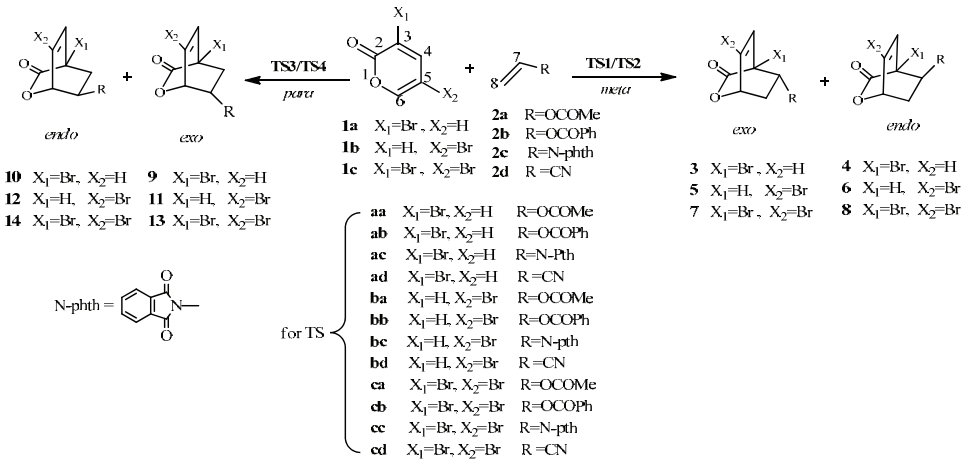

Scheme 1. The calculated possible reaction channels for the DA reaction of bromo-substituted 2*H*-pyran-2-ones **1a**–**c** with the vinyl derivatives **2a**–**d** at the B3LYP/cc-pVDZ level.

COMPUTATIONAL DETAILS

The density functional theory calculations were realized using the Gaussian 09 package.[10] The relative energies and free energies were computed at 298 K for the various stationary points at the B3LYP/cc-pVDZ level. The electronic structures of the stationary points were analyzed by the natural bond orbital (NBO) method.[11] The global reactivity indexes were estimated according to the equations recommended by Parr.[12] The global electrophilicity index, ω, is given by the following expression:[13]

$$\omega = \frac{\mu^2}{2\eta} \tag{1}$$

in terms of the electronic chemical potential, μ, and the chemical hardness, η. Both quantities may be approached in terms of the one-electron energies of the frontier molecular orbitals HOMO and LUMO, ε_H and ε_L,[14] as:

$$\mu = (\varepsilon_H + \varepsilon_L)/2 \tag{2}$$

$$\eta = \varepsilon_L - \varepsilon_H \tag{3}$$

Recently, Domingo introduced an empirical (relative) nucleophilicity index, N,[15] based on the HOMO energies obtained within the Kohn Sham scheme,[13] and defined as:

$$\varepsilon_{HOMO}(\text{Nu}) - \varepsilon_{HOMO}(\text{TCE}) \tag{4}$$

Nucleophilicity is referred to tetracyanoethylene (TCE), because it presents the lowest HOMO energy in a large series of molecules already investigated within the context of polar cycloadditions. This choice allows the convenient handling of a nucleophilicity scale of positive values. Recently, Domingo proposed two new electrophilic, P_k^+, and nucleophilic, P_k^-, Parr functions based on the atomic spin density distribution at the radical anion and cation of a neutral molecule.[16] The electrophilic, P_k^+, and nucleophilic, P_k^-, Parr functions, were obtained through the analysis of the Mulliken atomic spin density of the radical anion and cation by single-point energy calculations over the optimized neutral geometries using the

unrestricted UB3LYP formalism for radical species. The local electrophilicity indices, ω_k,[17] the local nucleophilicity indices, N_k,[198] were calculated using the following expressions:

$$\omega_k = \omega P_k^+ \quad (5)$$

$$N_k = N P_k^- \quad (6)$$

where P_k^+ and P_k^- are the electrophilic and nucleophilic Parr functions,[16] respectively.

RESULTS AND DISCUSSIONS

In the present study, the regio- and stereoselectivity of the cycloaddition reaction between bromo-substituted 2*H*-pyran-2-ones **1a**–**c** and vinyl substituents **2a**–**d** were studied, and then an analysis based on the reactivity indices of stationary points was performed.

*Study of the DA reactions of bromo-substituted 2*H*-pyran-2-ones **1a–c** with some vinyl derivatives (**2a–d**)*

Due to the asymmetry of bromo-substituted 2*H*-pyran-2-ones **1a**–**c**, four regio-isomeric channels are feasible for each of the DA reactions, *meta* and *para*, which are related to the *endo* and *exo* approach modes of the diene systems **1a**–**c** relative to the R group of the vinyl compounds **2a**–**d** (Scheme 1).

Analysis of the stationary points associated with these DA reactions indicated that they could occur *via* a one-step mechanism and consequently, four stereoisomeric TSs, named **TS1**, **TS2**, **TS3**, and **TS4**, and the corresponding products **3**–**13** were located and characterized. The activation and relative energies associated with these stationary points are given in Table I. Analysis of the geometries at the **TS** structures shows that the **TS**s of *meta* pathways correspond to asynchronous bond formation processes. The extent of bond formation along a reaction pathway is provided by the concept of bond order (BO).[19] These values are within the range of 0.180 to 0.636. These results show that for all DA reactions, **TS1** and **TS2** (*meta* pathways) are more asynchronous than **TS3** and **TS4** (*para* pathways), and that the **TSca**, **TScb** and **TScc** (for the *N*-phthalimide substituent) are the most asynchronous ones. The asynchronicity shown by the geometrical data is accounted for by the BO values.

Furthermore, the asynchronicity in bond formation at the **TS**s measured by $\Delta r = (r_2 – r_1)$ ranges from 0.72 to 1.10 at **TS1** and **TS2**, indicating that the **TS**s of *meta* process correspond to highly asynchronous bond-formation processes. Natural population analysis (NPA)[11] allowed the evaluation of the charge transfer (CT) along these DA reactions, at the TSs. Charge transfer (CT) plays a relevant role in most of organic reactions. In fact, in Diels–Alder reactions, the *CT* value is one of the most relevant characteristics of their transition states (**TS**s) and, in most cases, it is responsible of the height of their energy barrier. The calculated *CT* values for these DA reactions are given in Fig. 1. In general, the *CT* values in the **TS**s associated with the *para* pathways were lower than 0.090 e, in clear agree-

TABLE I. Activation energies, $\Delta E^{\#}$, activation free energies, $\Delta G^{\#}$, and reaction energies, ΔE_r, (all in kJ mol^{-1}), with the formation of DA cycloadducts between bromo-substituted 2*H*--pyran-2-ones **1a**–**c** and vinyl derivatives **2a**–**d** in the *meta* pathways

Entry	Species	**TS**	$\Delta E^{\#}$	$\Delta G^{\#}$	ΔE_r
1	**1a+2a→3a**-*exo*	**TS1aa**	108.48	166.33	–48.53
2	**1a+2a→4a**-*endo*	**TS2aa**	112.94	169.31	–46.22
3	**1a+2b→3b**-*exo*	**TS1ab**	112.12	168.26	–49.94
4	**1a+2b→4b**-*endo*	**TS2ab**	116.66	170.56	–45.98
5	**1a+2c→3c**-*exo*	**TS1ac**	106.75	163.59	–28.80
6	**1a+2c→4c**-*endo*	**TS2ac**	112.64	168.23	–27.73
7	**1a+2d→3d**-*exo*	**TS1ad**	117.59	171.64	–29.45
8	**1a+2d→4d**-*endo*	**TS2ad**	107.65	161.71	–33.67
9	**1b+2a→5a**-*exo*	**TS1ba**	92.82	150.75	–69.94
10	**1b+2a→6a**-*endo*	**TS2ba**	102.04	157.18	–65.45
11	**1b+2b→5b**-*exo*	**TS1bb**	98.36	154.17	–68.60
12	**1b+2b→6b**-*endo*	**TS2bb**	100.47	155.97	–66.38
13	**1b+2c→5c**-*exo*	**TS1bc**	64.58	120.92	–75.89
14	**1b+2c→6c**-*endo*	**TS2bc**	76.74	131.41	–71.40
15	**1b+2d→5d**-*exo*	**TS1bd**	108.51	162.17	–51.16
16	**1b+2d→6d**-*endo*	**TS2bd**	100.17	153.82	–54.83
17	**1c+2a→7a**-*exo*	**TS1ca**	94.23	151.39	–62.01
18	**1c+2a→8a**-*endo*	**TS2ca**	100.63	156.30	–59.89
19	**1c+2b→7b**-*exo*	**TS1cb**	98.40	153.68	–63.50
20	**1c+2b→8b**-*endo*	**TS2cb**	100.22	155.34	–59.66
21	**1c+2c→7c**-*exo*	**TS1cc**	91.26	148.47	–43.06
22	**1c+2c→8c**-*endo*	**TS2cc**	101.83	157.25	–41.22
23	**1c+2d→7d**-*exo*	**TS1cd**	106.23	160.32	–41.75
24	**1c+2d→8d**-*endo*	**TS2cd**	98.22	152.36	–45.00

ment with the non-polar character of these pathways. On the other hand, the *CT* values at the **TS**s of the DA reactions of **1a**–**c** and **2a**–**c** in the most favorable regioisomeric pathways (*meta–exo*), were between 0.205 and 0.157 e, which indicate the polar nature of the *meta* channels in these DA reactions. Only the most unfavorable DA reactions of **1a**–**c** and **2d** presented low *CT* values (lower than 0.050 e). These results with the proposal that for the DA reactions of **1a**–**c** with **2a**–**d**, an increase in the polar character as the reaction proceeds is accompanied by an acceleration of the reaction.[7–9]

The energy barrier ($\Delta E^{\#}$) and activation Gibbs free energy values ($\Delta G^{\#}$), related to the occurrence of transition states for the DA reactions of **1a**–**c** with **2a**–**d** are lower for the *meta* approaches than those for the *para* ones (Table I). The measured stereoselectivity indicated that the *meta–exo* cyclization modes are more favorable than the *meta–endo* ones, leading to the formation of *meta–exo* adducts for the DA reactions of **1a**–**c** with **2a**–**c**, while the lowest barrier energies for the DA reactions of **1a**–**c** with **2d** occur on the *meta–endo* pathway, which yields the *meta–endo* cycloadducts **4d**, **6d** and **8d**. Therefore, the presence of a cyano group

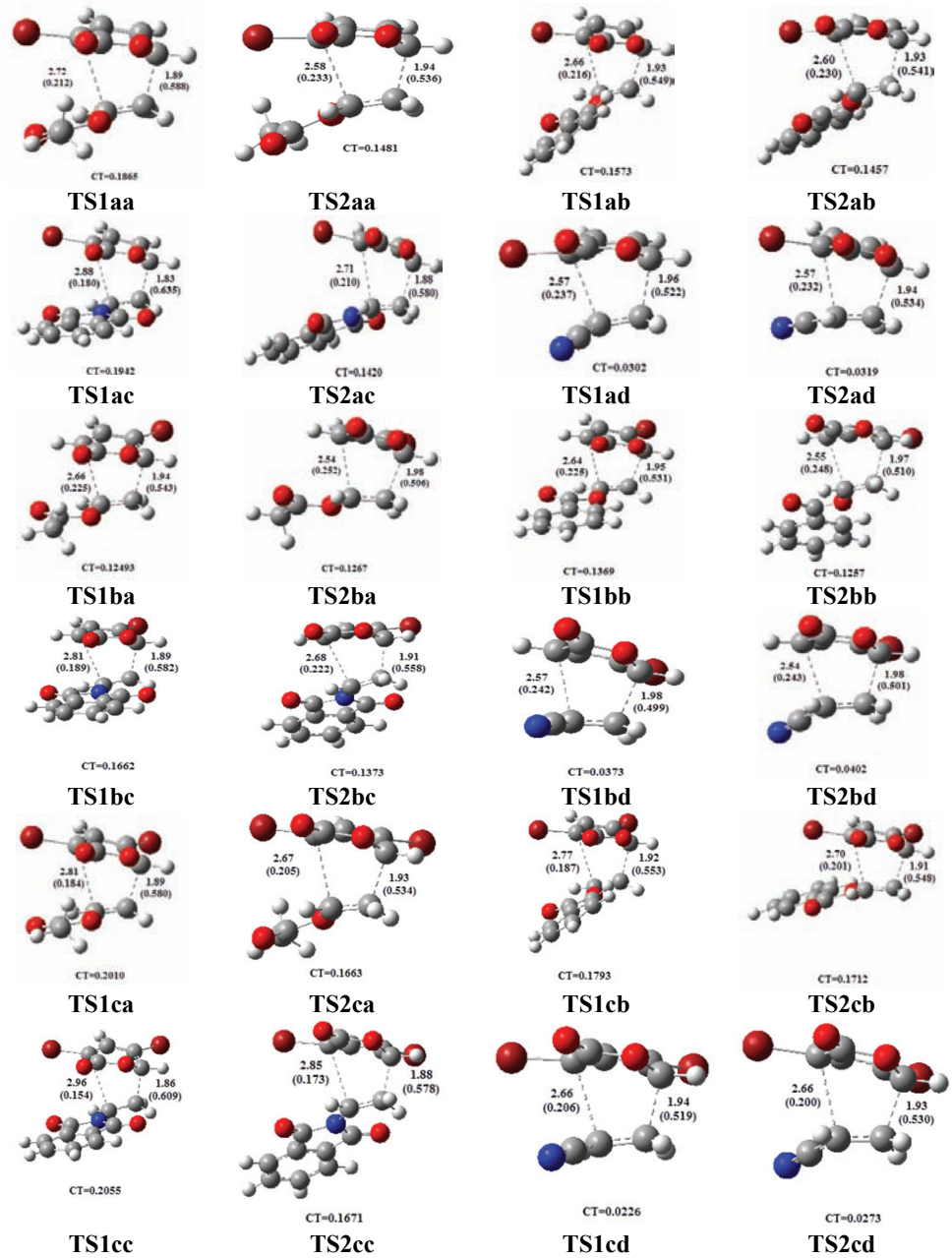

Fig. 1. Optimized geometries (B3LYP/cc-pVDZ) of the transition structures involved in the *meta* pathways of the DA reactions between the bromo-substituted 2*H*-pyran-2-ones **1a**–**c** and the vinyl derivatives **2a**–**d**. The bond distances are given in Å, the Wiberg bond indices are given in parenthesis and the natural charges (*CT*) of the **TS**s are also given.

on the dienophile, neither changes the stereoselectivity (*exo* to *endo*), nor increase the energy barriers relative to the other dienophiles.

On the other hand, the results of energy values in Table I showed that the DA reactions of **1a**–**c** with **2a** and **2b** are less stereoselective than the cycloadditions to dienophiles **2c** and **2d**. These differences in stereoselectivity could be explained as follows.

The lack of stereoselectivity in the cycloadditions of vinyl acetate **2a** presumably arises from a lack of strong secondary orbital interactions, suggesting that the cycloaddition to the weakly activated dienophile may be much more susceptible to steric interaction.[7] This was confirmed from the results of the cycloadditions of 2-ethenyl-1*H*-isoindole-1,3(2*H*)-dione (**2c**), where the reactions are highly *exo* selective. Here, the steric congestion arises directly from an unfavorable steric interaction between the second nitrogen substituent and the bromine atom in the **TS**, leading to the *endo* cycloadduct. Therefore, **TS1ac**, **TS1bc** and **TS1cc** leading to the *exo* cycloadduct are favored. This does not arise in the **TS** of *endo* cycloadduct of vinyl benzoate **2b** since the benzoate group can swing away from the bromine in the transition state. Moreover, the *endo* predomination in the cycloaddition of 2-propenenitrile (**2d**) is attributed to secondary orbital interactions and therefore it was not expected that cycloaddition to the bromo-2*H*-pyran-2-ones **1a**–**c** would give an *endo* to *exo* ratio of nearly one.

As can be seen in Table I and Scheme 1, it is possible to correlate the calculated energy of the transition state to the final yield of the cycloadducts **3**–**13**. The calculated values of all transition states confirmed that the ones likely to be the most abundant are the **3**, **5** and **7** isomers in all cases, which occurred in the DA reactions of **1a**–**c** with **2c**. The cycloadditions of **1a**–**c** with **2d** in all of reactions had the highest relative energy and it was expected to be the most disfavored cycloadduct.

The results of calculated free activation energies ($\Delta G^{\#}$) for DA reactions of 3,5-dibromo-2*H*-pyran-2-one (**1c**) with **2a**, **2b** and **2d** demonstrate the lowest activation free energy, while an increasing barrier energy has been seen for **1c** and **2c**.With considering FMO approach (Table II), broadly speaking, 3-bromo, 5-bromo and 3,5-dibromo-2*H*-pyran-2-one should undergo normal and inverse electron demand cycloadditions with dienophiles bearing weakly electron-donating (**1a**–**c**) and electron-withdrawing (**2d**) substituents, respectively.

DFT-based reactivity indices

The molecular DFT-based parameters, electronic chemical potential (μ), chemical hardness (η), global electrophilicity (ω) and global nucleophilicity (N) of the reactants **2a–d** and **1a–c** are displayed in Table II.

As can be seen in Table II, the bromo-2*H*-pyran-2-one derivatives **1a**–**c** are more electrophilic than the dienophiles **2a**–**d** and 3,5-dibromo-2*H*-pyran-2-one

(**1c**) with the highest electrophilicity (ω = 2.43 eV) being classified as a strong electrophile on the electrophilicity scale.[20] On the other hand, **1a** has a high nucleophilicity index, N = 2.52 eV, and thus is classified as a strong nucleophile on the nucleophilicity scale.[21] This ambiphilic behavior is the consequence of the presence of the enone and oxygen atom inside **1a**–**c**. The electronic chemical potential (μ) of the bromo-2*H*-pyran-2-one derivatives **1a**–**c** are lower than those of the dienophiles, **2a** (–0.134), **2b** (–0.156) and **2c** (–0.130), indicating that charge transfer along the corresponding reactions will occur from the dienophiles **2a**–**c** to the electron deficient dienes **1a**–**c**. While as expected, a CN group (**2d**) decreases the chemical potential and increases the electrophilicity toward the dienophiles **2a**–**d**, and hence, these results are in agreement with the increase in the activation energy.

TABLE II. HOMO and LUMO energies, electronic chemical potential, μ, chemical hardness, η, (all in a.u.), global electrophilicity, ω, and nucleophilicity, N (both in eV), for the reactants obtained at the B3LYP/cc-pVDZ level of theory

Species	E_{HOMO}	E_{LUMO}	μ	η	ω	N
1a	–0.24366	–0.07747	–0.160	0.166	2.09	2.52
1b	–0.24586	–0.07990	–0.162	0.166	2.15	2.40
1c	–0.24777	–0.08881	–0.168	0.158	2.43	2.41
2a	–0.25309	–0.01470	–0.134	0.238	1.02	2.27
2b	–0.25205	–0.06044	–0.156	0.192	1.71	2.29
2c	–0.24195	–0.01862	–0.130	0.223	1.03	2.57
2d	–0.26633	–0.08384	–0.178	0.182	2.28	1.90

The polar character of a cycloaddition process can be predicted using the electrophilicity difference of the reaction pair, $\Delta\omega$.[22] In this sense, the electrophilicity differences between the diene **1c** and the dienophiles **2a** and **2c** are about 1.40, indicating a large polar character for these cycloadditions, while the small $\Delta\omega$ between **1a** and **2b** (0.38 eV) and between **1b** and **2d** (0.21 eV) show a low polar character for these cycloaddition reactions. The Parr indices, local electrophilicity indices and local nucleophilicity indices for the atoms C6 and C3 of the pyrones **1a**–**c**, and C7 and C8 of the dienophiles **2a**–**d** are given in Table III (see Scheme 1 for atom numbering). The Parr functions (the electrophilic, P_k^+, and nucleophilic, P_k^-) were computed based on Mulliken atomic spin density analysis.

According the Domingo model,[15,17] along a polar cycloaddition involving asymmetric reagents, the most favorable reactive channel is that involving the initial two-center interaction between the most electrophilic center (ω_k) at the electrophile and the most nucleophilic center (N_k) at the nucleophile. According to this model, in the cycloaddition reactions of **1a–c** with dienophiles **2a–d**, the most favorable two-center interaction occurs between C6 of the dienes and C8 of

dienophiles **2a–d**, leading to the formation of the **3**–**13** regioisomers, which is in agreement with the experimental results.[7–9]

TABLE III. The Parr functions (P_k^-, P_k^+ / au), local electrophilicity indices (ω_k / eV) and local nucleophilicity (N_k / eV) indices for the C6 and C3 atoms of the pyrones **1a**–**c** and for atoms C7 and C8 of the dienophiles at the reactive sites for the reactants obtained at the B3LYP/cc-pVDZ level of theory

Species	k	P_k^-	P_k^+	N_k	ω_k
1a	C6	0.188	0.381	0.474	0.795
	C3	0.253	0.204	0.639	0.426
1b	C6	0.394	0.205	0.945	0.492
	C3	0.232	0.264	0.558	0.634
1c	C6	0.240	0.384	0.580	0.932
	C3	0.188	0.222	0.453	0.540
2a	C7	0.181	0.171	0.410	0.174
	C8	0.291	0.548	0.660	0.559
2b	C7	0.018	0.074	0.040	0.127
	C8	0.092	0.357	0.212	0.610
2c	C7	0.009	0.037	0.024	0.038
	C8	0.019	0.476	0.050	0.490
2d	C7	0.219	0.260	0.146	0.594
	C8	0.606	0.426	1.152	0.972

CONCLUSIONS

DFT computations using the B3LYP functional in conjunction with the cc-pVDZ basis set were used to analyze the outcome of the DA reactions of the bromo-2*H*-pyran-2-ones **1a**–**c** with some weakly activated and unactivated vinyls. The following conclusions could be inferred from the results of the energies:

I. The activation energies associated with the DA reaction of cyclic dienes **1a**–**c** with dienophile **2c** is more favorable than those for the reactions with **2a**, **b** and **2d**. The low reactivities of the dienophiles in these DA reactions correspond with their nucleophilic character.

II. While the DA reactions with **2a**–**c** are *exo* selective, the reaction with **2d** is *endo* selective.

III. 3,5-Dibromo-2*H*-pyran-2-one is more active than 3- and 5-bromo-2*H*--pyran-2-ones, having a lower energy barrier.

IV. These DA reactions proceed *via* a polar, regioselective and highly asynchronous process.

ИЗВОД

ТЕОРИЈСКА СТУДИЈА ДИЛС–АЛДЕРОВЕ РЕАКЦИЈЕ БРОМО-СУПСТИТУИСАНИХ 2*H*-ПИРАН-2-ОНА И НЕКИХ СУПСТИТУИСАНИХ ВИНИЛА

MINA HAGHDADI, HAMED AMANI и NASIM NAB

Department of Chemistry, Islamic Azad University, P. O. Box 755, Babol branch, Babol, Iran

Извршено је DFT испитивање реактивности, регио- и стереоселективности Дилс–Алдерове реакције између 3-бромо, 5-бромо и 3,5-дибромо-2*H*-пиран-2-она и неких слабо активираних и неактивираних алкена. Истражена су четири могућа реакциона пута, који обухватају формирање *мета*-, *пара*-, *ендо*- и *егзо*-циклоадукта. Анализа заснована на енергији и природним орбиталама показује да је преферирана *мета*-региоселективност и *егзо*-реакциони механизам.

(Примљено 5. децембра 2014, ревидирано 8. фебруара, прихваћено 8. фебруара 2015)

REFERENCES

1. K. Afarinkia, T. D. Nelson, M. V. Viader, G. H. Posner, *Tetrahedron* **48** (1992) 9111
2. B. T. Woodward, G. H. Posner, *Adv. Cycloaddit.* **5** (1999) 47
3. a) C.-G. Cho, Y.-W. Kim, Y.-K. Lim, J.-S. Park, H. Lee, S. Koo *J. Org. Chem*. **67** (2002) 290; b) C.-G. Cho, J.-S. Park, I.-H, Jung, H. Lee, *Tetrahedron Lett*. **42** (2001) 1065
4. G. H. Posner, T. D. Nelson, C. M. Kinter, K. Afarinkia, *Tetrahedron Lett.* **32** (1992) 5295
5. K. Afarinkia, G. H. Posner, *Tetrahedron Lett*. **33** (1992) 7839
6. G. H. Posner, K. Afarinkia, H. Dai, *Org. Synth.* **73** (1995) 231
7. K. Afarinkia, N. T. Daly, S. Gomez-Farnos, S. Joshi, *Tetrahedron Lett.* **83** (1997) 2369
8. K. Afarinkia, M. J. Bearpark, A. Ndibwami, *J. Org. Chem*. **70** (2005) 1122
9. K. Afarinkia, M. J. Bearpark, A. Ndibwami, *J. Org. Chem.* **68** (2003) 7158
10. Gaussian 09, Revision A, Gaussian, Inc., Wallingford, CT, 2009
11. A. E. Reed, R. B. Weinstock, F. Weinhold, *J. Chem. Phys.* **83** (1985) 735
12. R. G. Parr, R. G. Pearson, *J. Am. Chem. Soc.* **105** (1983) 7512
13. R. G. Parr, L. Von Szentpaly, S. Liu, *J. Am. Chem. Soc*. **121** (1999) 1922
14. R. G. Parr, W. Yang, *Density functional theory of atoms and molecules*, Oxford University Press, New York, 1989, p 16
15. L. R. Domingo, P. Pérez, *J. Org. Chem.* **73** (2008) 4615
16. L. R. Domingo, P. Pérez, J. A. Saez, *RSC Adv*. **3** (2013) 1486
17. L. R. Domingo, M. J. Aurell, P. Pérez, *J. Phys. Chem., A* 106 (2002) 6871
18. P. Pérez, L. R. Domingo, M. Duque-Noreña, E. Chamorro, *J. Mol. Struct.*: *THEOCHEM* **895** (2009) 86
19. K. B. Wiberg, *Tetrahedron* **24** (1968) 1083
20. L. R. Domingo, M. J. Aurell, P. Perez, R. Contreras, *Tetrahedron* **58** (2002) 4417
21. I. Kim, K. A. Hoff, E. T. Hessen, T. Haug-Warberg, H. F. Svendsen, *Chem. Eng. Sci*. **64** (2009) 2027
22. H. Chemouri, S. M. Mekelleche, *Int. J. Quantum Chem*. **112** (2012) 2294.

Journal of the Serbian Chemical Society
JSCS-info@shd.org.rs • www.shd.org.rs/JSCS
J. Serb. Chem. Soc. 80 (9) 1149–1160 (2015)
JSCS–4787
UDC 546.92+66.081+546.56+
546.47:544.35–131:544.726
Original scientific paper

Sorption recovery of platinum(II,IV) in presence of copper(II) and zinc(II) from chloride solutions

OLGA N. KONONOVA*, NATALIYA S. KARPLYAKOVA and EVGENIYA V. DUBA

Institute of Non-Ferrous Metals and Material Science, Siberian Federal University, 660041 Krasnoyarsk, Svobodny Pr., 79 Russian Federation

(Received 17 December 2014, revised 22 January, accepted 19 February 2015)

Abstract: The sorption pre-concentration of platinum(II,IV) ions was investigated in presence of accompanying copper(II) and zinc(II) ions from chloride solutions on new previously unexplored ion exchangers (Cybber, Russia). The initial concentrations of platinum and the accompanying ions were 0.25 and 2.0 mmol L^{-1}, respectively, and the acidity of medium was 0.001–4.0 mol L^{-1} HCl. It was shown that the investigated resins – strong and weak basic anion exchangers as well as chelate ion exchangers – possessed good sorption and kinetic properties. The simultaneous sorption of the investigated ions results in the complete recovery of platinum, while the non-ferrous metal ions were sorbed at less than 20 %. Followed by the selective elution of platinum by a thiourea (80 g L^{-1}) solution in 0.3 M H_2SO_4, the quantitative isolation of platinum was achieved (more than 90 %). Therefore, the studied ion exchangers could be recommended for the recovery and separation of Pt(II,IV), Cu(II) and Zn(II) ions.

Keywords: ion exchange; platinum; copper; zinc; chloride solutions.

INTRODUCTION

With growing global demand for the platinum group metals (PGM), these metals are being recovered not only from natural deposits, but also from non-traditional sources (*e.g.*, metal-bearing high-carbon complexes) and secondary sources,[1] including spent automobile and chemical catalysts, electronic scrap and the so-called tailings (wastes of ore-dressing plants at platinum-containing deposits).[1–4]

The distinctive feature of both primary and secondary PGM sources is their multicomponent composition. This means that the noble metals are contained in raw materials together with other metals, such as Ni, Zn, Cu, Co, Pb, *etc.* Moreover, the noble metals are micro components, whereas the accompanying metals

* Corresponding author. E-mail: cm2@bk.ru
doi: 10.2298/JSC141217018K

are macro components.[1,3–5] Therefore, after the breakdown of such raw materials by acids ("*aqua regia*"), chlorination, fusion, *etc*., the obtained industrial solutions have low concentrations of noble metals.[2,4–6] These solutions contain PGM complexes, varying in their stability and chemical inertness.[2,4,7–9] Moreover, it is known[2,4,7–10] that PGM complexes are affected by aquation and hydrolysis. The sophisticated composition of the solutions makes it essential to use selective methods for the isolation of the noble metals.

As a rule, the PGM are isolated from such solutions by precipitation or electrowinning. However, these methods basically do not provide a high degree of recovery, and the solid products formed in such cases make further processing significantly harder.[4,6,11,12] These problems could be solved by means of sorption methods, known not only for their selectivity and efficiency, but also for environmental safety and compatibility with a variety of post-determination methods.[6,11–16]

Among a variety of sorbents, ion exchangers with different functional groups are of special interest because of their high exchange capacity, osmotic and mechanical stability and good kinetic properties.[2,12,13,15,17] These characteristics allow the recovery of even trace amounts of PGM through their pre-concentration, and also the removal of interfering components. As a result, the obtained noble metals can be of high purification grades.[2,11,12,17,18]

The selectivity of the ion exchangers is a matter of great importance, given that the ionic state of noble metals in solutions is distinguished by a variety of complex forms with different stabilities and kinetic inertness, and the solutions themselves are multicomponent systems. The selectivity could be improved through the complex-forming properties of ion exchangers.[17]

Previously, the recovery of platinum (II,IV) from chloride solutions on Purolite ion exchangers was investigated.[19] Since the recovery of platinum in the presence of accompanying components is a matter of practical interest, the present work is focused on the simultaneous recovery of Pt(II,IV), Cu(II) and Zn(II) because these ions are often contained in real solutions obtained after breakdown of platinum-containing raw materials.[2–6] It should also be noted that these non-ferrous metals are valuable materials and are the subject of industrial recycling.

The sorption recovery of copper(II) and zinc on Purolite ion exchangers were also studied.[20] For the present investigation, new, previously unexplored cybber ion exchangers made in Russia were used.

EXPERIMENTAL

The Cybber ion exchangers, produced by $SYNTEZ_{NVK}$ Company, St. Petersburg, Russia, were taken for investigation. Their physicochemical characteristics are summarized in Table I. It could be seen from the data that anion exchangers, chelate resins and strong acidic cation exchangers were used to study copper and zinc sorption. Before use, the resins were

prepared according to standard methods and loaded by 2 M HCl, to convert them into the Cl^- form (anion exchangers) or H^+ form (cation exchanger and chelate sorbents).

TABLE I. Physicochemical characteristics of the investigated macroporous ion exchangers Cybber. Resin matrix: styrene (St) – divinylbenzene (DVB); Functionalization: QAB – quaternary ammonia base, TAG – tertiary amino-groups; AMPA – aminomethyl-phosphonic acid; IDAA – iminodiacetic acid; SG – sulfo-groups

Trade name	Exchanger type	Functional group	Exchange capacity, mmol g^{-1}, in the form:		Swelling grade, %	Moisture %	Working pH range
			Cl^-	H^+			
AX 400	Strong base anion exchanger	QAB	1.20	–	19	44	0–14
ALX 220	Weak base anion exchanger	TAG	1.45	–	21	50	0–8
CRX 300	Chelating resin	AMPA	–	1.80	23	40	1–14
CRX 210	Chelating resin	IDAA	–	1.10	21	55	1–6
EV 023	Strong acid cation exchanger	SG	–	1.80	17	45	0–14

The initial platinum stock solution of concentration 9.669 mmol·L^{-1} was prepared by dissolution of an accurately weighed quantity H_2PtCl_6 in concentrated hydrochloric acid, with the subsequent dilution of the solution to 500 mL with distilled water. The working platinum solutions with concentration 0.25 mmol L^{-1} and acidity 0.001–4.0 M HCl were prepared from this initial solution. In the present work, only freshly prepared platinum solutions were used.

The solutions of copper(II) and zinc(II) of concentration 2.0 mmol L^{-1} were prepared from accurately weighed quantities of $CuCl_2{\cdot}2H_2O$ and $ZnCl_2$, respectively, which were dissolved in hydrochloric acid solutions of different concentrations (0.001–4.0 mol L^{-1}). All the reagents were of analytical purification grade.

The initial concentrations of the studied ions were selected with the aim of making the experiments similar to the real industrial conditions, *i.e.* to the technical solutions obtained after the processing of secondary materials.[2,5,18] The acidity range of initial solutions was intentionally wide, to study the sorption properties of the investigated resins.

The concentrations of platinum and non-ferrous metal ions were determined by spectrophotometrical methods, *i.e.*, platinum with $SnCl_2{\cdot}2H_2O$,[7,9] and copper(II) and zinc(II) with PAR (4-(2-pyridylazo)resorcinol)[21,22] using a Specol 1300 spectrophotometer (Carl Zeiss, Germany).

The sorption of the investigated ions was realized under batch experimental conditions. The equilibrium time determined by special tests was 24 h.

The efficiency of sorption recovery of the ions investigated was estimated by means of the recovery degree, R / %, and the distribution coefficient, D.

Moreover, the separation coefficients S of the recovered metal ions were calculated as follows:

$$S = \frac{K_{Me_1}}{K_{Me_2}} \quad (1)$$

where K_{Me_1} is the distribution coefficient of platinum (or copper) and K_{Me_2} is the distribution coefficient of copper (or zinc).

The sorption isotherms were plotted by varying the molar ratio of resins to the amount of metal ions in the contacting solution.[23,24] The apparent constants of the ion exchange equilibrium were calculated based on these isotherms according to the law of mass action for the investigated equilibria.[23,24]

The kinetic behavior of ion exchangers investigated during sorption of the metal ions was studied by the "limited bath" method.[23,25] After a certain time, the resins and solutions were quickly separated by filtration through a porous glass filter. Then the concentrations of platinum, copper and zinc were determined in the solutions by the spectrophotometrical methods. Using the obtained results, the degree of saturation F was calculated as follows:

$$F = \frac{Q_t}{Q_\infty} \quad (2)$$

where Q_t and Q_∞, mmol, are the amounts of the metal ion sorbed at time t and at equilibrium, respectively.

Then the kinetic curves were plotted as dependences $F = f(t)$ and the half-exchange times, $t_{1/2}$ / s, were determined from these curves at $F = 0.5$. Subsequently, the diffusion coefficients of metal ions in a resin grain, $\bar{D}_S$ / cm^2 s^{-1}, were calculated from the following equation:

$$\bar{D}_S = \frac{r^2}{4\pi^2 t_{1/2}} \quad (3)$$

where r / cm is the radius of the resin grain.

Moreover, the process rate, v / mmol g^{-1} s^{-1}, was calculated using the formula:

$$v = \frac{a_i}{t_i} \quad (4)$$

where a_i / mmol g^{-1} is the quantity of metal ion sorbed by the resin at time t_i / s.

All the results were subjected to statistical processing according to conventional procedures.[26,27] The average experimental error for 3–4 parallel runs was less than 6 %.

The details regarding the batch and kinetic experiments, as well as the sorption preconcentration and recovery data, are given in the Supplementary material to this paper.

RESULTS AND DISCUSSION

The ionic state of platinum in chloride solutions was investigated in detail.[2,4,7–10] The electron absorption spectrum of a freshly prepared platinum (II,IV) solution in 2 M HCl, which had two absorption maxims at 218 and 251 nm, was recorded This spectrum is in full compliance with literary data and corresponds to the presence of complexes $[PtCl_4]^{2-}$ (218 nm) and $[PtCl_6]^{2-}$ (251 nm).[2,9,10]

The ionic states of copper(II) and zinc(II) in chloride solutions were previously investigated in detail[21,22] and are described in a previous work.[20] There-

fore, the initial investigated solution contained different chloride complexes of the studied ions, and their subsequent sorption on the ion exchangers depended on the form of their complex compounds.

Since the Cybber ion exchangers were investigated for the first time, the sorption recovery of platinum (II,IV), copper(II) and zinc ions were initially studied from their individual solutions of different acidities.

These studies revealed that the studied anion exchangers and chelate sorbents exhibited high affinity for platinum (II,IV) ions, with no dependence on the acidity of medium. As for copper (II) and zinc (II) recovery under the same conditions, the results correlated with their ionic state in the solutions. Thus, the anion exchangers and chelate resins recovered copper(II) ions only from the strong acidic solutions, indicating the sorption of copper anionic chloride complexes. Copper was only recovered from the 0.001–0.1 mol L^{-1} HCl solutions by the strong acidic cation exchanger EV 023, meaning that cationic copper complexes are present in these solutions. It should be noted that the ion exchangers in a strong acidic medium exhibited high affinities for copper(II) ions.

Moreover, only the chelate ion exchanger Cybber CRX 300 recovered zinc ions over the whole range of investigated HCl concentrations. The other resins did not sorb Zn(II) from strong acidic solutions, although it is known from the literary data that negatively charged complexes $[ZnCl_4]^{2-}$ are present in such solutions. This was also supported by the fact that the cation exchanger EV 023 did not recover zinc ions from 2–4 M HCl solutions. This phenomenon is of academic interest and will be the subject of further investigations. However, the fact that copper(II) and zinc(II) ions could be recovered in different ways and from different media provides the opportunity to separate these ions by varying the HCl concentration in the contacting solution.

Based on this, the simultaneous recovery of copper and zinc from strong and weak acidic media was further investigated. The results are presented in Table II. It can be seen from these data that the presence of zinc did not affect copper(II) sorption, which means that copper is not recovered from weakly acidic solutions by the investigated resins. As for the sorption of zinc in presence of Cu(II), in this case they were recovered from strong acidic solutions, and at a quite satisfactory level (86–89 %). No doubt, it could be considered the effect of synergy, *i.e.*, the increase in sorption ability of ion exchanger to an ion that was not sorbed (or poorly sorbed) from individual solutions in the presence of another ion.[28–30] Therefore, the simultaneous action of both components has an effect on the sorption ability of the ion exchangers. The data in Table II also show that the studied sorbents were more selective towards copper(II) ions than to zinc ions.

The separation coefficients of non-ferrous metal ions during their recovery from 2 M HCl solution are shown in Table III. It can be seen that all the values exceed 1 and, therefore, copper and zinc could be completely separated.

TABLE II. Simultaneous recovery of copper(II) and zinc(II) from chloride solutions of different acidity on the investigated ion exchangers (c_0(Cu) = c_0(Zn) = 2.0 mmol L^{-1})

Trade name	Parameter	Recovery of:			
		Cu(II) in presence of Zn(II) at c_0(HCl) / mol L^{-1}		Zn(II) in presence of Cu(II) at c_0(HCl) / mol L^{-1}	
		2.0	0.01	2.0	0.01
AX 400	R / %	≈100	–	86±4	89±5
	log D	5.08±0.31	–	3.78±0.23	3.89±0.23
ALX 220	R / %	≈100	–	86±4	89±5
	log D	4.79±0.29	–	3.79±0.23	3.91±0.23
CRX 300	R / %	≈100	–	88±4	88±5
	log D	5.11±0.31	–	3.85±0.23	3.86±0.23
CRX 210	R / %	≈100	–	87±4	87±4
	log D	4.99±0.29	–	3.82±0.23	3.81±0.22

TABLE III. Separation coefficients of Cu and Zn during their sorption from strong acidic chloride solutions (c_0(HCl) = 2.0 mol L^{-1}; c_0(Cu) = c_0(Zn) = 2.0 mmol L^{-1})

Trade name	Separation coefficient	Trade name	Separation coefficient
AX 400	20	CRX 300	18
ALX 220	10	CRX 210	13

Furthermore, the sorption pre-concentration of platinum (II,IV) in the presence of copper(II) and zinc(II) was studied from strong acidic chloride solutions, given that under industrial conditions, the noble metals are mostly present in strong acidic media after the breakdown. The results are summarized in Table IV, from which it could be seen that the presence of copper and zinc ions in the system had no effect on the sorption pre-concentration of platinum, and hence, it could be completely recovered from the solution by the investigated sorbents. Simultaneously, the copper ions and, especially, the zinc ions were sorbed at low levels (not more than 20 % for Cu and 16 % for Zn). These data clearly illustrate the distinct selectivity of ion exchangers towards noble metal complexes. On the one hand, this could be explained by the fact that complexes with greater stability are "preferable" for the resins during sorption from multicomponent solutions.[31] As the stability of platinum chloride complexes is much higher than those of copper and zinc,[8] the sorption centers of the resin are preoccupied by platinum complexes.

However, on the other hand, it is known[17,32,33] that complex-forming sorbents that contain nitrogen or sulfur atoms in their functional groups show especially high selectivity towards noble metal ions. From the investigated range of sorbents, the weak basic anion exchanger ALX 220 and chelate resin CRX 210 belong to this group. It is important that CRX 210 contains iminodiacetic acid as functional groups, *i.e.* two carboxylic groups. The Lewis theory of acids and bases states that platinum ions are "soft" acids, and possess lower affinity to oxy-

gen donor atoms,[8,34] which explains the lower degree of recovery of platinum on the chelate resin CRX 210 in comparison with that on ALX 220. The strong basic anion exchanger AX 400 with quaternary ammonia bases as functional groups has a high selectivity to platinum ions, due to the strong electrostatic interaction between these large-sized and practically not hydrated groups and the aquatic complex ions of the noble metal.[31]

TABLE IV. Sorption pre-concentration of platinum(II,IV) from strong acidic chloride solutions in the presence of copper(II) and zinc(II) on the investigated ion exchangers (c_0(HCl) = 2.0 mol L^{-1}; c_0(Pt) = 0.25 mmol L^{-1}; c_0(Cu) = c_0(Zn) = 2.0 mmol L^{-1})

Trade name	Parameter	Recovery of:		
		Pt(II,IV) in the presence of Cu(II) and Zn(II)	Cu(II) in the presence of Pt(II,IV) and Zn(II)	Zn(II) in presence of Pt(II,IV) and Cu(II)
AX 400	R / %	95±5	14±1	10±1
	log D	4.43±0.27	2.30±0.14	2.01±0.12
ALX 220	R / %	95±5	20±2	16±2
	log D	4.45±0.27	2.48±0.15	2.32±0.14
CRX 210	R / %	77±4	12±1	7±1
	log D	3.53±0.21	2.04±0.12	1.97±0.12

The separation coefficients of platinum and the accompanying metals were calculated and the results are given in Table V. The values were much greater than 1, indicating the possibility of isolation of platinum from the non-ferrous metal ions.

TABLE V. Separation coefficients of Pt and non-ferrous metal ions during their sorption from strong acidic chloride solutions (c_0(HCl) = 2.0 mol L^{-1}; c_0(Pt) = 0.25 mmol L^{-1}; c_0(Cu) = c_0(Zn) = 2.0 mmol L^{-1})

Trade name	Separation coefficients of Pt(II,IV) towards:	
	Cu (II)	Zn (II)
AX 400	137	273
ALX 220	91	137
CRX 210	34	34

Thus, the obtained data led to the conclusion that the sorption pre-concentration of platinum(II,IV) proceeded on the strong basic anion exchanger according to the anion exchange mechanism:

$$2\overline{RCl} + [PtCl_n]^{2-} \leftrightarrow \overline{R_2[PtCl_n]} + 2Cl^- \quad (5)$$

The weak basic anion exchanger sorbed platinum ions not only through anion exchange, but also through additional complexation between the metal ions and the nitrogen atoms of the functional groups:

$$\overline{\mathrm{RN}} + [\mathrm{PtCl}_n]^{2-} \leftrightarrow \left[\overline{\mathrm{RNPtCl}_{n-1}}\right] + \mathrm{Cl}^- \qquad (6)$$

where $n = 4$ or 6.

The chelate ion exchanger CRX 210 recovered platinum(II,IV) ions according to the complex-formation mechanism:

$$[\mathrm{PtCl}_n]^{2-} + m\overline{\mathrm{RL}} \cdots \mathrm{S} \leftrightarrow (\mathrm{PtCl}_{n-m}\overline{\mathrm{RL}_m})^{2-(n-m)-zm} + m\mathrm{L} + m\mathrm{S} \qquad (7)$$

where $n = 4$ or 6; m is the number of functional groups o the resin RL with the charge z; S is the dissolvent.

The sorption isotherms of platinum in presence of accompanying copper and zinc ions are shown in Fig. 1 for the strong and weak basic anion exchangers. It can be seen that the curves are convex, *i.e.*, the anion exchangers are selective towards Pt(II,IV) ions.[23,24] Based on the isotherms, the apparent constants of the ion exchange equilibrium were 3.0 and 2.4 for ALX 220 and AX 400, respectively. These values correlate with the selectivity of the sorbents.

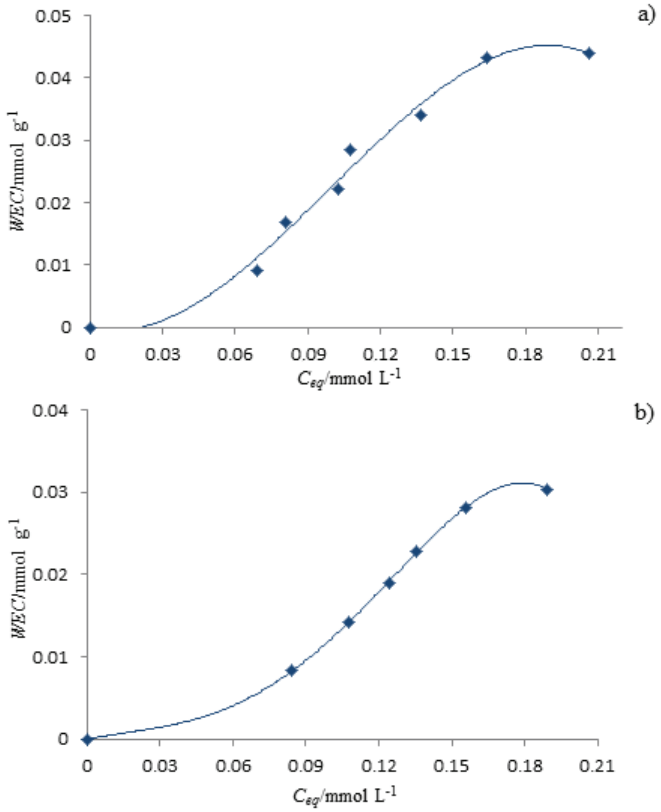

Fig. 1. Isotherms of platinum sorption in presence of copper(II) and zinc(II) from strong acidic solutions onto: a) ALX 220 and b) AX 400; c_0(HCl) = 2.0 mol L^{-1}.

Furthermore, the kinetic properties of ion exchangers during the recovery of platinum(II,IV) ions in presence of copper(II) and zinc(II) were investigated. The dependences of the process rate on time are presented in Fig. 2. It could be seen that the process rate increased sharply at the beginning of ion exchange and then decreased gradually before reaching equilibrium.

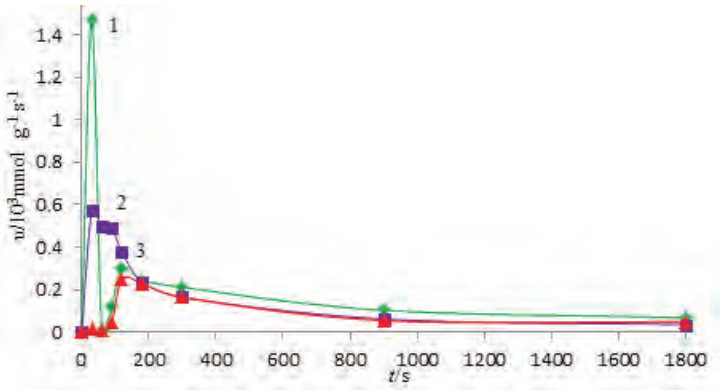

Fig. 2. Dependences of process rate on time during sorption pre-concentration of platinum(II,IV) in presence of copper(II) and zinc(II) on the investigated ion exchangers; c_0(HCl) = 2.0 mol L^{-1}; c_0(Pt) = 0.25 mmol L^{-1}; c_0(Cu) = c_0(Zn) = 2.0 mmol L^{-1}; ◆ (1) – ALX 220; ■ (2) – AX 400; ▲ (3) – CRX 210.

The calculated main kinetic parameters for sorption pre-concentration of Pt(II,IV) in the presence of the accompanying ions are summarized in Table VI. According to the data, it proceeds coherently, with high process rate. The other kinetic parameters – half-exchange time and diffusion coefficients – correlate with the previously discussed data on selectivity.

TABLE VI. Kinetic parameters during sorption pre-concentration of platinum(II,IV) in the presence of copper(II) and zinc(II) from strong acidic chloride solutions on the investigated ion exchangers (c_0(HCl) = 2.0 mol L^{-1}; c_0(Pt) = 0.25 mmol L^{-1}; c_0(Cu) = c_0(Zn) = 2.0 mmol L^{-1}); $\bar{v}$ is the average process rate

Trade name	Kinetic parameter		
	$t_{1/2}$ / s	$\bar{D}_S \times 10^7$ / cm^2 s^{-1}	$\bar{v} \times 10^5$ / mmol g^{-1} s^{-1}
AX 400	7200	1.1	1.8
ALX 220	1800	4.6	1.9
CRX 210	2700	2.3	0.7

Finally, the desorption of platinum from the ion exchangers was investigated. As the amount of accompanying non-ferrous metal ions was no higher than 20 % (Table IV), after the sorption pre-concentration of platinum, it was enough to wash the ion exchangers with 0.5 M HNO_3 once for their complete removal. Then, the elution of platinum by thiourea solution (80 g L^{-1}) in 0.3 M

H_2SO_4 was performed, given that acidic thiourea solutions are conventional desorption agents for noble metals.[2,9] As a result, 93 % of the platinum was eluted from the resin AX 400, and 90 % of the platinum – from ALX 220. Therefore, the anion exchangers CYBBER AX 400 and ALX 220 could be recommended for the recovery of platinum(II,IV) ions and their quantitative separation from accompanying copper(II) and zinc ions.

CONCLUSIONS

Sorption recovery of platinum(II,IV) in the presence of copper(II) and zinc(II) ions from chloride solutions on new CYBBER ion exchangers produced in Russia was investigated. Since these resins were studied for the first time, their sorption properties were investigated during recovery of each component from its individual solutions over a wide range of HCl concentrations (0.001–4.0 mol L^{-1}). High affinities of the ion exchangers for platinum(II,IV) complexes were revealed. However, copper(II) ions were sorbed only from strong acidic solutions, while zinc ions, only from weak acidic media.

An investigation of the simultaneous recovery of Cu(II) and Zn(II) from weak and strong acidic chloride solutions showed that zinc ions were sorbed at a high level in the presence of copper(II) from both weak and strong acidic media. This phenomenon was the result of synergy.

A study of sorption pre-concentration of platinum(II,IV) in the presence of copper(II) and zinc(II) has revealed the high selectivity of the investigated ion exchangers towards the noble metal ions, whereas the non-ferrous metal ions were recovered to no more than 20 %.

The investigation of kinetic properties of the resins revealed high rate of ion exchange process during Pt(II,IV) recovery in the presence of the accompanying ions. The main kinetic parameters, *i.e.*, half-exchange time and diffusion coefficients in the resin grain, correlated with the previously found selectivity of the sorbents.

The elution of the investigated components from the resins after sorption was realized using 0.5 M HNO_3 (for copper and zinc) and thiourea solution (80 g L^{-1}) in 0.3 M H_2SO_4 (for platinum). As a result, the quantitative isolation and separation of the ions was achieved.

The obtained results allowed the recommendation of the anion exchangers CYBBER AX 400 and ALX 220 for sorption pre-concentration of platinum(II,IV) in presence of accompanying Cu(II) and Zn(II) ions from strong acidic chloride solutions and for the subsequent isolation of the noble metal by selective elution.

SUPPLEMENTARY MATERIAL

Details of the batch and kinetic experiments, considerations about the ionic states of the metal in chloride solutions and sorption pre-concentration and recovery data, Tables S-I–S-III,

are available electronically from http://www.shd.org.rs/JSCS/, or from the corresponding author on request.

Acknowledgements. The authors express deep gratitude to the $SYNTEZ_{NVK}$ Company (St. Petersburg, Russia) for the resin samples kindly provided for investigation.

ИЗВОД

СОРПЦИОНО ИЗДВАЈАЊЕ ПЛАТИНЕ(II,IV) У ПРИСУСТВУ БАКРА (II) И ЦИНКА (II) ИЗ ХЛОРИДНИХ РАСТВОРА

OLGA N. KONONOVA, NATALIYA S. KARPLYAKOVA и EVGENIYA V. DUBA

Institute of Non-Ferrous Metals and Material Science, Siberian Federal University, 660041 Krasnoyarsk, Svobodny Pr., 79 Russian Federation

Концентровање јона платине (II,IV) сорпцијом је испитивано у присуству пратећих јона бакра (II) и цинка (II) из хлоридних раствора на новим јоно-измењивачима Cybber (Русија), који до сада нису испитивани. Почетна концентрација платине и пратећих јона је била 0,25 и 2,0 mmol L^{-1}, редом, а киселост средине је била 0,001–4,0 mol L^{-1} HCl. Показано је да испитиване смоле – јаки и слаби базни анјонски измењивачи као и измењивачи хелатних јона – имају добре сорпционе и кинетичке особине. Истовременом сорпцијом испитиваних јона платина је потпуно издвојена, док су јони бакра и цинка сорбовани мање од 20 %. Након тога, селективним издвајањем платине раствором тиоурее (80 g L^{-1}) у 0,3 M H_2SO_4, постигнута је квантитативна изолација платине (више од 90 %). На основу добијених резултата може се закључити да се испитивани јоно-измењивачи могу користити за одвајање јона Pt(II,IV), Cu(II) и Zn(II).

(Примљено 17. децембра 2014, ревидирано 22. јануара, прихваћено 19. фебруара 2015)

REFERENCES

1. Anon, *Novel, non-traditional sources of platinum group metals,* http://www.ural-gold.ru/pt_innova.html (accessed 01.07.2010)
2. Y. A. Zolotov, G. M. Varshal, V. M. Ivanov, *Analytical Chemistry of Platinum Group Metals,* Editorial URSS, Moscow, 2003, p. 592
3. G. V. Semenchenko, A. S. Mukusheva, L. L. Osipovskaya, *Direct leaching of noble metals from refractory ores of Kazakhstan's deposits*, *Proceedings of the 2nd International Congress "Non-Ferrous Metals in Siberia"*, Krasnoyarsk, 2010, p. 288
4. T. M. Buslaeva, *Chemistry and Technology of Platinum Group Metals*, Nauka, Moscow, 1999, p. 251
5. Y. A. Kotlyar, M. A. Meretukov, L. S. Strizhko, *Metallurgy of Noble Metals*, MISIS, Moscow, 2005, p. 392
6. O. V. Spektor, A. L. Ryumin, M. G. Pochekutova, *Tsvetnye Metally* **7** (1998) 31
7. F. E. Beamish, *The Analytical Chemistry of the Noble Metals*, Pergamon Press, Oxford, 1966, p. 702
8. F. A. Cotton, C. Wilkinson, *Advanced Inorganic Chemistry. A Comprehensive Text*, Wiley, New York, 1969, p. 582
9. S. I. Ginzburg, V. I. Ezerskaya, I. V. Prokofieva, Y. I. Shlenskaya, N. K. Belskiy, *Analytical Chemistry of Platinum Group Metals,* Nauka, Moscow, 1975, p. 615
10. N. M. Sinitsyn, T. M. Buslaeva, *Chemistry of Complex Halides of Platinum Group Metals,* A. O. Rosvuznauka, Ed., Moscow, 1992, p. 79
11. F. I. Bernardis, R. A. Grant, D. C. Sherrington, *React. Funct. Polym.* **65** (2005) 205

12. A. A. Blokhin, N. D. Abovskiy, Y. V. Murashkin, M. A. Mikhaylenko, in *Proceedings of the 1st International Congress "Non-Ferrous Metals of Siberia",* Krasnoyarsk, Russia, 2009, p. 587
13. E. R. Els, I. Lorenzen, C. Aldrich, *Miner. Eng.* **13** (2000) 401
14. V. I. Bogdanov, L. D. Gorbatova, S. V. Grokhovskiy, *Tsvetnye Metally* **9**–**10** (2001) 33
15. P. Liu, G.-F. Liu, D.-I. Chen, S.-Y. Cheng, N. Tang, *Transact. Nonferrous Metals Soc.China* **19** (2009) 1509
16. S. I. Pechenyuk, *Vestnik Kol'skogo Nauchnogo Zentra RAN* **2** (2013) 64
17. G. Friss,. in *Proceedings of the 1st International Congress "Non-Ferrous Metals of Siberia",* Krasnoyarsk, Russia, 2009, p. 578
18. A. A. Palant, O. M. Levchyuk, V. A. Bryukvin, *Tsvetnye Metally* **5** (2012) 38
19. O. N. Kononova, A. M. Melnikov, T. V. Borisova, A. S. Krylov, *Hydrometallurgy* **105** (2011) 341
20. O. N. Kononova, M. A. Kuznetsova, A. M. Mel'nikov, N. S. Karplyakova, Y. S. Kononov, *J. Serb. Chem. Soc.* **79** (2014) 1037
21. V. P. Zhivopistsev, V. A. Seleznyova, *Analytical Chemistry of Zinc,* Nauka, Moscow, 1975, p. 44
22. V. I. Podchanova, L. N. Simonova, *Analytical Chemistry of Copper,* Nauka, Moscow, 1990, p. 62
23. F. Helfferich, *Ion Exchange,* McGraw Hill, New York, USA, 1962, p. 481
24. Y. A. Kokotov, V. A. Pasechnik, *Ion Exchange Equilibrium and Kinetics of Ion Exchange,* Khimiya, Leningrad, 1979, p. 374
25. F. Helfferich, *Ion Exchange Kinetics*, In *Ion Exchange. A Series of Advances,* J. A. Marinsky, Ed., McGraw Hill, Buffalo, NY, 1966, p. 281
26. D. C. Harris, *Quantitative Chemical Analysis,* W. H. Freeman Co., New York, 2007, p. 51
27. J. H. Pollard, *Handbook of Numerical and Statistical Techniques,* Cambridge University Press, Cambridge, 1977, p. 374
28. A. P. Rao, S. P. Dubey, *Anal. Chem.* **44** (1972) 686
29. A. Girija, R. K. Sunivasan, *Rasayan J. Chem.* **6** (2013) 212
30. Y. N. Kim, M. Choi, *Environ. Sci. Technol.* **48** (2014) 7503
31. R. M. Diamond, D. C. Whitney, in *Ion Exchange. A Series of Advances,* J. A. Marinsky, Ed., McGraw Hill, Buffalo, NY, 1966, p. 174
32. K. M. Saldadze, V. D. Kopylova-Valova, *Complex-Forming Ion Exchangers,* Nauka, Moscow, 1980, p. 562
33. R. Hering, *Chelatbildende Ionenaustauscher,* Akademie-Verlag, Berlin, GDR, 1967, p. 268
34. H. Remy, *Lehrbuch der Anorganischen Chemie,* Akademische Verlags Gesellschaft Geest & Portig K.-G., Leipzig, GDR, 1960, p. 1074.

Journal of the Serbian Chemical Society
JSCS@tmf.bg.ac.rs • www.shd.org.rs/JSCS
J. Serb. Chem. Soc. 80 (9) S292–S294 (2015) *Supplementary material*

SUPPLEMENTARY MATERIAL TO

Sorption recovery of platinum(II, IV) in the presence of copper(II) and zinc(II) from chloride solutions

OLGA N. KONONOVA*, NATALIYA S. KARPLYAKOVA and EVGENIYA V. DUBA

Institute of Non-Ferrous Metals and Material Science, Siberian Federal University, 660041 Krasnoyarsk, Svobodny Pr., 79 Russian Federation

J. Serb. Chem. Soc. 80 (9) (2015) 1149–1160

BATCH EXPERIMENTS

The sorption of the investigated ions was performed under batch experiment conditions: resin mass, 0.1–0.2 g; volume of contacting solution, 10.0–20.0 mL; stirring in a thermostat at 20±1 °C. The equilibrium time determined by special tests was 24 h.

The efficiency of sorption recovery of the ions investigated was estimated by means of the recovery degree R / % and the distribution coefficient K, which were calculated as follows:

$$R = 100\frac{c_0 - c_{eq}}{c_0} \quad (1S)$$

$$K = \frac{WEC}{c_{eq}} \quad (2S)$$

where c_0 and c_{eq} are the initial and equilibrium molar concentrations of the metal ions, respectively; WEC / mmol g^{-1} is the working exchange capacity of the ion exchanger towards the recovered metal ions. The latter was calculated from the equation:

$$WEC = \frac{(c_0 - c_{eq})V}{m} \quad (3S)$$

where V / L is the volume of the contacting solution and m / g is the resin mass.

* Corresponding author. E-mail: cm2@bk.ru

KINETIC EXPERIMENTS

The resin quantities (0.1 g) were stirred with 10.0 mL of solution at 20±1 °C over a period from 1 min to 24 h. The saturation times were 1, 2, 3, 5, 15, 20, 30 and 45 min and 1, 2, 3, 6 and 24h. The suspensions were intensively stirred (more than 800 rev·min^{-1}). After a certain time, the resins and solutions were quickly separated by filtration through a porous glass filter. Then the concentrations of platinum, copper and zinc were determined in the solutions.

PLATINUM IONIC STATE IN CHLORIDE SOLUTIONS

It is known that the ionic state of platinum depends on the acidity of the medium, the concentration of chloride ions and the temperature. It was shown that the hexachloro-platinate (IV) complex $[PtCl_6]^{2-}$ predominates in strong acidic solutions (c(HCl) ≥ 3 mol L^{-1}). With dilution and increase in the pH value of these solutions, complexes of platinum(II) appear in the system, and co-exist in different proportions with the chloride complexes of platinum(IV). Moreover, the dilution leads to hydration and hydrolysis. This causes the formation of different aqua chloro- and aqua hydroxo-complexes of platinum(II) and platinum(IV): $[Pt(H_2O)_nCl_{4-n}]^{n-2}$, $[Pt(H_2O)_k(OH)_mCl_{4m-k}]^{k-2}$, $[Pt(OH)_nCl_{4-n}]^{2-}$, $[Pt(H_2O)_nCl_{6-n}]^{n-2}$, $[Pt(H_2O)_k(OH)_mCl_{6m-k}]^{k-2}$, $[Pt(OH)_nCl_{6-n}]^{2-}$ (where n = = 1,2; k = 1,2 and m = 1–6).

COPPER AND ZINC IONIC STATE IN CHLORIDE SOLUTIONS

The ionic states of copper and zinc were described it in a previous work.[1] It is noteworthy that, depending on acidity of the medium, both non-ferrous metal ions can form chloride complexes $[CuCl_4]^{2-}$ and $[ZnCl_4]^{2-}$ in 1–6 M HCl and $[Cu(H_2O)_6]^{2+}$, $[ZnCl_4(H_2O)_2]^{2-}$, $[Zn(H_2O)_6]^{2+}$, $[ZnCl]^-$ and $[ZnCl_2]^0$ in 0.001––0.01 M HCl. Therefore, the initial investigated solution contained different chloride complexes.

TABLE S-I. Sorption pre-concentration of platinum(II,IV) from individual chloride solutions with different acidity on the investigated ion exchangers (c_0(Pt) = 0.25 mmol L^{-1})

Trade name	Parameter	c_0(HCl) / mol L^{-1}					
		4.0	2.0	1.0	0.1	0.01	0.001
AX 400	R / %	≈100	≈100	≈100	≈100	≈100	≈100
	log D	3.13±0.19	3.52±0.21	3.60±0.22	3.51±0.18	3.33±0.21	3.17±0.19
ALX 220	R / %	≈100	≈100	≈100	≈100	≈100	≈100
	log D	3.39±0.19	3.60±0.22	3.84±0.23	3.71±0.22	3.44±0.17	3.16±0.19
CRX 300	R / %	≈100	≈100	≈100	≈100	≈100	≈100
	log D	2.48±0.15	2.87±0.17	2.84±0.14	2.63±0.16	2.58±0.13	2.42±0.15
CRX 210	R / %	≈100	≈100	≈100	≈100	≈100	≈100
	log D	2.59±0.16	2.55±0.15	2.85±0.15	3.20±0.19	3.51±0.21	3.60±0.22

TABLE S-II. Sorption recovery of copper(II) from individual chloride solutions of different acidities on the investigated ion exchangers (c_0(Cu) = 2.0 mmol L^{-1})

Trade name	Parameter	c_0(HCl) / mol L^{-1}					
		4.0	2.0	1.0	0.1	0.01	0.001
AX 400	*R* / %	94±5	93±6	94±5	–	–	–
	log *D*	4.21±0.25	4.12±0.25	4.17±0.26	–	–	–
ALX 220	*R* / %	94±5	93±5	94±5	–	–	–
	log *D*	4.24±0.25	4.15±0.24	4.18±0.25	–	–	–
CRX 300	*R* / %	94±5	93±6	93±6	–	–	–
	log *D*	4.22±0.25	4.14±0.25	4.11±0.25	–	–	–
CRX 210	*R* / %	94±5	95±5	95±5	–	–	–
	log *D*	4.23±0.25	4.28±0.26	4.24±0.25	–	–	–
EV 023	*R* / %	–	–	–	95±5	≈100	≈100
	log *D*	–	–	–	4.45±0.27	5.51±0.28	5.89±0.28

TABLE S-III. Sorption recovery of zinc (II) from individual chloride solutions of different acidities on the investigated ion exchangers (c_0(Zn) = 2.0 mmol L^{-1})

Trade name	Parameter	c_0(HCl) / mol L^{-1}					
		4.0	2.0	1.0	0.1	0.01	0.001
AX 400	*R* / %	–	–	–	86±4	92±6	94±6
	log *D*	–	–	–	4.81± 0.29	5.08 ± 0.31	5.18 ± 0.31
ALX 220	*R* / %	–	–	–	84±4	92±5	92±5
	log *D*	–	–	–	4.73± 0.28	5.08 ± 0.31	5.09 ± 0.31
CRX 300	*R* / %	90±5	89±4	89±4	89±4	95±5	95±5
	log *D*	4.96±0.29	4.89±0.29	4.88±0.29	4.89±0.29	5.26±0.32	5.34±0.32
CRX 210	*R* / %	–	–	–	84±4	90±5	92±5
	log *D*	–	–	–	4.71±0.28	4.99±0.31	5.09±0.31
EV 023	*R* / %	–	–	–	93±5	95±4	≈100
	log *D*	–	–	–	5.12±0.31	5.29±0.32	5.57±0.33

REFERENCES

1. O. N. Kononova, M. A. Kuznetsova, A. M. Mel'nikov, N. S. Karplyakova, Y. S. Kononov, *J. Serb. Chem. Soc.* **79** (2014) 1037.

Journal of the Serbian Chemical Society
JSCS-info@shd.org.rs • www.shd.org.rs/JSCS
J. Serb. Chem. Soc. 80 (9) 1161–1175 (2015)
JSCS–4788
UDC 547.475.2+543.55+544.6.076.32–033.5–039.6
Original scientific paper

Electrochemical determination of ascorbic acid at *p*-phenylenediamine film–holes modified glassy carbon electrodes

BIKILA NAGASA OLANA, SHIMELES ADDISU KITTE and TESFAYE REFERA SORETA*

Department of Chemistry, College of Natural Sciences, Jimma University, P. O. Box 378, Jimma, Ethiopia

(Received 4 November, revised 30 December 2014, accepted 19 January 2015)

Abstract: In this work, the determination of ascorbic acid (AA) at a glassy carbon electrode (GCE) modified with a perforated film produced by reduction of diazonium generated *in situ* from *p*-phenylenediamine (PD) is reported. Holes were intentionally created in the modifier film by stripping pre-deposited gold nanoparticles. The modified electrodes were electrochemically characterized using common redox probes: hydroquinone, ferrocyanide and hexaminеruthenium(III). The cyclic voltammetric and amperometric responses of AA using the modified electrodes were compared with those of a bare GCE. The bare GCE showed a linear response to AA in the concentration range of 5 mM to 45 mM with detection limit of 1.656 mM and the modified GCE showed a linear response to AA in the concentration range from 5 to 45 μM with detection limit of 0.123 μM. The effects of potential interferents on amperometric signal of AA at the modified GCE were examined and found to be minimal. The inter-electrode reproducibility, stability, and accuracy were determined. The modified electrode showed excellent inter-electrode reproducibility, accuracy and stability. The modified electrode reported is a promising candidate for use in the electro-analysis of AA.

Keywords: diazonium; *p*-phenyldiamine; gold nanoparticles; ascorbic acid; glassy carbon electrode.

INTRODUCTION

Ascorbic acid (AA) naturally occurs in a wide number of foods, such as fruits and vegetables. It is a water-soluble organic compound involved in many biological processes. It is known for its reductive properties that make it useful as an antioxidant agent in foods and drinks. Moreover, pharmaceuticals often contain AA as a supplementary source to human diets as a free-radical scavenger. It

* Corresponding author. E-mail: tesfaye.refera@ju.edu.et
doi: 10.2298/JSC141104006O

has been used for the prevention and treatment of the common cold, mental illness, scurvy and cancer.[1] However, the intake of excess AA can lead to undesirable health effects, such as gastric irritation, excessive oxidative stress, diabetes mellitus, liver disease[2] and renal problems.[3] Excessive quantities of AA in food may result in the inhibition of the occurrence of natural processes and hence may contribute to taste deterioration.[4]

AA is a labile substance that easily degrades due to interaction with enzymes and atmospheric oxygen. Excessive heat, exposure to light, and interaction with heavy metal cations can accelerate the oxidation of AA.[5] Due to its susceptibility to oxidation, the analysis of the level of AA in foodstuffs and beverages helps to indicate their quality. Hence, the level of AA has to be carefully monitored to estimate the relative variation of AA from manufacture, storage up to consumption. For this reason, there is a necessity for an easy-to-use, inexpensive method for the detection of AA in food, beverages and pharmaceuticals.[6]

Many analytical methods have been reported in the literature for the determination of AA.[7,8] Electrochemical techniques are known to offer some benefits such as fast analysis, low cost, higher sensitivity and accuracy. However, the major problem frequently encountered in the electro-analysis of AA is the effect of interferents caused by substances with similar redox potentials at conventional electrodes, which results in poor selectivity. In the presence of co-existing oxidizable species, the determined amount of vitamin C could be overestimated.[9–12] Thus, it is difficult to detect specifically one substance in the presence of others substances in real biological samples at conventional electrodes. AA exists in the anionic form at physiological pH values. Based on this property; different techniques were developed to detect AA selectively. Modification of the working electrode with modifiers such as tetrabromo-*p*-benzoquinone,[13] electronically conductive anion exchange polymers based on polypyrrole[14] and polyaniline[15] showed promising applications in the fabrication of sensors for sensitive and selective detection of AA.

The most distinguishing feature of chemically modified electrodes is their modification by a selected substance that is coated onto the electrode surface thereby imparting certain desirable properties to the electrode. The use of nanomaterials for nanostructuring of an electrode surface has aroused the interest of analysts[16] because nanostructured materials can be tailored to improve the selectivity and sensitivity of sensors. Further investigation of these new materials in the fabrication chemically modified electrodes is required to exploit the systems.

In this work, a glassy carbon working electrode was modified with electronucleated gold nanoparticles and passivated with an organic film by grafting diazonium obtained from *p*-phenylenediamine. Holes were formed on the electrodeposited film by stripping the nucleated gold nanoparticles. Improvement in the

selectivity and sensitivity of the electrode surface modified using the developed method for the determination of AA was demonstrated.

EXPERIMENTAL

Chemicals

Ascorbic acid (99 %, Finkem), *p*-phenylenediamine (100 %, Aldrich), sodium nitrite (96 %, Wardle), potassium nitrate (99 %, Nice), potassium teterachloroaurate (99.99 %, Aldrich), 2-mercaptoethanol (100 %, Aldrich), hydrochloric acid, (37 %, Riedel-de Haen), sulfuric acid, (98 %, Merck), hydroquinone (99 %, KIRAN), potassium hexacyanoferrate(III) (97 %, Labmerk Chemicals), hexamineruthenium chloride(III), (98 %, Aldrich), potassium iodide (99 %, Nice), iodine resublimed (99.5 %, Nice), potassium chloride (99 %, Finkem), sodium citrate dihydrate (99 %, Finkem), citric acid (99 %, Wardle), sodium acetate trihydrate (99.8 %, Chem. Rein), glacial acetic acid (100 %, BDH Laboratory), potassium hydrogen phosphate (98 %, Finkem) and potassium dihydrogen phosphate (99 %, Nice) were of analytical grade and used as received. The vitamin C tablet 500 mg [Batch number 11202023, Ethiopian Pharmaceuticals] was purchased from a local drug store. Double distilled water was used to prepare all solutions.

Instrumentation

Cyclic voltammetry (CV) and amperometric experiments were performed using BASi Epsilion EC-Version 1.40.67 voltammetric analyzer (Bio-analytical Systems, USA) controlled with basic epsilon software. A conventional three-electrode setup was used with a glassy carbon electrode (3 mm diameter, BASi, MF 2012) as the working electrode and a platinum wire counter electrode (BASi, MW 1032). An Ag/AgCl electrode (BASi, MF 2079) served as the reference electrode. All potentials were reported with respect to this reference electrode. For stirring the electrolytes in the cell, a small magnetic bar was used in the BASi C3 Cell stand at 500 rpm.

Methods

Electrode preparation. Prior to electrode modification, a bare glassy carbon electrode (GCE) was polished with polishing paper and then further polished to a mirror finish with alumina slurries (0.3 micron, BASi) and rinsed thoroughly with distilled water. The procedure reported by Soreta *et al.*[17] was used for electrochemical conditioning of the employed electrodes.

Fabrication of PD film–hole modified GCE. PD represents the aryldiazonium generated from *p*-phenylenediamine. Fabrication of the PD film–hole modified electrode was undertaken in several steps. The major steps were sequential electronucleation of gold nanoparticles (AuNPs) on the GCE (three rounds), grafting of a diazonium film from *p*-phenyldiamine (PD) on a GCE modified with AuNPs and stripping of the nucleated AuNPs.

i. Electrodeposition of AuNPs. Sequential electronucleation of gold nanoparticles on a GCE was performed following the procedure reported by Soreta *et al.*[18] Sequential electronucleation was used to increase the number of gold nanoparticles deposited on the GCE surface while preventing the growth of the already nucleated particles so that they remain in the nano-size range.

ii. Grafting of diazonium film generated from p*-phenylenediamine (modifier film).* The AuNPs-modified GCE was covered with *in situ* generated *p*-phenylenediamine diazonium cations based on literature information.[19,20] Briefly, 5 mL solution of 3 mmol L^{-1} *p*-phenylenediamine in 0.5 mol L^{-1} HCl and 5 mL of 3 mmol L^{-1} sodium nitrite in 0.5 mol L^{-1} HCl

were kept separately in an ice jacketed beaker for 1 h. Then, 2 mL of the $NaNO_2$ solution was added to 2 mL of the *p*-phenylenediamine solution under stirring at room temperature and CV was used to graft the phenylenediamine film onto the AuNPs nucleated GCE within potential window from 0.6 to –0.2 V at a scan rate of 0.1 V s^{-1} for 3 cycles. It was reported that an aryldiazonium film could be grafted on both carbon and gold particles surfaces.[21]

iii. Electrochemical formation of random holes on the modifier film. This is the only new step introduced in the fabrication of the modified electrode. After the modifier film had been grafted on the GCE on which gold nanoparticles were electronuclated in three rounds, the deposited AuNPs were stripped off by running three CV scans in the potential range of 0 to 1400 mV in 0.1 mol L^{-1} KCl. This step is used to create holes (could be in the nanometer diameter size) on the modifier film electrode. The size of the formed holes presumably reflected the size of the nanoparticle that was deposited on the surface of the GCE. An as such prepared modified electrode is refers to as a PD film–hole modified GCE.

Fabrication of a PD film modified GCE

This modified electrode is different from the PD film–hole modified electrode. The main difference is that gold nanoparticles were not deposited on the polished and electrochemically conditioned GCE and hence there was no AuNPs striping step. This electrode was prepared by just grafting the *in situ* prepared diazonium cation from *p*-phenylenediamine onto the bare GCE surface by running CV within a potential window from 0.6 to –0.2 V at a scan rate of 0.1 V s^{-1} for three scans.

Electrochemical characterization of the modified GCEs

The prepared modified electrodes were electrochemically characterized by CV using common redox probes: hydroquinone, hexamineruthenium chloride $Ru(NH_3)_6Cl_3$ and ferrocyanide $K_3Fe(CN)_6$. The selection of the redox probes was intentional so that hydroquinone represented molecular probes, while hexamineruthenium chloride $Ru(NH_3)_6Cl_3$ represented cationic probes and ferrocyanide $K_3Fe(CN)_6$ anionic probes in aqueous solution. The voltammetric signals of these probes at the modified GCEs were compared to the signals of those of the bare GCE.

Preparation of AA solutions

A 2 mmol L^{-1} stock solution of AA was prepared in 0.1 mol L^{-1} acetate buffer solution (pH 5) and AA solutions of other concentrations were prepared by appropriate dilution of the stock solution in acetate buffer (pH 5).

Real sample solutions, preparation and analysis

For real sample analysis, orange fruit, which was obtained from a local market in Jimma, Ethiopia, and vitamin C tablets, purchased from local drug stores in Jimma, Ethiopia, were used. Fresh orange juice was obtained by squeezing orange fruit into a glass beaker. Then, after filtering the juice through a filter paper to remove the fiber and pulp, 1 mL was diluted with 5 mL of 0.1 mol L^{-1} sodium acetate buffer (pH 5). Vitamin C tablet solution was prepared according to a literature procedure.[22] Briefly a weighed tablet was crushed with a pestle and mortar, and the powder dissolved in 20 mL of distilled water and then 10 mL of 1 mol L^{-1} H_2SO_4 was added. From this solution, 9.3 mL were taken and diluted with 20 mL sodium acetate buffer. The concentration of AA in orange fruit and vitamin C tablet was determined by standard iodimetric titration. Amperometric analysis was performed three times at 0.237 V at the PD film–hole modified GCE and average results of the three measurements were taken. Concentration of AA was determined by the standard addition method.

Study of the effect of pH on the oxidation peak current of AA

Effect of pH of the supporting electrolyte (buffer) on oxidation peak current of AA was studied within range 2 to 9. Citrate buffer of 0.1 mol L^{-1} was used to study effect of pH within the range of 2 to 4, 0.1 mol L^{-1} acetate buffer was used within range of 4.5 to 6 and 0.1 mol L^{-1} phosphate buffer of was used within the range 6 .5 to 8.5. Dilute NaOH or HCl were used to adjust the pH of the buffer solutions.

RESULTS AND DISCUSSION

Electrode fabrication

Grafting of a PD film onto a GCE. In situ generated diazonium from *p*-phenylenediamine was electrochemically grafted onto a GCE surface and the resulting film was electrochemically characterized using common redox probes. The CV of the PD film grafted onto a bare GCE is shown in Fig. 1A. A broad, irreversible cathodic peak was observed in the first cycle. In the subsequent scans, the reduction peak current decreases due to the insulation effect of the grafted surface film.

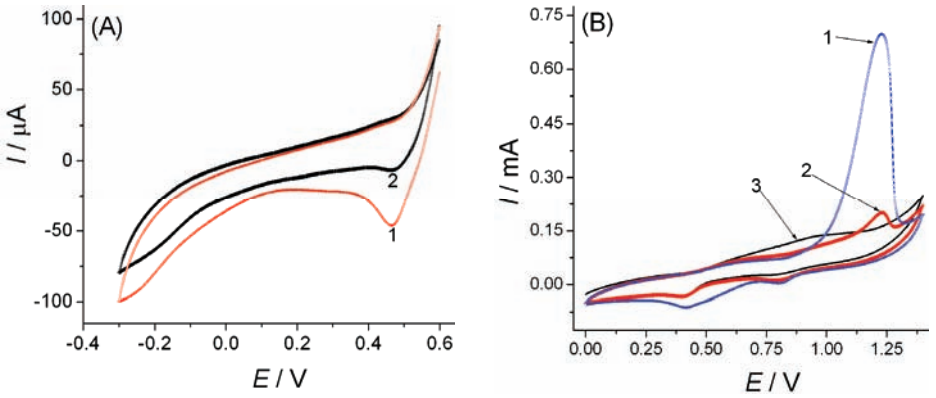

Fig. 1. A) CVs of the grafting of a diazonium film from 3 mmol L^{-1} *p*- phenylenediamine in 0.5 mol L^{-1} HCl at a bare GCE in 2 cycles (1 and 2 representing first and second cycles, respectively); B) CVs for the striping of the electronucleated gold nanoparticles from a GCE surface in 0.1 mol L^{-1} KCl in 3 cycles (1, 2 and 3 representing first, second and third cycles, respectively). In all cases, the scan rate was 100 mV s^{-1}.

Electronucleation of gold nanoparticles and stripping of the particles

Gold nanoparticles were sequentially electronucleated from a solution of 0.1 mmol L^{-1} $KAuCl_4$ in 0.5 mol L^{-1} H_2SO_4 following the procedure reported by Soreta *et al.*[18] The nucleation of gold nanoparticles was confirmed by linear a voltammetric scan from 1.4 to 0 V, when the characteristic gold oxide reduction peak appeared at 0.953 V. After three rounds of gold nanoparticles electronucleation, the electrode was passivated by electro-grafting of diazonium *in situ* generated from *p*-phenylenediamine. Pores on the modifier film were intentionally

created by stripping the deposited Au NPs by running three CV scans in the potential range of 0 to 1400 mV in 0.1 mol L^{-1} KCl (Fig. 1B). As depicted Fig. 1B, the anodic peaks at around 1.2 V, associated with gold stripping, decreased as the number of scans increases. The gold was stripped by electro-oxidation due to the presence of excess chloride that encourages the oxidation of gold to form its water-soluble chlorocomplex.

Electrochemical characterization of the modified GCEs

CV of hydroquinone (HQ). The CV of HQ at the bare GCE and at the PD film–hole modified GCE are depicted in Fig. 2, curves a and b, respectively. The anodic peak currents are comparable for the two electrodes except the peak current was slightly higher and the peak potential slightly shifted anodically at the modified electrode. When the voltammogram of hydroquinone on the PD film modified GCE (Fig. 2, curve c), was compared with the two former cases, the following differences were registered, *i.e.*, the anodic peak current was lower and shifted to a higher anodic potential. However, the modified PD–film could not prevent hydroquinone from interacting with the electrode. Hydroquinone is a molecular redox probe and diffusion of the probe towards the electrode surface was not very influenced by the surface charge of the electrodes that was developed due to the presence of modifier molecules on the GCE, *i.e.*, the modifier film does not effectively block the approach of hydroquinone to the electrode.

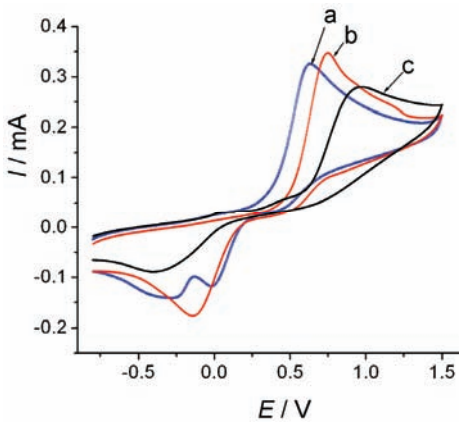

Fig. 2. CV of 10 mmol L^{-1} HQ in 0.1 mol L^{-1} $NaClO_4$ at: a) bare GCE, b) PD film–hole modified GCE and c) PD film modified GCE. The scan rate was100 mV s^{-1} in all cases.

CV of hexaminеruthenium(III)

The CVs of $Ru(NH_3)_6Cl_3$ at the bare and the modified GCEs are depicted in Fig. 3. Electrochemical response of $Ru(NH_3)_6Cl_3$ was significantly suppressed at the PD film–hole modified GCE (Fig. 3, curve c) relative to that at the bare GCE (Fig. 3, curve a). At the PD film modified GCE, redox peak of $Ru(NH_3)_6^{3+}$ was significantly diminished (Fig. 3, curve b). From the voltammograms, it was

concluded that the modified electrodes were positively charged as the signal for the cationic redox probe was significantly diminished due to its repulsion from the surface of the electrode.

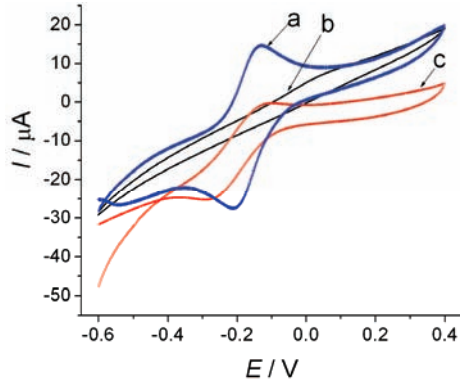

Fig. 3. CVs of 10 mmol L^{-1} $Ru(NH_3)_6Cl_3$ in 0.1 mol L^{-1} KNO_3 at: a) bare GCE, b) PD film modified GCE and c) PD film–hole modified GCE. The scan rate was 50 mV s^{-1} in all cases.

CV of hexacyanoferrate

The CVs of $K_3Fe(CN)_6$ at the modified GCEs (Fig. 4, curves a and b) were compared to that at the bare GCE (Fig. 4, curve c). The redox peaks for the modified GCEs were significantly higher than that for the bare GCE. Comparing the CV response of $K_3Fe(CN)_6$ at the PD film–hole modified GCE (Fig 4, curve a) to that at the PD film GCE (Fig 4, curve b), the redox peak current of the probe at the modified GCE was found to be higher. From this observation, it was concluded that the modification imparted a positive charge on the surface of the organic film and hence the ferrocyanide approached the electrode surface not only by diffusion, but also by electrostatic interaction between the positively charged PD film and the negatively charged ferricyanide. The presence of holes on the PD film–hole modified GCE could be responsible for the extra enhancement for the ferrocyanide signal due to the three-dimension diffusion of the anionic redox probes towards nanoelectrodes. The produced holes could change diffusion of

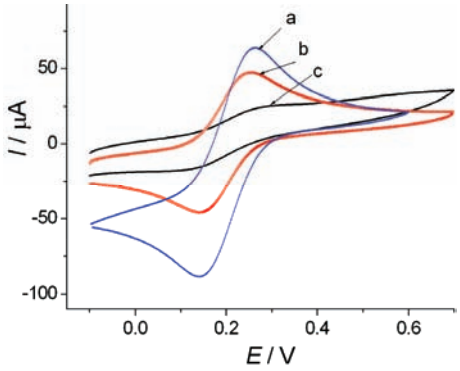

Fig. 4. CV of 10 mmol L^{-1} $K_3Fe(CN)_6$ in 0.1 mol L^{-1} KCl at: a) the PD film-hole modified GCE, b) the PD film modified GCE and c) the bare GCE. The scan rate was 50 mV s^{-1} in all cases.

ions from planar to three dimensional.[23,24] Compton and his coworkers[25] demonstrated that modifying an electrode with porous layers of a conducting material could affect voltammetric peaks because of a change in the mass-transport mode from planar diffusion to one with a thin-layer character.

The observation from the studied redox probes indicated that the modified PD–film was positively charged and repelled $Ru(NH_3)_6^{3+}$ but strongly attracted the $Fe(CN)_6^{3-}$ probe. From this, it was decided to use the modified electrode for electro-analysis of the negatively charged analyte. The advantage could be two-fold: enhancement in the signal of the analyte and improvement in the selectivity as cationic interferents would not approach the modified electrode surface. With this in mind, the PD film–hole modified GCE was used for the electro-analysis of AA.

CV of ascorbic acid (AA) at the PD film–hole modified GCE

The CV curves of AA at the bare GCE and the PD film–hole modified GCE over a wide range of potentials are depicted in Fig. 5. It is clearly presented that the oxidation peak current of AA is enhanced and shifted to a lower potential at the PD film–hole modified GCE relative to those at the bare GCE. The electro oxidation of AA at a bare GCE generally occurs at a relatively high oxidation potential, indicating a slow electron transfer rate.[26]

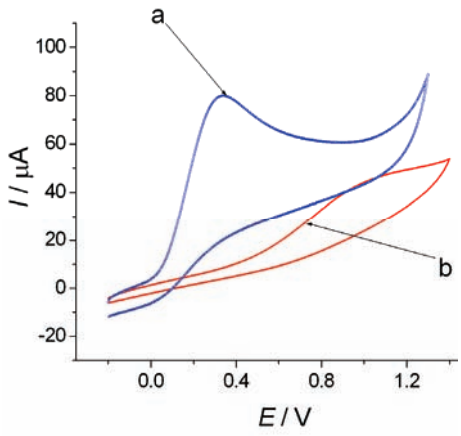

Fig. 5. CVs of 2 mmol L^{-1} AA in 0.1 mol L^{-1} acetate buffer (pH 5) at: a) PD film–hole modified GCE and b) bare GCE; in all cases scan rate 100 mV s^{-1}.

The oxidation of AA ($C_6H_8O_6$) involves a two-electron and two-proton irreversible reaction to produce dehydroascorbic acid ($C_6H_6O_6$).[27] From the voltammograms, the oxidation potential of AA is close to 0.8 and 0.237 V for bare and PD film–hole modified GCE, respectively. These potentials for were selected for the amperometric determination of AA at the studied electrodes.

Effect of the pH of the supporting electrolyte on the electro-analysis of AA

The pH of the electrolyte is one of the important parameters that could influence the response of the electrode in the analysis of AA. The pH is an important parameter that controls the surface charge of the modifier film and the state in which AA could be available in the solution. The pH of the supporting electrolyte was varied within the range of 2 to 8.5 to study the effect of pH on oxidation peak current of AA at the PD film–hole modified GCE.

Oxidation peak current of AA was found to increase as the pH was changed from pH 2 to 5 (Fig. 6, curve a). A further increase in pH of the buffer led to a decrease in the response of AA. This observation is in agreement with the proposed interaction model. In the pH range in which the modifier film can be made positive film and the AA in its anionic form, the interaction of the modified GCE surface with AA enhances the redox signal. At higher pH conditions, the film might develop a negative charge (due to adsorption free hydroxyl ions) and cause the anionic form of AA to be repelled. Thus, pH 5 is the condition that favors the formation of cationic film and anionic form of AA. Hence, a pH value of 5 was selected as optimum condition for the electro-analysis of AA at the PD film–hole modified GCE. For the sake of comparison, similar study on the effect of pH on the oxidation peak current of AA at bare GCE was conducted. The oxidation peak current for AA consistently decreased with increasing pH (Fig. 6, curve b). A comparison of the two results clearly demonstrated the difference in surface property between the modified and the unmodified GCE.

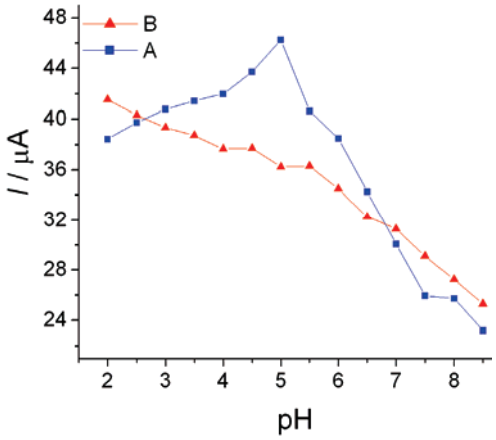

Fig. 6. Oxidation peak current of 2 mol L^{-1} AA in different pH supporting electrolytes at: a) the PD film–hole modified GCE and b) the bare GCE.

Amperometric determination of AA

In this work, amperometric measurements were performed and the results compared for the determination of AA at the two electrodes, *i.e.*, the PD film––hole modified GCE and the bare GCE. For the PD film–hole modified GCE, the

amperometric measurement was performed at 0.237 V while for bare the GCE, it was at 0.8 V (the potential at which the highest oxidation peak current was observed). The amperometric response of both the modified and the bare GCE, for successive additions of AA, increased stepwise with increasing concentration of AA in 0.1 mol L^{-1} acetate buffer (pH 5). The bare GCE showed a linear response to AA in the concentration range from 5 to 45 mmol L^{-1} with detection limit of 1.656 mmol L^{-1} and a correlation coefficient of 0.995 (Fig. 7A). The PD film–hole modified GCE showed a linear response to AA in the concentration range from 5 to 45 μmol L^{-1} with a detection limit of 0.123 μmol L^{-1} and a correlation coefficient of 0.998 (Fig. 7B). The average of three measurements for each concentration was calculated to plot the calibrations curves. The limit of detection ($LOD = 3\sigma$/slope) at the bare GCE and the PD film–hole modified GCE were 1.656 mmol L^{-1} and 0.123 μmol L^{-1}, respectively. The PD film–hole modified GCE had improved characteristics, such as, detection of a lower concentration of AA and better reproducibility of the signal for the studied concentrations. Thus, the observed attributes are encouraging for the potential application of the modified electrode as an electrochemical sensor for the determination of AA.

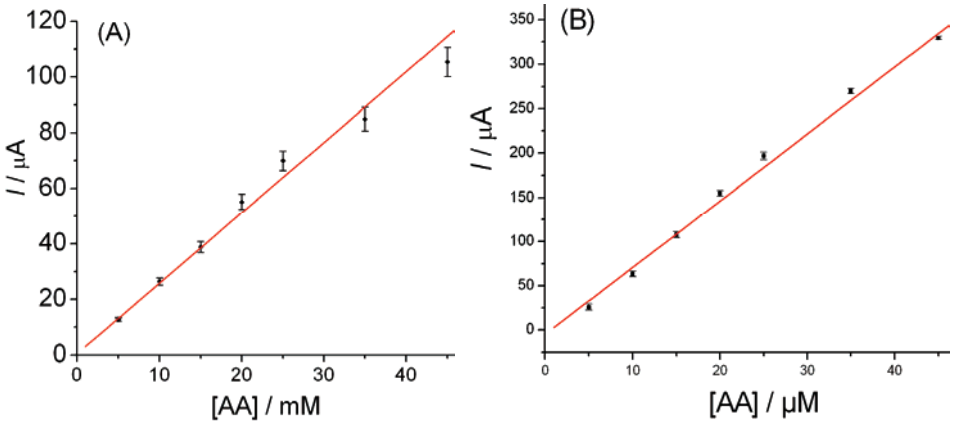

Fig. 7. Amperometric calibration curve for determination of AA in acetate buffer (pH 5) at: A) bare GCE; B) PD film–hole modified GCE.

Effect of interferents

The influence of compounds, such as caffeine (CAF), starch (STA), which could coexist in the pharmaceutical dosages, vitamin C, glucose (GLU), citric acid (CA) and tartaric acid (TA), which may co-exist in fruit juices,[28–30] and compounds such as GLU, dopamine (DA) and uric acid (UA), which co-exist in human fluid,[31] may interfere with the determination of AA. Amperometric signal for AA in the presence of the above possible interfering substances was studied at a fixed concentration of 1 mmol L^{-1} AA and 1 mmol L^{-1} each interferent at

the bare GCE at 0.8 V (Fig. 8A). For the PD film–hole modified GCE, amperemetric signal of AA in the presence of the above possible interfering substances was studied at a fixed concentration of 1 mmol L^{-1} AA and 200-fold excesses of interfering species at 0.237 V (Fig. 8B and C).

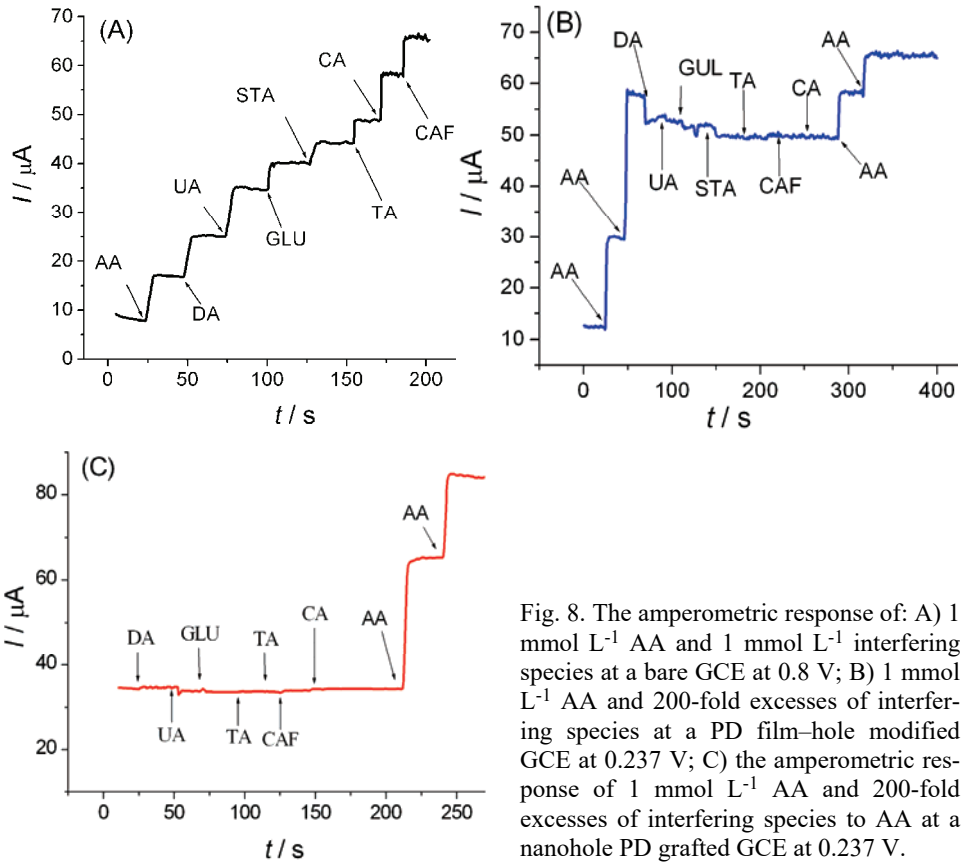

Fig. 8. The amperometric response of: A) 1 mmol L^{-1} AA and 1 mmol L^{-1} interfering species at a bare GCE at 0.8 V; B) 1 mmol L^{-1} AA and 200-fold excesses of interfering species at a PD film–hole modified GCE at 0.237 V; C) the amperometric response of 1 mmol L^{-1} AA and 200-fold excesses of interfering species to AA at a nanohole PD grafted GCE at 0.237 V.

As can be seen from Fig. 8, the influence of even very high concentrations of the studied potential interferents on the amperometric response of AA at the PD film–hole modified GCE was found to be minimal. This could be due to a lowering of the oxidation potential of AA at the modified electrode compared to at the bare GCE and the repulsion by the modifier film of species, such as DA, that are available in cationic form.

Inter-electrode reproducibility and stability tests

The inter-electrode reproducibility was investigated for PD film–hole modified GCE by preparing five electrodes under the same conditions. Amperometric measurement at 0.237 V for 2 mmol L^{-1} AA at five different electrodes, prepared

with the same electrode modification strategy, was used to estimate the reproducibility. The reproducibility expressed by the relative standard deviation was found to be 5.18 % (n = 5) for PD film–hole modified GCE, thereby showing the good reproducibility of the modified electrode.

The stability of the PD film–hole modified electrode was studied by comparing the current response of a freshly prepared PD film–hole modified GCE with the response of electrodes after storage for 28 days in 0.1 mol L^{-1} acetate buffer (pH 5) at room temperature. For 2 mmol L^{-1} AA, the modified electrodes retained 98 % of the initial current response. The result showed that the PD film––hole modified GCE has a good stability and long life.

Comparison of the PD film–hole modified GCE with previously reported methods

The detection limit of the PD film hole modified GCE is compared in Table I with those of previously reported modified electrodes. As can be seen from Table I, the electrode modification strategy reported herein resulted in an electrode with a better detection limit than most of those previously reported.

TABLE I. Comparison of the modified electrode with previously reported modified electrodes for the determination of ascorbic acid

Electrode	Detection limit μM	Ref.
Bi_2O_2 microparticles modified GCE	8.1	32
Tiron modified GCE	1.79	33
GCE modified with carbon-spheres (linear range 2–300 μM)	0.60	34
GCE modified with a nickel(II)-bis(1,10-phenanthroline) complex (linear range 10–630 μM)	4.0	35
Quaternized carbon nanotubes/ionic liquid–polyaniline composite film modified GCE (linear range 20 nM–4 μM)	0.25	36
Nitrogen doped porous carbon nanopolyhedra (linear range 80–2000 μM)	0.74	37
Graphene modified GCE (linear range 10.0–1000 μM)	1.20	38
Gold electrode modified with a flower-like gold nanostructure (linear range 60–500 μM)	10	39
Over oxidized *p*-aminophenol polymer film on GCE	1.0	40
GCE modified with poly(ethylene oxide)	50	41
Methionine modified carbon paste electrode	5.0	42
Electropolymerized aniline on GCEs	1.0	15
PD film–hole modified GCE	0.123	This work

Real sample analysis

To demonstrate the applicability of the PD film–hole modified GCE for real sample analysis, orange fruit and vitamin C tablet samples were analyzed (Table II). The bulk concentration of AA was first determined by titration. The concentration of AA obtained in orange fruit and vitamin tablet were 23.33±0.01 mg per

100 mL and 504.97±0.03 mg per tablet, respectively. Then the AA was determined by amperometry using PD film–hole modified GCE. The relative error for PD film–hole modified GCE was 0.04 % for the determination of AA in orange and 0.37 % for the determination of AA in vitamin C tablet. The data presented clearly showed that the method reported herein is accurate.

Table II Accuracy test for the modified electrode against the standard titration method

Working electrode	Concentration of AA, mean ± *SD*, *n* = 3 for each sample	
	In orange fruit, mg/100mL	In vitamin C tablet, mg/tablet
PD film–hole modified GCE	23.34±0.17	506.87±0.39
Standard titration method	23.33±0.01	504.97±0.03

CONCLUSIONS

In this work, the fabrication and electrochemical characterization of PD film–hole modified GCE was reported. The modified GCE was demonstrated for the amperometric determination of AA. The PD film–hole modified GCE was found to have very good selectivity towards AA and high sensitivity for the determination of AA and could be applied in different matrices. The electrode modification strategy could be used as a means for the selective determination of anionic analytes in the presence of cationic interfering species. Further study is required to understand fully the reported surface modification strategy and to explore different modifying films and other important analytes.

Acknowledgements. We would like to acknowledge the Department of Chemistry, Jimma University, Ethiopia, for providing the laboratory facilities. Financial support from Jimma University School of Graduate Studies is also acknowledged.

ИЗВОД

ЕЛЕКТРОХЕМИЈСКО ОДРЕЂИВАЊЕ АСКОРБИНСКЕ КИСЕЛИНЕ НА ЕЛЕКТРОДИ ОД СТАКЛАСТОГ УГЉЕНИКА МОДИФИКОВАНОЈ ПЕРФОРИРАНИМ ФИЛМОМ *p*-ФЕНИЛЕНДИАМИНА

BIKILA NAGASA OLANA, SHIMELES ADDISU KITTE и TESFAYE REFERA SORETA

Department of Chemistry, College of Natural Sciences, Jimma University, P. O. Box 378, Jimma, Ethiopia

У раду је приказано одређивање аскорбинске киселине (АА) на електроди од стакластог угљеника која је модификована перфорираним филмом формираним редукцијом диазонијум јона генерисаним *in situ* из *p*-фенилендиамина. Перфорације филма постигнуте су растварањем претходно исталожених наночестица злата. Модификоване електроде су електрохемијски карактерисане коришћењем уобичајених редокс реакција хидрохинона, јона гвожђе(II)-цијанида и јона рутенијум(II)-хексамина. Струје оксидације АА одређене цикличном волтаметријом и хроноамперометријом на модификованим електродама су упоређене са струјама на немодификованој електроди од стакластог угљеника. Немодификована електрода је показала линеаран одговор у опсегу концентрација АА од 5 до 45 mM уз границу детекције од 1,656 mM, док је модификована електрода показала линеаран одговор у опсегу концентрација АА од 5 до 45 μM уз границу детекције од 0,123 μM. На модификованој електроди је испитан утицај суп-

станци које могу да ометају амперометријски сигнал АА и нађено је да је он минималан. Такође је утврђено да су репродуктивност самих модификованих електрода, њихова стабилност и тачност одлични. Модификована електрода приказана у овом раду има потенцијалну примену за електроаналитичко одређивање АА.

(Примљено 4. новембра, ревидирано 30. децембра 2014, прихваћено 19. јануара 2015)

REFERENCES

1. O. Arrigoni, M. C. De Tullio, *BBA-Gen. Subjects* **1569** (2002) 1
2. K. J. Stutts, P. M. Kovach, W. G. Kuhr, R. M. Wightman, *Anal. Chem.* **54** (1983) 1632
3. A. Hodgkinson, *Oxalic Acids in Biology and Medicine*, Academic Press, London, 1977
4. J. Wawrzyniak, A. Ryniecki, W. Zembrzuski, *Acta Sci. Pol. Technol. Aliment.* **42** (2005) 5
5. H. S. Burdurlu, N. Koca, F. Karadeniz, *J. Food Eng.* **74** (2006) 211
6. H. M. Nassef, L. Civit, A. Fragoso, C. K. O'Sullivan, *Analyst* **133** (2006) 1736
7. A. M. Pisoschi, A. Pop, A. I. Serban, C. Fafaneata, *Electrochim. Acta* **121** (2014) 443
8. A. Hossu, V. Magearu, *Rom. Biotechnol. Lett.* **9** (2004) 1497
9. Z. H. Sheng, X. Q. Zheng, J. Y. Xu, W. J. Bao, F. B. Wang, X. H. Xia, *Biosens. Bioelectron.* **34** (2012) 125
10. A. T. Markas, J. Gilmartin, P. Hart, *Analyst* **120** (1995) 1029
11. L. F. Xiao, J. Chen, C. S. Cha, *J. Electroanal. Chem.* **495** (2000) 27
12. M. Ardakani, A. Talebi, H. Naeimi, M. Barzoky, N. Taghavinia, *J. Solid State Electrochem.* **13** (2009) 1433
13. H. Zare, N. Nasirizadeh, M. Mazloum Ardakani, *J. Electroanal. Chem.* **577** (2005) 25
14. H. Mao, P. G. Pickup, *J. Electroanal. Chem.* **265** (1989) 127
15. I. G. Casella, M. R. Guascito, *Electroanalysis* **9** (1997) 1381
16. F. W. Campbell, R. G. Compton, *Anal. Bioanal. Chem.* **396** (2010) 241
17. T. R. Soreta, J. Strutwolf, C. K. O'Sullivan, *Langmuir* **23** (2007) 10823
18. T. R. Soreta, J. Strutwolf, C. K. O'Sullivan, *ChemPhysChem* **9** (2008) 920
19. M. H. Nassef, A. D. Radi, C. O' Sullivan, *J. Electrochem.* **592** (2006) 139
20. J. Lyskawa, D. Belanger, *Chem. Mater.* **18** (2006) 4755
21. S. Griveau, D. Mercier, C. Vautrin-Ul, A. Chausse, *Electrochem. Commun.* **9** (2007) 2768
22. M. Arvand, S. Sohrabnezhad, M. F. Mousavi, M. Shamsipur, M. A. Zanjanchi, *Anal. Chim. Acta* **491** (2003) 193
23. S. Lupu, A. Mucci, L. Pigani, R. Seeber, C. Zanardi, *Electroanalysis* **14** (2002) 519
24. H. Zhao, Y. Zhang, Z. Yuan, *Anal. Chim. Acta* **441** (2001) 117
25. M. C. Henstridge, E. J. F. Dickinson, M. Aslanoglu, C. B. McAuley, R. G. Compton, *Sensors Actuators, B* **145** (2010) 417
26. M. Zhang, K. Gong, H. Zhang, L. Mao, *Biosens. Bioelectron.* **20** (2005) 1270
27. I. F. Hu, T. Kuwana, *Anal. Chem.* **58** (1986) 3235
28. R. Deinhammer, M. Ho, M. Anderegg, M. D. Porter, *Langmuir* **13** (1994) 123
29. P. Allongue, M. Delamar, B. Desbat, O. Fagebaume, R. Hitmi, K. Pinson, J. M. Saveant, *J. Am. Chem. Soc.* **119** (1997) 201
30. D. Arrigan, *Analyst* **129** (2004) 1157
31. M. Bernard, A. Chausse, E. Cabet-Deliry, M. Chehimi, J. Pinson, F. Podvorica, C. Vautrin-Ul, *Chem. Mater*. **15** (2003) 3450
32. M. Zidan, T. W. Tee, A. H. Abdullah, Z. Zainal, K. J. Kheng, *Int. J. Electrochem. Sci.* **6** (2011) 6289
33. A. A. Ensafi, M. Taei, T. Khayamian, *Int. J. Electrochem. Sci.* **5** (2010) 116
34. J. Zhou, M. Sheng, X. Jiang, G. Wu, F. Gao, *Sensors* **13** (2013) 14029

35. X. Liu, X. Li, Y. Xiong, Q. Huang, X. Li, Y. Dong, P. Liu, C. Zhang, *Microchim. Acta* **180** (2013) 1309
36. X. Lingling, Z. Zuoyi, W. Fengli, *J. Electrochem. Soc.* **160** (2013) H327
37. P. Gai, H. Zhang, Y. Zhang, W. Liu, G. Zhu, X. Zhang, J. Chen, *J. Mater. Chem., B* **1** (2013) 2742
38. X. Ma, M. Chao, M. Chen, *Russ. J. Electrochem.* **50** (2014) 154
39. Y. Zheng, Z. Huang, C. Zhao, S. Weng, W. Zheng, X. Lin, *Microchim. Acta* **180** (2013) 537
40. Ç. C. Koçak, Z. Dursun, *J. Electroanal. Chem.* **694** (2013) 94
41. W. Gong, Z.-Y. Dou, P. Liu, X.-Y. Cai, X.-Q. He, *J. Electroanal. Chem.* **666** (2012) 62
42. B. K. Chethana, Y. Arthoba Naik, *Anal. Methods* **4** (2012) 3754.

Journal of the Serbian Chemical Society
JSCS-info@shd.org.rs • www.shd.org.rs/JSCS
J. Serb. Chem. Soc. *80* (9) 1177–1192 (2015) UDC 547.462.3+678.744:66.081.2:661.742.2
JSCS–4789 *Original scientific paper*

Poly(methyl methacrylate) denture base materials modified with ditetrahydrofurfuryl itaconate: Significant applicative properties

PAVLE SPASOJEVIĆ[1*#], VESNA PANIĆ[1], SANJA ŠEŠLIJA[2#], VLADIMIR NIKOLIĆ[3#], IVANKA G. POPOVIĆ[4#] and SAVA VELIČKOVIĆ[4]

[1]Innovation Centre, Faculty of Technology and Metallurgy, University of Belgrade, Karnegijeva 4, 11000 Belgrade, Serbia, [2]Institute of Chemistry, Technology and Metallurgy, University of Belgrade, Njegoševa 12, 11000 Belgrade, Serbia, [3]Innovation Centre, Faculty of Chemistry, University of Belgrade, Studentski trg 12–16, 11000 Belgrade, Serbia and [4]Faculty of Technology and Metallurgy, University of Belgrade, Karnegijeva 4, 11000 Belgrade, Serbia

(Received 23 January, revised 9 April, accepted 22 April 2015)

Abstract: The aim of this work was to examine the possibility of modification of commercial denture base materials with itaconic acid esters, in order to obtain materials with lower toxicity and higher biocompatibility. Despite their relatively higher price compared to methacrylates, itaconic acid and itaconates are materials of choice for environmentally friendly applications, because they are not produced from petrochemical sources, but from plant products. A commercial system based on poly(methyl methacrylate) was modified using ditetrahydrofurfuryl itaconate (DTHFI), whereby the ratio of DTHFI was varied from 2.5 to 10 % by weight. Copolymerization was confirmed using FTIR spectroscopy, while SEM analysis showed the absence of micro defects and pores in the structure. The effects of the itaconate content on the absorption of fluids, the residual monomer content, thermal, dynamic-mechanical and mechanical properties (hardness, toughness, stress and elongation at break) were investigated. It was found that the addition of DTHFI significantly reduced the amount of residual methyl methacrylate, which made these materials less toxic. It was shown that increasing the DTHFI content resulted in materials with decreased glass transition temperatures, as well as with decreased storage modulus, ultimate tensile strength and impact fracture resistance; however the mechanical properties were in the rang prescribed by ADA standards, and the materials could be used in practice. The deterioration in mechanical properties was therefore worthwhile in order to gain lower toxicity of the leached monomer.

Keywords: dental; itaconic; methyl methacrylate; absorption, tensile.

* Corresponding author. E-mail: pspasojevic@tmf.bg.ac.rs
# Serbian Chemical Society member.
doi: 10.2298/JSC150123034S

INTRODUCTION

Poly(methyl methacrylate) (PMMA) is one of the most significant acrylic polymers. Although it was discovered and commercialized many years ago, PMMA is still the subject of intense scientific research. Poly(methyl methacrylate) is used as a substitute for transparent glass and dielectric films,[1] acrylic paints,[2] micro-cell foam,[3] *etc*. However, biomedicine represents the most attractive application area where this material is used to create denture bases,[4] contact lenses, bone cement,[5] inhalers,[6] *etc*. Materials based on PMMA are often used as biomaterials due to their good biocompatibility, non-toxicity, stability of colour and shape,[7] the absence of taste, smell and irritation of the surrounding tissue,[8] good adhesion to teeth, insolubility in body fluids, the ease of handling and design, as well as good aesthetic properties.[9] In spite of these advantages of the material, dental prosthesis based on PMMA have several drawbacks. The most important of these drawbacks are toxicity of residual monomer,[10–13] susceptibility to distortions as well as limitations in terms of mechanics.[14] As a result of these deficiencies, residual monomer may leak out by diffusion from prosthesis and irritate the surrounding tissue. This leakage creates cracks and other structural damages to the dental prosthesis that could lead to mechanical fracture of the prosthesis and create an environment suitable for the development of different types of bacteria, moulds and fungi.

In order to overcome the drawbacks and the limitations of PMMA denture base materials, the possibility of modifying a commercial PMMA-based formulation using itaconic acid derivatives was investigated. Itaconic acid is structurally very similar to methacrylic acid, except that at the α-carbon atom a carboxyl group is attached instead of the H atom. Despite the slightly higher market price compared to methacrylic acid, itaconic acid and itaconates are more acceptable in terms of ecology and sustainable development.[15,16] The reason for this lies in the fact that the itaconic acid is obtained from plants (mostly by enzymatic transformations of molasses[17]), while methacrylic acid is derived from petrochemical sources. As a dibasic acid, itaconic acid provides more options when making its esters compared to methacrylic acid. Due to the many similarities of itaconates with the corresponding methacrylates and the mentioned advantages, itaconates represent an interesting alternative to methacrylates in the synthesis of a variety of materials.

In dentistry, itaconic acid and its esters are known. They have been widely used in the production of glass ionomer cements.[18–20] Itaconic acid and its derivatives are used as components in many systems for controlled drug release.[21–26] It is important to note that itaconates have been extensively used in varies medical applications because of their very low toxicity.[19] Furthermore, itaconic acid and its derivatives are increasingly used in the preparation of paints and coatings,[27–29] composite resins,[30,31] contact lenses,[32,33] and products for personal care.[34]

Due to the structural similarities of the methacrylates and the itaconates, numerous studies concerning copolymers of methyl methacrylate and dialkyl itaconates have been published.[11,12] Fernandez-Garcia and Madruga[13] examined the effect of copolymer composition on the glass transition temperature and came to the conclusion that the glass transition temperature of the copolymers decreased with increasing amount of itaconate, as well as with the increasing alkyl chain length of the ester group. Investigation of the thermal stability of the copolymers of the methyl methacrylate and dialkyl itaconates showed that the relative thermal stability increased with increasing proportion of methyl methacrylate in the copolymer, following a similar trend as the change of glass transition temperature.[14]

In a previous study, the residual monomer content and water sorption for PMMA denture base materials modified with dimethyl itaconate and dibutyl itaconate were investigated.[35] It was shown that the addition of itaconate led to a reduction in the water uptake and greatly reduced the residual methyl methacrylate content. In this way, the applicative properties and biocompatibility of PMMA denture base materials for the production of dental prostheses were greatly improved.

In order to further investigate the effect of the substitution of methyl methacrylate in denture base materials with the esters of itaconic acid, in this study, a commercial denture base material was modified by ditetrahydrofurfuryl itaconate (DTHFI). The applicative properties of significance of the novel materials were investigated.

EXPERIMENTAL

Materials

A commercial system for denture base materials Biokril® (Galenika AD, Serbia) was used as received. The system was delivered as two-components; one part was solid and the other was liquid. Liquid component included monomer (MMA) and ethylene glycol dimethacrylate (EGDMA) as crosslinker, while solid component included PMMA powder and benzoyl peroxide (BPO) as initiator. Itaconic acid (2-methylidenebutanedioic acid) was a commercial product (Fluka), while ditetrahydrofurfuryl itaconate (DTHFI) was synthesized as previously described in the literature.[16]

Synthesis of PMMA denture base materials modified with itaconates

The liquid component was mixed with a precisely defined amount of ditetrahydrofurfuryl itaconate. The amount of DTHFI that was added in liquid component was determined in a manner that mixture obtained by mixing modified liquid component with solid commercial component had satisfying characteristics (“working hours” and curing time). The mass percent of DTHFI in the new procedures were 0, 2.5, 5.0, 7.5 and 10 (Table I).

Polymerization under heating in a water bath

Polymerization was realised under pressure in metal mould that was placed in a water bath at 100 °C for 30 min. Round moulds with diameter of 25 mm and thickness of 3 mm were used for the preparation of the samples for measurement of the material hardness, while

moulds for the measurement of elongation, viscoelastic properties and toughness had a rectangular shape with the dimensions of 60 mm× 10 mm× 4 mm, 60 mm× 12 mm× 2 mm and 80 mm× 10 mm× 4 mm, respectively.

TABLE I. Feed composition

Sample	Component		
	Biokril® PMMA powder, %	Biokril® liquid component, %	DTHFI, %
PMMA	66.0	34.0	–
PMMA/2.5PDTHFI	64.5	33.0	2.5
PMMA/5PDTHFI	63.0	32.0	5.0
PMMA/7.5PDTHFI	61.5	31.0	7.5
PMMA/10PDTHFI	59.5	30.5	10

Determination of the amount of residual monomer in the obtained materials by high pressure liquid chromatography with a UV detector (HPLC-UV)

The amount of the residual monomer after polymerization was determined by high pressure liquid chromatography with a UV detector (HPLC-UV). The residual monomers were extracted from samples with an average mass of 0.5 g. The samples were placed in cups and then immersed in 20 mL of methanol. To complete the extraction, the cups were closed, covered with Parafilm® and stored in the dark for 10 days. A Surveyor HPLC system (Thermo Fisher Scientific, Waltham, MA, USA) was used for the determination of the amount of the residual monomers (MMA and DTHFI). The chromatographic separation of monomers was realised on the Zorbax Eclipse® XDB-C18 column that was preceded by a pre-column of the same producer. The mobile phase consisted of methanol (A) and deionised water (B). Chromatographic separation of MMA and DTHFI was performed isocratically for a duration of 10 min and mobile phase consisted of 70 % A and 30 % B at a constant flow of 1.1 mL min^{-1}. A 10-µl sample was injected into the HPLC system. The UV spectra of monomers were obtained by a Surveyor PDA detector. Only one absorption maximum for both monomers (λ = 210 nm) was observed in the obtained UV spectra. This absorption maximum was used for quantitative determination of the monomers.

Fourier transform infrared spectroscopy (FTIR)

FTIR spectra were recorded by Bomen MB 100 spectrophotometer (Hartmann and Braun, Canada). The KBr pellet technique was used whereby the KBr:sample ratio was 10:1. The Spectra were recorded with 10 repetitions at a resolution of 4 cm^{-1}. Win Bomen software was used for the processing of the spectra.

Scanning electron microscopy (SEM)

Prior to SEM analysis, the samples were covered with platinum vapour in a Leica SCD005 nebulizer. The SEM observations were performed using a Jeol JSM 5800 scanning electron microscope at an acceleration voltage of 20 kV.

Water absorption

Water absorption of the commercial PMMA and DTHFI-modified materials for denture base was investigated gravimetrically at 37 °C. First, the masses of the dry samples were measured and then the samples were immersed in distilled water. In the first 3 days, the samples were measured in intervals of 3 h and then once per day until equilibrium were

reached. Before measuring, the excess water was removed by wiping the samples with filter paper. All of the calculations were realised using data from the second absorption cycle. The second absorption cycle lasted 28 days. Water-soluble oligomers and other impurities were leached from the sample during the first adsorption cycle and hence, the results obtained from the second cycle were accepted as relevant for the water absorption–desorption process.

Equilibrium absorption (M_∞ / %) was calculated using the equation:

$$M_\infty = 100\frac{(m_\infty - m_0)}{m_0} \quad (1)$$

where m_0 is mass of the dry sample and m_∞ is the mass of the sample at equilibrium.

Water diffusion coefficient

The diffusion of water into the synthesized materials was modelled by the Higuchi Equation:

$$\frac{M_t}{M_\infty} = Kt^n \quad (2)$$

where M_t is the % adsorption by the sample at time t, K is a kinetic constant and n is the diffusion exponent. In case of Fickian diffusion, n is 0.5, but in literature values between 0.43 and 0.5 could be found.[36] A value of n higher than 0.5 is indicative of an anomalous diffusion mechanism, while in case when n = 1, the diffusion kinetics is zero order, *i.e.*, time-independent.

According to the Fickian second law, at the initial period of diffusion (M_t/M_∞), diffusion through a solid material could be calculated using the equation:[37]

$$\frac{M_t}{M_\infty} = 2\left(\frac{Dt}{\pi L^2}\right)^{1/2} \quad (3)$$

where D is the effective diffusion coefficient and 2L is the sample thickness.

The dependence between M_t/M_∞ and $t^{1/2}$ is linear and the diffusion coefficient can be calculated from the linear part using Eq. (3).

Differential scanning calorimetry (DSC)

The glass transition temperatures (T_g) of the samples were determined by differential scanning calorimetry on a Perkin Elmer DSC-2 instrument under an inert nitrogen atmosphere. The heating and the cooling rates were 20 °C min^{-1} in the temperature range of 50 to 200 °C. The measurements were performed in two cycles in order to remove unreacted monomers in the first cycle. All calculations were performed using the data from the second cycle.

Dynamic mechanical analysis (DMA)

The dynamic mechanical properties of the samples were tested on a Rheometrics mechanical spectrometer 605. The samples were exposed to a constant shear stress of 0.3 % at a frequency of 1 Hz. The heating rate was 3 °C min^{-1} in the temperature range from 25 to 180 °C. The obtained experimental data were as follows: storage modulus (G' / GPa), loss modulus (G'' / MPa) and damping factor (tan δ), while the T_g was determined as the temperature at which tan δ had a maximum value.

Tensile properties

The analysis of the mechanical tensile properties was performed on an Instron-1332 (FastTrack 8800 control system, High Wycombe, UK) testing machine. The specimens (Fig. S-1 of the Supplementary material to this paper) were clamped by mechanical jaws. The testing speed was 0.5 mm min^{-1}. For each sample five measurements were performed. The average values of the ultimate stress and deformation at break, as well as the standard deviations, were calculated. During the test, the deformations were continuously registered as a function of the stress.

Hardness

The hardness of derived materials was measured on an Instron D-XD durometer (Instron, Norwood, USA). Five repetitions were performed for each sample.

Impact strength

Impact strength was measured on Charpy pendulum using samples with a V notch (Fig. S-2 of the Supplementary material). Length of pendulum was 60 mm with impact energy of 8.73 J. The impact edge of the cone-shaped pendulum with an angle of 30±1°, rounded with a radius R1= 2±0.5 mm, was made of hard steel. All tests were performed at 23 °C and repeated 5 times.

For the calculation of the Charpy impact strength for notched specimens, a_{cN} / KJ m^{-2}, the following equation was used:

$$a_{cN} = 10^3 \left(\frac{w}{h b_N} \right) \quad (4)$$

where w / J is the corrected energy absorbed by the fracture of the specimen, h / mm is the thickness and b_N / mm is the remaining width of the specimen at the notch.

RESULTS AND DISCUSSION

A commercial formulation of denture base material based on PMMA was modified with DTHFI. The modification was performed in order to obtain a material with better biocompatibility, minor risks for an immune response and preserved significant physicochemical properties. Polymerization in moulds was used for the syntheses of the modified denture base materials in which a part of the MMA in liquid phase was replaced with specified amounts of itaconate (Table I).

The samples prepared this way, including PMMA and PDTHFI homopolymers, were characterized by FTIR spectroscopy. The FTIR spectra of PMMA and PDTHFI homopolymers are shown in Fig. 1, while the FTIR spectra of PMMA/PDTHFI containing 2.5 and 10 wt. % itaconate are presented in Fig. 2. From Fig. 1, it could be seen that the FTIR spectra of PMMA and PDTHFI were similar and the characteristic peaks were at the same wavenumbers (3000 and 2950 cm^{-1} for the C–H stretching vibrations of the methyl group, 1730 cm^{-1} for the C=O stretching vibrations of the ester group, 1450 and 1300 cm^{-1} for the asymmetric and symmetric C–H deformation vibrations, 1165 cm^{-1} for the stretching vibrations of the ester group and at 990, 850 and 750 cm^{-1} for the out

of ring C–H vibrations). The FTIR spectrum of PDTHFI contained an absorption peak at 1266 cm^{-1} (C–O–C asymmetric stretching vibrations) but in the case of PMMA, this peak was moved toward slightly a lower wavenumber. From Fig. 2, it could be seen that if the amount of DTHFI residues in monomer feed was increased, the absorption peak at 1266 cm^{-1} had a higher intensity; this led to the conclusion that polymerization between MMA and DTHFI had occurred.

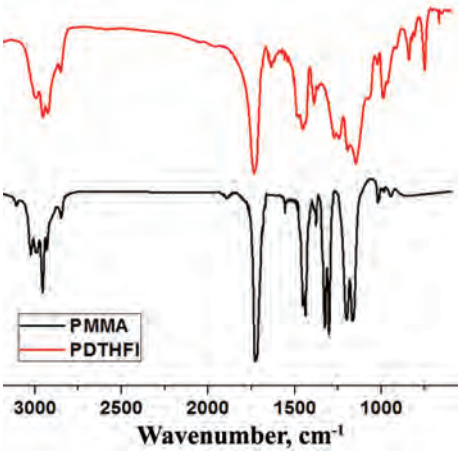

Fig. 1. FTIR spectra of the synthesized PMMA and PDTHFI homopolymers.

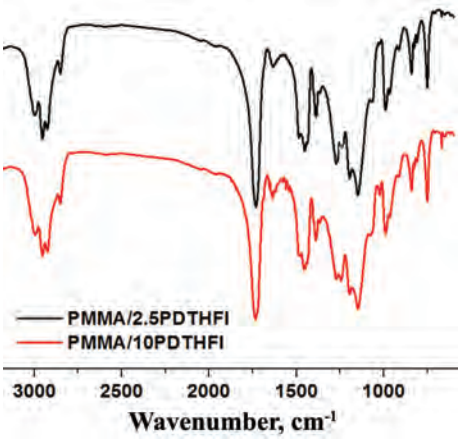

Fig. 2. FTIR spectra of the synthesized copolymers PMMA/PDTHFI containing 2.5 and 10 wt. % of itaconate.

The morphology of the samples of PMMA denture base materials modified with DTHFI is shown in Fig. 3. Serious micro defects in the structure could not be observed in the samples, as presented in micrographs of the representative samples modified with 2.5 and 10 wt. % of DTHFI (Fig. 3). Macro pores (>200 μm) were not present in any of the prepared samples, indicating that during the polymerization process, no boiling of the residual monomer occurred and that the mechanical characteristics of the materials were preserved. The obtained results

justified the continuation of the testing and detailed characterization of the PMMA denture base materials modified with DTHFI.

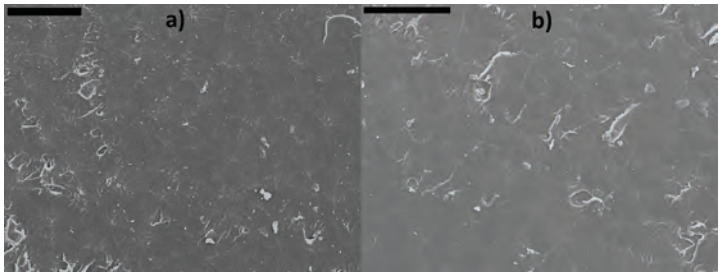

Fig. 3. SEM micrographs of the denture base materials a) PMMA/2.5DTHFI and b) PMMA/10DTHFI; bar: 200 μm.

The residual monomer contents of the synthesized PMMA/PDTHFI samples, as well as of the referent PMMA sample, were analyzed using high-performance liquid chromatography with ultraviolet detection (Table II).

TABLE II. Residual MMA and DTHFI contents and total residual monomer (TRM) content of the PMMA and PMMA/PDTHFI denture base materials

Sample	Residual monomer, %		*TRM* / %
	MMA	DTHFI	
PMMA	1.27	–	1.27
PMMA/2.5DTHFI	0.79	0.95	1.74
PMMA/5DTHFI	0.62	1.66	2.28
PMMA/7.5DTHFI	0.27	2.37	2.64
PMMA/10DTHFI	0.33	2.97	3.30

The results presented in Table II showed that the highest amount of residual MMA was found in case of the referent sample and its value was in accordance with literature data.[27,38,39] It is clear from Table II that the addition of DTHFI decreased the residual MMA content in the synthesized samples. Considering the lower toxicity of itaconates compared to methacrylates,[40] the replacement of MMA leads to the safer usage of denture base materials. At the same time, with increasing DTHFI content in the copolymer, the amount of residual itaconate increased. This could be explained by the analysis of the kinetic parameters of the copolymerization reaction between MMA and DTHFI. It was found that the overall rate of copolymerization increased with increasing MMA content in the feed composition. This also meant that a greater amount of itaconate in the system would result in a lower overall copolymerization rate and lead to a greater amount of total residual monomer for the same polymerization time. Furthermore, the reactivity of MMA monomer towards polymer radicals is greater compared to the reactivity of DTHFI monomer and therefore, as the copolymerization

reaction proceeded, the ratio of MMA to DTHFI decreased. From Table II it could easily seen be that even the minimum modification of denture base material with DTHFI (2.5 wt. %) led to a decrease in the residual MMA content by 37.8 %. Modification with higher amounts of itaconate (> 7.5wt. %) led to the minimal residual MMA content. The values of the residual MMA and DTHFI content were similar as in the case of the polymerization reaction between DMI and MMA, as well as DBI and MMA.[35]

The use of denture base materials implies absorption of water and others oral fluids. If the absorption is very pronounced, the dimensions of dental prosthesis could be significantly increased so they would not fit properly. The absorbed molecules act as plasticizers and hence they affect the mechanical properties of the material and the rate of aging of the material. Furthermore, the fluids absorbed in micropores make the perfect environment for the propagation of many microorganisms. For these reasons, it is very important to determine the mechanism and rate of absorption.

The adsorption–desorption characteristics of the denture base material modified with DTHFI were investigated (Fig. S-3 of the Supplementary material). The water diffused from both the top and the bottom surfaces of the samples until equilibrium. Many authors have used the weight gain as a parameter defining the capability of a material to absorb water, but this phenomenon needs a more detailed insight. Namely, the weight of the samples after desorption were smaller than the initial weight, which indicates that a certain amount of impurities had leached from the sample during the first adsorption cycle. As already mentioned, the denture base materials produced by free radical polymerization have a small percentage of residual monomer as an undesirable part of the product. After the immersion of the samples, two processes occurred – entry of water into the sample, and desorption of residual monomer, water-soluble oligomers and other impurities.[27] Since the variation in weight is the cumulative result of both the increase in weight due to water penetration, and the decrease in weight due to elution of low-molecular weight components, it is impossible to conclude the exact amount of absorbed water only by measuring the increase in weight. Several studies showed that the greatest amount of residual monomers leached during the first seven days of immersion, while the rest leached out over a longer period of time.[28] According to this, in the present study, all results concerning the maximum water uptake and the diffusion coefficients were calculated using the data obtained from the second absorption cycle, as it was reasonable to assume that most of the impurities had diffused out from the samples during the first 28 days of absorption.

The plots of water uptake in the second absorption cycle for the denture base materials modified with DTHFI as a function of $t^{1/2}$ / $h^{1/2}$ are shown in Figs. 4 and 5. The shape of the curves was the same for all the samples and hence, for

better clarity, curves are shown for only three samples. The plots were initially linear with the respect to $t^{1/2}$ (Fig. 5), and thus, it could be concluded that the uptake was diffusion controlled.

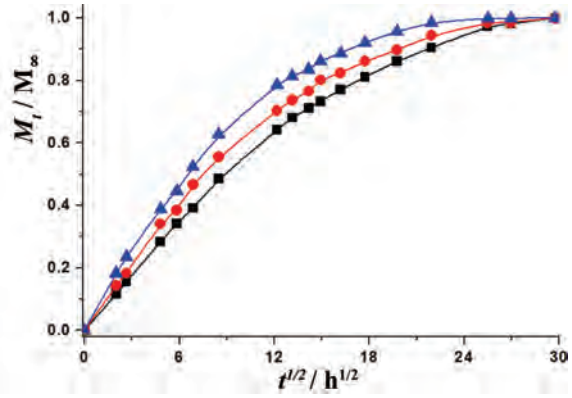

Fig, 4. Plot of water uptake in the second absorption cycle as a function of $t^{1/2}$ for denture base material modified with ■ – 0, ● – 5 and ▲ – 10 % DTHFI.

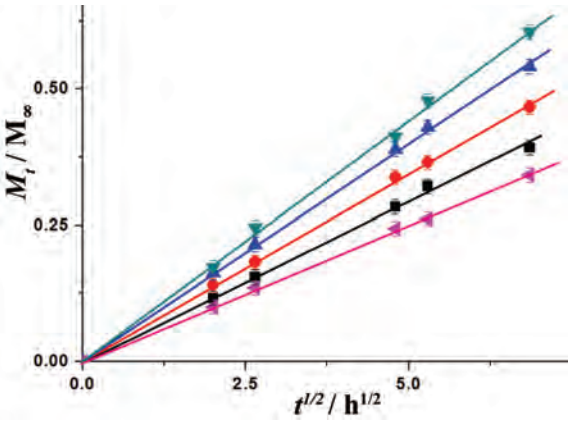

Fig. 5. Plot of initial water uptake of the second absorption cycle as a function of $t^{1/2}$ for denture base material modified with ◄ – 0, ■ – 2.5, ● – 5, ▲ – 7.5 and▼ – 10 % DTHFI.

The results for the diffusion exponent (n), the weight loss (ΔM / %), the maximum degree of absorption (M_∞ / %) and desorption (M'_∞ / %), as well as the calculated values of the diffusion coefficient for absorption (D_a / m^2 s^{-1}) and desorption (D_d / m^2 s^{-1}) are summarised in Table III for the denture base materials modified with DTHFI. The ratio D_d/D_a is also presented, which is an index of the degree of the concentration dependence of the diffusion coefficient. $D_d/D_a > 1$ indicates that the diffusion coefficient decreases with concentration.

Weight loss for the denture base materials (ΔM) involved a single absorption–desorption cycle. This loss was caused by the leaching of residual monomers, soluble oligomers and other impurities. After the polymerization was completed, residual monomer remained between the macromolecular chains: absorbed into the polymer network or trapped in micropores. Furthermore, linear

correlations of the total residual monomer content and weight loss as a function of DTHFI content were found (Fig, S-4 of the Supplementary material). Furthermore, the slopes of these linear correlations were almost the same indicating that the weight loss in this kind of materials depended mostly on the total residual monomer content.

TABLE III. Kinetic parameter (n), weight loss (ΔM), the maximum degree of absorption (M_∞) and desorption (M'_∞), and diffusion coefficients for absorption (D_a) and desorption (D_d) for the studied denture base materials

Sample	n	M_∞ / %	M'_∞ / %	$D_a \times 10^{12}$ m^2 s^{-1}	$D_d \times 10^{12}$ m^2 s^{-1}	D_d / D_a	ΔM / %
PMMA	0.49	1.87	2.04	3.00	7.27	2.42	0.34
PMMA/2.5DTHFI	0.47	1.94	2.15	3.27	4.44	1.36	0.75
PMMA/5DTHFI	0.49	1.93	2.11	3.83	5.32	1.39	1.21
PMMA/7.5DTHFI	0.53	1.96	2.20	3.76	4.54	1.21	1.49
PMMA/10DTHFI	0.51	1.98	2.20	4.06	5.32	1.31	1.87

The thermal properties of PMMA denture base materials modified with DTHFI were investigated *via* differential scanning calorimetry (Fig. S-5 of the Supplementary material). The commercial PMMA denture base material had a single glass transition temperature (T_g) at around 123 °C. The PMMA materials modified with DTHFI also showed a single T_g indicating that copolymers were homogeneous in the range of 10–30 nm.[41] Substitution of a part of MMA with DTHFI lowered the values of the glass transition temperature of the polymer. The greater the amount of DTHFI, the lower was the T_g. However, the observed decrease in the T_g was not as pronounced as in the case of modification of PMMA denture base materials with monomers such as dimethyl itaconate (DMI) and dibutyl itaconate (DBI).[42] This could be attributed to the presence of the tetrahydrofuran ring in the structure of DTHFI, which is a not so movable side group.

During the use of a denture, it undergoes diverse tensions that appear at different places and have enormously wide magnitude of intensities. The most common reason for denture deterioration is due to its breakage, and therefore, it is of a great importance to investigate the dynamic-mechanical properties of new materials. The dependences of the storage modulus (G' / GPa) on temperature for all cured samples were of a similar shape. In the temperature range of 25–100 °C, the investigated denture base materials behaved like homogeneous rigid solids (Fig. S-6 of the Supplementary material). Further increase in temperature led to a sharp decrease in the storage modulus, indicating transition from the glassy to the rubbery state. Above 160 °C, storage moduli for all samples entered into a plateau. As the operating temperature for dentures is around 37 °C, special attention was paid on to values of the DMA parameters precisely at this temperature.

The values of the storage modulus (G' / GPa), loss modulus (G'' / MPa) and damping factor (tan δ_{37}) at 37 °C, the damping factor (tan δ_{max}) and glass transition temperatures calculated from DMA ($T_{g,DMA}$ / °C) and DSC ($T_{g,DSC}$ / °C) measurements for the PMMA denture base materials modified with DTHFI are listed in Table IV.

TABLE IV. Dynamic-mechanical parameters at 37 °C and glass transition temperatures calculated from DMA ($T_{g,DMA}$) and DSC ($T_{g,DSC}$) measurements for the PMMA denture base materials modified with DTHFI

Sample	G' / GPa	G'' / MPa	tan δ_{37}	tan δ_{max}	$T_{g,DSC}$ / °C	$T_{g,DMA}$ / °C
PMMA	4.03	359	0.089	1.31	123.2	141.5
PMMA/2.5DTHFI	4.01	369	0.092	1.34	121.2	140.1
PMMA/5DTHFI	3.79	451	0.119	1.48	118.9	137.8
PMMA/7.5DTHFI	3.52	471	0.134	1.58	117.3	136.0
PMMA/10DTHFI	3.24	509	0.157	1.76	114.6	133.6

The "ideal" material for a denture base should exhibit great rigidity and strength (large G'), moderate deformation under the stress (G'') and the ability to return to the previous shape shortly after removal of a load (low tan δ). It could be noticed in Table IV that increasing the DTHFI content in the PMMA denture base materials led to decreases in the values of the storage modulus and increases in the loss modulus and tan δ. These results indicated reduced stiffness and increased deformation under the load in the case of the materials modified with DTHFI, which was due to the plasticizing effect of the side group of the employed itaconate. Despite the noticed effect, the addition of small amounts of DTHFI (see sample with 2.5 wt. % of DTHFI) caused only negligible decreases in G' (< 1 %) and ensured the same dynamic-mechanical properties as those of the commercial PMMA denture base material.

It could be noticed that the T_g values determined from DMA measurements, as temperature corresponding to the maximal value of damping factor (tan δ_{max}), were somewhat higher than those obtained by DSC measurement, but the trend in the change in T_g was the same for both methods. A similar observation was reported earlier.[42] The differences in the T_g values arise from the fact that the $T_{g,DSC}$ represents the temperature at which the material undergoes the maximum change in polymer chain mobility, which corresponds to the chemical definition of the T_g, while $T_{g,DMA}$ describes the damping characteristics of the material and has historical significance.

As previously presented, the modified materials had better biocompatibility than the commercial PMMA denture base material, but in order to prevent denture breakage during use, it was also necessary that they possess appropriate mechanical properties. For this reason, for all the modified and the commercial PMMA denture base materials, the ultimate tensile strength (σ_{ult} / MPa), elon-

gation at break (ε / %), the Shore D hardness and the Charpy impact strength were determined and are listed in Table V.

TABLE V. Values of the ultimate tensile strength (σ_{ult}), elongation at break (ε), Shore D hardness and Charpy impact strength of the investigated denture base materials

Sample	σ_{ult} / MPa	ε / %	Shore D	Charpy, J cm^{-2}
PMMA	63.8±2.3	6.26±0.55	96.0±0.37	0.285±0.03
PMMA/2.5PDTHFI	63.7±2.5	6.3±0.31	96.3±0.17	0.313±0.02
PMMA/5PDTHFI	63.5±3.2	10.8±0.27	96.1±0.37	0.304±0.04
PMMA/7.5PDTHFI	64.2±1.7	9.5±0.35	94.8±0.28	0.295±0.03
PMMA/10PDTHFI	62.5±4.2	9.4±0.37	90.2±0.49	0.287±0.05

The tensile properties of modified denture base materials were investigated on an Instron testing machine. Modification of commercial PMMA denture base material with DTHFI gave materials with slightly lower values of the ultimate tensile strength. On the other hand, the modified materials elongated more at break. This behaviour could be explained by the fact that the DTHFI molecule possesses an oxygen atom in its structure that might establish hydrogen bonds with hydrogen atoms. Formed H-bonds were very weak and had no effect on the values of stress at break but affected the values of elongation at break. It should be noted that for all samples, the values of tensile strength were within the framework of the prescribed standards.[43]

The mean values of the Shore D hardness for PMMA denture base materials modified with DTHFI ranged between 90.2 and 96.3 and thus fulfilled the required hardness values for denture base materials, as prescribed by the American Dental Standards Institute.[43] Bearing in mind that many material properties, such as composition, surface porosity, residual monomer concentration, *etc*., affect its hardness, it could be concluded that investigated modifications of PMMA denture base material did not have an effect on the Shore D hardness.

Inclusion of DTHFI in commercial PMMA denture base formulation led to increase in the impact resistance of prepared samples (Table V) except in the case of the sample with the highest DTHFI content (10 wt. %). It was observed in all impact tests experiments that the specimens broke with a sharp fracture, exhibiting typical brittle fracture behaviour characterized by a lack of distortion of the broken parts.

CONCLUSIONS

In this study, an itaconate (a sustainable, non-petrochemical raw material) was used as a co-monomer in the preparation of denture base materials. Quantities of 2.5; 5.0; 7.5 and 10 wt. % of methyl methacrylate were replaced by ditetrahydrofurfuryl itaconate. Copolymerization of MMA and DTHFI was confirmed by FTIR, and DSC analysis. Using liquid chromatography, it was found that the addition of itaconate led to a reduction in the amount of residual MMA

and, therefore, made the base material significantly more biocompatible and drastically reduced the risk of a variety of immune responses. The glass transition temperatures of the synthesized samples were shifted to lower values, indicating that the side groups of DTHFI acted as plasticizers. By DMA, it was found that increasing the DTHFI content led to a lowering the values of the storage modulus and stress at break. However, analysis of the mechanical properties showed that all the modified materials possessed characteristics prescribed by ADA standards, and could be used in practice. The magnitude of the measured values indicated that the PMMA denture base materials modified with DTHFI could be developed into a less toxic, more environmentally and patient-friendly product than commercial pure PMMA denture base material. The optimal mechanical properties were exhibited by the sample with the minimal DTHFI modification (2.5 wt. %).

SUPPLEMENTARY MATERIAL

The geometry of the specimens and additional analysis are available electronically from http://www.shd.org.rs/JSCS/, or from the corresponding author on request.

Acknowledgements. The authors acknowledge funding from the Ministry of Education, Science and Technological Development of the Republic of Serbia, Project No. 172062 “Synthesis and characterization of novel functional polymers and polymeric nanomaterials”.

ИЗВОД

ПОЛИ(МЕТИЛМЕТАКРИЛАТНИ) МАТЕРИЈАЛИ ЗА БАЗУ ПРОТЕЗА МОДИФИКОВАНИ ДИТЕТРАХИДРОФУРФУРИЛ-ИТАКОНАТОМ: СВОЈСТВА ВАЖНА ЗА ПРИМЕНУ

ПАВЛЕ СПАСОЈЕВИЋ[1], ВЕСНА ПАНИЋ[1], САЊА ШЕШЛИЈА[2], ВЛАДИМИР НИКОЛИЋ[3], ИВАНКА Г. ПОПОВИЋ[4] и САВА ВЕЛИЧКОВИЋ[4]

[1]Иновациони центар, Технолошко–металуршки факултет, Универзитет у Београду, Карнегијева 4, 11000 Београд, [2]Институт за хемију, технологију и металургију, Универзитет у Београду, Његошева 12, 11000 Београд, [3]Иновациони центар, Хемијски факултет, Универзитет у Београду, Студентски трг 12–16, 11000 Београд и [4]Технолошко–металуршки факултет, Универзитет у Београду, Карнегијева 4, 11000 Београд

Циљ овог рада је испитивање могућности модификације комерцијалних система за добијање материјала за базу зубних протеза естрима итаконске киселине, ради добијања материјала смањене токсичности и већег степена биокомпатибилности. Упркос већој цени итаконата у односу на метакрилате они се често користе у “зеленим” системима због чињенице да се добијају из биообновљивих, а не петрохемијских извора. Комерцијални систем на бази поли(метил-метакрилата) (PMMA) модификован је дитетрахидрофурфурил-итаконатом (DTHFI), при чему је вариран удео DTHFI од 2,5 до 10 мас. %. ФТИР спектроскопијом узорака утврђено је да је у систему дошло до кополимеризације, док је SEM анализа потврдила одсуство озбиљнијих микродефеката и пора у структури. Испитан је утицај итаконата на: апсорпцију течности (вода), количину заосталог мономера, као и термичке, динамичко-механичке и механичке карактеристике (тврдоћа, жилавост, напон и издужење при кидању) синтетисаних материјала. Утврђено је да додатак итаконата у састав комерцијалних система значајно смањује количину заосталог метил-метакрилата што материјал чини биокомпатибилнијим. Синтетисани узорци су

имали задовољавајуће механичке карактеристике. Нађено је да са повећањем удела DTHFI долази до смањења вредности температуре остакљивања, модула сачуване енергије, напона кидања и ударне жилавости, међутим механичке карактеристике су и даље у границама прописаним ADA стандардима тако да се нови материјали могу користити у пракси.

(Примљено 23. јануара, ревидирано 9. априла, прихваћено 22. априла 2015)

REFERENCES

1. J. F. McCabe, R. M. Basker, *Br. Dent. J.* **140** (1976) 347
2. C. Y. K. Lung, B. W. Darvell, *Dent. Mater.* **21** (2005) 1119
3. D. C. Smith, *Brit. Dent. J.* **111** (1961) 9
4. A. Moshaverinia, N. Roohpour, S. Ansari, M. Moshaverinia, S. Schricker, J. A. Darr, I. U. Rehman, *Dent. Mater.* **25** (2009) 1240
5. A. Moshaverinia, S. Ansari, Z. Movasaghi, R. W. Billington, J. A. Darrhtesham, U. Rehman, *Dent. Mater.* **24** (2008) 1381
6. K. Kinashita, *J. Chem. Soc.* **50** (1929) 583
7. B. Axelsson, G. Nyquist, *Odontol. Revy* **27** (1962) 370
8. J. K. Anusavice, *Phillips' Science of Dental Materials*, W. B. Saunders Co., Philadelphia, PA, 2003, p. 176
9. D. C. Smith, M. E. Bains, *Br. Dent. J.* **98** (1955) 55
10. B. E. Tate, *Vinyl and Diene Monomers*, Wiley-Interscience, New York, 1979, p. 205
11. M. Fernandez-Garcia, E. L. Madruga, *Polymer* **37** (1996) 263
12. E. L. Madruga, M. Fernandez-Garcia, *Polymer* **35** (1994) 4437
13. M. Fernandez-Garcia, E. L. Madruga, *Polymer* **38** (1997) 1367
14. M. Fernandez-Garcia, J. L. Fuente, E. L. Madruga, *Polym. Eng. Sci.* **41** (2001) 1616
15. J. Velickovic, S. Vasovic, *Makromol. Chem.* **153** (1972) 207
16. *ISO 20795-1: Dentistry -- Base polymers -- Part 1: Denture base polymers*, 2013
17. G. Giavaresi, E. B. Minelli, M. Sartori, A. Benini, A. Parrilli, M. C. Maltarello, F. Salamanna, P. Torricelli, R. Giardino, M. Fini, *J. Mater. Sci.: Mater. Med.* **23** (2012) 1247
18. J. Zheng, Q. Su, C. Wang, G. Cheng, R. Zhu, J. Shi, K. Yao, *J. Mater. Sci.: Mater. Med.* **22** (2011) 1063
19. M. I. Shtilman, *Polymeric Biomaterials*, VSP BV, Utrecht, 2003, p. 47
20. S. Shen, W. Kiong, Z. Shi, L. Chia, K. G. Neoh, R. B. H. Tan, *J. Mater. Sci.: Mater. Med.***22** (2011) 2283
21. W. I. Higuchi, T. Higuchi, *J. Am. Pharm. Assoc. Sci. Ed.* **49** (1960) 598
22. R. W. Korsmeyer, R. Gurny, E. Doelker, P. Buri, N. A. Peppas, *Int. J. Pharm.* **15** (1983) 25
23. J. Crank, *The Mathematics of Diffusion*, Oxford University Press, London, 1999, p. 203
24. M. F. Burrow, S. Inokoshi, J. Tagami, *Am. J. Dent.* **12** (1999) 295
25. D. T. Turner, *Polymer* **28** (1987) 293
26. G. Bayraktar, B. Guvener, C. Bural, Y. Uresin, *J. Biomed. Mater. Res., B* **76** (2006) 340
27. P. K. Vallittu, V. Miettinen, P. Alakuijala, *Dent. Mater.* **11** (1995) 338
28. S. Baker, S. C. Brooks, D. M. Walker, *J. Dent. Res.* **67** (1988) 1295
29. C. Y. K. Lung, B. W. Darvell, *Dent. Mater.* 23 (2007) 88
30. K. Sato, K. Kodama, (Fuji Photo Film Co., Ltd) US 6,777,160 (2004)
31. K. Shirakawa, Y. Adegawa, S. Yasunami, (Fuji Photo Film Co., Ltd) US 6,773,862 (2004)
32. A. Berube, C. Lapalme, (André Berube) US 6,733,125 (2004)

33. T. Watanabe, E. Ito, S. Tanikawa, S. Ichinohe, T. Yamazaki, M. Lamrani, (Menicon Co., Ltd.) US 6,770,728 (2004)
34. E. R. Lukenbach, C. Kaminski, S. Pascal-Suisse, M. Tahar, M. Ruggiero, (Johnson & Johnson Consumer Companies, Inc.) US 6,762,158 (2004)
35. P. Spasojevic, D. Stamenkovic, R. Pjanovic, N. Boskovic-Vragolovic, J. Dolic, S. Grujic, S. Velickovic, *Polym. Int.* **61** (2012) 1272
36. P. Neogi, *Diffusion in polymers*, Marcel Dekker, New York, 1996, p. 184
37. E. P. Lautenschlager, S. I. Stupp, J. C. Keller, *Functional behavior of orthopedic biomaterials*, CRC Press, Boca Raton, FL, 1984, p. 206
38. S. H. Mohamed, Alb. M. Al-Jadi, T. Ajaal, *J. Phys. Sci.* **19** (2008) 127
39. P. Pfeiffer, E. U. Rosenbauer, *J. Prosthet. Dent.* **92** (2004) 72
40. SIDS Initial Assessment Profile CAS No. 97-65-4, JETOC–Japan Chemical Industry Ecology-Toxicology and Information Center, Tokyo; Inchem, http://www.inchem.org/documents/sids/sids/97654.html (29.09.2015)
41. L. A. Utracki, *Polymer alloy and blends*, Hanser Publishers, Munich, Germany, 1989, p. 189
42. R. J. Sayler, *Assignment of the glass transition*, American Society for Testing and Materials, Philadelphia, PA, 1994, p. 114
43. ADA12-2002: ANSI/ADA *Specification No. 12 for Denture Base Resins*, 2002.

Journal of the Serbian Chemical Society
JSCS@tmf.bg.ac.rs • www.shd.org.rs/JSCS
J. Serb. Chem. Soc. 80 (9) S295–S297 (2015) *Supplementary material*

SUPPLEMENTARY MATERIAL TO

Poly(methyl methacrylate) denture base materials modified with ditetrahydrofurfuryl itaconate: Significant applicative properties

PAVLE SPASOJEVIĆ[1*#], VESNA PANIĆ[1], SANJA ŠEŠLIJA[2#], VLADIMIR NIKOLIĆ[3#], IVANKA G. POPOVIĆ[4#] and SAVA VELIČKOVIĆ[4]

[1]Innovation Centre, Faculty of Technology and Metallurgy, University of Belgrade, Karnegijeva 4, 11000 Belgrade, Serbia, [2]Institute of Chemistry, Technology and Metallurgy, University of Belgrade, Njegoševa 12, 11000 Belgrade, Serbia, [3]Innovation Centre, Faculty of Chemistry, University of Belgrade, Studentski trg 12–16, 11000 Belgrade, Serbia and [4]Faculty of Technology and Metallurgy, University of Belgrade, Karnegijeva 4, 11000 Belgrade, Serbia

J. Serb. Chem. Soc. 80 (9) (2015) 1177–1192

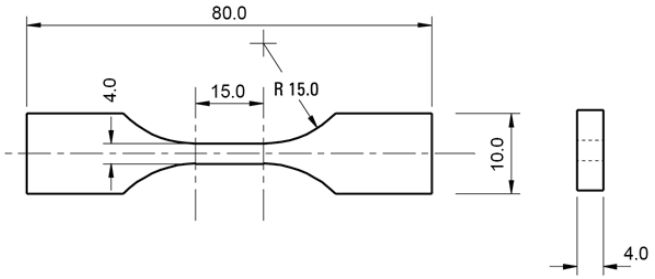

Fig. S-1. The geometry of the specimens used for tensile testing of materials (ASTM D882).

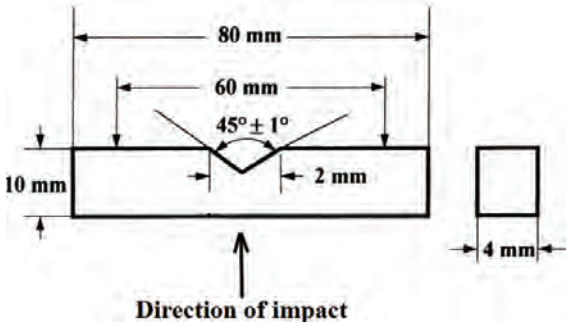

Fig. S-2. The geometry of the specimen used for testing the impact strength after Charpy.

* Corresponding author. E-mail: pspasojevic@tmf.bg.ac.rs

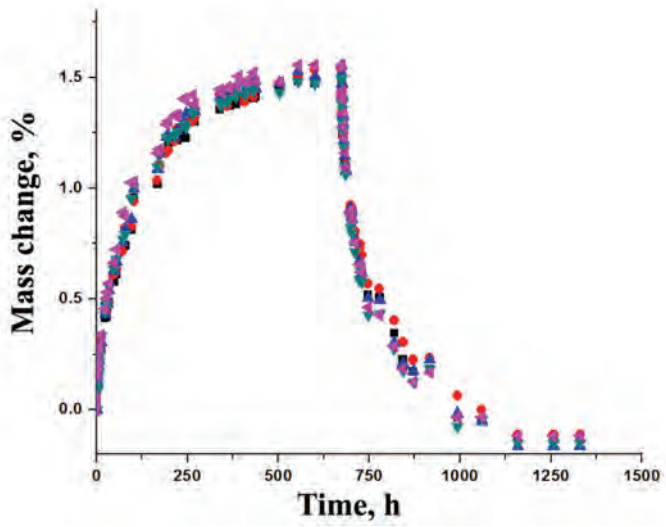

Fig. S-3. Percentage changes in weight of a commercial denture material modified with DTHFI (◄ – 0, ■ – 2.5, ● – 5, ▲ – 7.5 and ▼ – 10 %). The symbols represent mean values (n = 3). Since the standard deviations around all means were smaller than the size of the symbols, they are not shown.

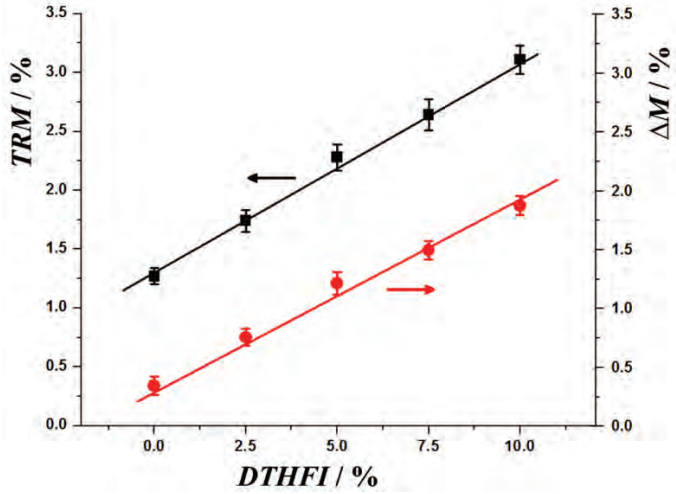

Fig. S-4. Plots of ■ – total residual monomer (TRM) content and ● – weight loss as a function of different DTHFI content in the systems.

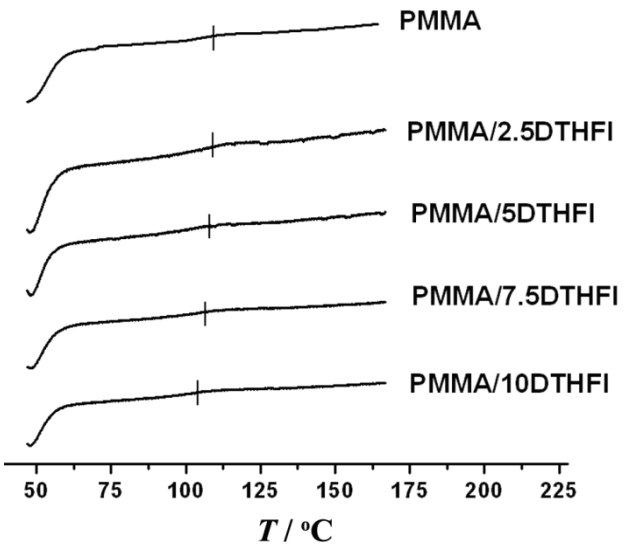

Fig. S-5. DSC curves of commercial PMMA denture base materials modified with DTHFI.

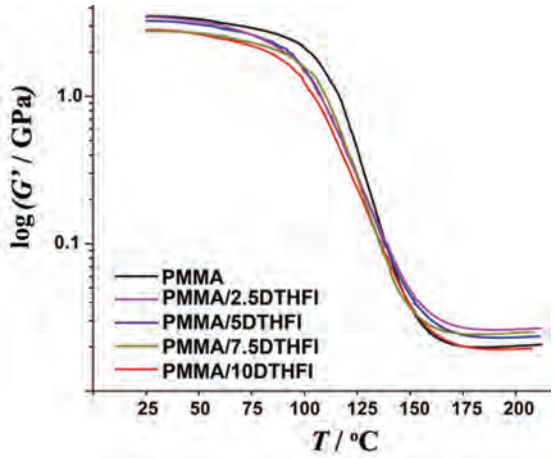

Fig. S-6. The storage modulus (G') of PMMA denture base materials modified with DTHFI in dependence on the temperature and composition of denture base materials.

Journal of the Serbian Chemical Society
JSCS-info@shd.org.rs • www.shd.org.rs/JSCS
J. Serb. Chem. Soc. 80 (9) 1193–1202 (2015)
JSCS–4790
UDC 549.623.83.004.12+547.292+546.28–36:543.44–77
Original scientific paper

Sepiolite functionalized with *N*-[3-(trimethoxysilyl)propyl]-ethylenediamine triacetic acid trisodium salt. Part I: Preparation and characterization

SLAVICA S. LAZAREVIĆ*, IVONA M. JANKOVIĆ-ČASTVAN, BOJAN M. JOKIĆ, DJORDJE T. JANAĆKOVIĆ and RADA D. PETROVIĆ

Faculty of Technology and Metallurgy, University of Belgrade, Karnegijeva 4, 11000 Belgrade, Serbia

(Received 19 February, revised 11 May, accepted 14 May 2015)

Abstract: Natural sepiolite from Andrici (Serbia) was functionalized by covalent grafting of *N*-[3-(trimethoxysilyl)propyl]ethylenediamine triacetic acid trisodium salt onto the Si–OH sepiolite groups. The functionalized material, MSEAS, was characterized by determination of the phase composition by X-ray diffraction (XRD) analysis, analysis of the morphological characteristics by scanning electron microscopy (SEM), using Fourier transform infrared (FTIR) spectroscopy, differential thermal analyses (DTA), determination of the specific surface areas and pore size distribution using the BET method and point of zero charge (pH_{pzc}) determination. The crystal structure of sepiolite did not change significantly upon surface modification. The FT-IR and DTA analyses confirmed that the modified sample maintained the basic structure of sepiolite and the presence of organic groups in the functionalized sepiolite sample. The point of zero charge of MSEAS in KNO_3 solutions of different concentrations, determined by the batch technique, was at pH 7.0±0.1.

Keywords: sepiolite; functionalization; *N*-[3-(trimethoxysilyl)propyl]ethylenediamine triacetic acid, trisodium salt.

INTRODUCTION

The variety of possible reactions of the active centres on the surface of clays allows the surface properties to be changed by introduction of new groups of atoms. Grafting is a process that links inorganic and organic components *via* strong bonds, such as covalent or ionic–covalent linkages, to obtain functionalized clays, *i.e.*, the formation organic–inorganic hybrid materials combining the mechanical stability of a clay framework and the reactivity of organofunctional groups. The alkoxysilane part of an organosilane molecule is capable of bonding

* Corresponding author. E-mail: slazarevic@tmf.bg.ac.rs
doi: 10.2298/JSC150219038L

with a variety of mineral or metal surfaces through complex hydrolysis/condensation reactions, whereby Si–O–metal bonds are ultimately formed.[1]

The reactions of clay minerals with reagents containing metal chelating functionalities have recently been explored in an effort to enhance the heavy metal binding capacities of clays and their selectivity to the type of metal considered.[2–9]

The surface of sepiolite has a great ability for grafting reactions with organosilanes due to its high content of silanol groups that are very susceptible to the reactions.[10] By hydrolysis, the alkoxy-groups of the organosilane ($R–SiX_3$, where X designates hydrolysable alkoxy groups (usually methoxy, $–OCH_3$, or ethoxy, $–OC_2H_5$)) are converted to silanol groups, which react with silanol groups of sepiolite forming Si–O–Si covalent bonds.[11] The most widely used functional silanes contain thiol (–SH) or amino ($–NH_2$) groups. The surface of sepiolite was previously functionalized using silane coupling agents: 3-mercaptopropyltrimethoxysilane (MPS),[2] triethoxy-3-(2-imidazolin-1-yl)propylsilane,[12] [3-(2-aminoethylamino)propyl]trimethoxy-silane).[13]

In previous papers, natural, acid activated and thermo-acid activated sepiolites were functionalized using (3-mercaptopropyl)trimethoxy-silane and [3-(2--aminoethylamino)propyl]trimethoxysilane and the capacities of the obtained sorbents for chromium(VI) sorption from aqueous solutions were investigated.[9,14,15] It was shown that adsorption capacities of the amine-functionalized sepiolites were much higher than those of mercapto-silane functionalized sepiolites under the same conditions, indicating that adsorption capacities of functionalized sepiolites depended on the type of groups covalently grafted to the sepiolite surface.

The present study is the first to investigate the modification of sepiolite with *N*-[3-(trimethoxysilyl)propyl]ethylenediamine triacetic acid trisodium salt in order to improve sorption capacity for metal ions from aqueous solutions. The silanation reagent *N*-[(3-trimethoxysilyl)propyl]ethylenediamine triacetic acid contains three methoxy groups, which could react with the OH groups on clays, and an EDTA group, which could chelate metals. This paper reports the preparation of the modified material and its characterization by XRD analysis, scanning electron microscopy (SEM), Fourier transform infrared (FTIR) spectroscopy, differential thermal analyses (DTA), surface-area analysis and determination of the point of zero charge (pH_{pzc}). In the second part of this paper, the adsorption properties of the functionalized sepiolite sample, the sorption of Ni^{2+} on the MSEAS as a function of the initial metal concentration, the equilibration time, the pH value and temperature are discussed.

EXPERIMENTAL

Materials

The natural sepiolite (SEP) used for the modification was obtained from Andrici (Serbia). The chemical composition, specific surface area, pore volume, pore radius, X-ray diffraction, and FTIR analyses of the sample were reported previously.[16] The functionalization of sepiolite was performed from aqueous solution[6,17] by mixing a mechanically stirred suspension of 50 g of sepiolite in distilled water, pH of 7.1, with 22.5 mL of a 45 % aqueous solution of *N*-[3-(trimethoxysilyl)propyl]ethylenediamine triacetic acid trisodium salt ($(CH_3O)_3Si(CH_2)_3N(CH_2COONa)N(CH_2)_2N(CH_2COONa)_2$), MSEA, Gelest). The mixture was filtered after 2 h and the modified sepiolite sample, MSEAS, was washed with water.

Characterization of the modified sepiolite

The scanning electron microscopic (SEM) analysis of the sepiolite powder was realized on a Tescan Mira 3 microscope. The powder was fused with a Pd–Pt alloy. X-Ray diffraction (XRD) analysis of the sample was performed using an Ital Structures APD 2000 diffractometer with CuKα radiation, in the 2θ angle range from 5 to 60°, with a 0.02° step.

Infrared spectroscopy analysis was made on a MB Boman Hartmann 100 instrument in the wave number range from 4000 to 400 cm^{-1}. The sample was prepared by the KBr method at a ratio of sample:KBr of 1:75. Differential thermal analysis in air was realized using an AMINCO instrument with computer-controlled temperature, at a heating rate of 10 °C min^{-1}.

The specific surface areas and pore size distribution of the modified sample was estimated using nitrogen adsorption–desorption isotherms determined using a Micrometrics ASAP 2020 instrument. Before the sorption measurement, the sample was degassed at 150 °C for 10 h under reduced pressure. The specific surface area of sample (S_{BET}) was calculated according to the Brunauer–Emmett–Teller (BET) method from the linear part of the nitrogen adsorption isotherm.[18] The total pore volume (V_{tot}) was given at $p/p_0 = 0.998$. The volume of the mesopores and pore size distribution were analyzed according to the Barrett, Joyner and Halenda method from the desorption isotherm.[19] The volume of the microspores was calculated according to *t*-plot analysis[20] using the Harkins–Jura thickness curve.

The point of zero charge (pH_{pzc}) of the modified sepiolite was determined in KNO_3 solutions having concentration 0.1, 0.01 and 0.001 mol L^{-1}, using the batch equilibration method as described previously.[21] In order to determine the degree of dissolution of the modified sepiolite powder, the concentration of Mg^{2+} in the solutions after equilibration with a 0.01 mol L^{-1} KNO_3 solution was measured by atomic absorption spectroscopy (AAS, Perkin Elmer 730).

RESULTS AND DISCUSSION

Characterization of modified sepiolite

The characteristic peak positions in the XRD spectrum of the sepiolite sample had not changed after modification with *N*-[3-(trimethoxysilyl)propyl]-ethylenediamine triacetic acid trisodium salt (Fig. 1), indicating that the structure and crystallinity of sepiolite were maintained, which could be attributed to the functionalization occurring mainly on the surface or by the partial replacement of zeolitic water.

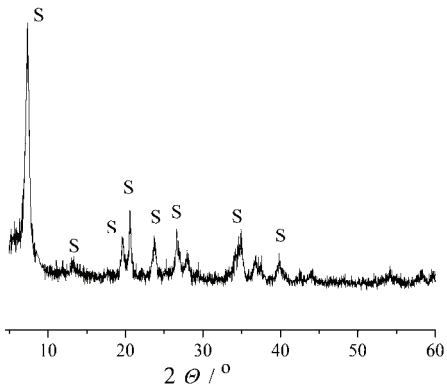

Fig. 1. XRD spectrum of the MSEAS sample (S – sepiolite).

The SEM micrograph of MSEAS is shown in Fig. 2. It could be seen that the modified sepiolite had a fibrous structure, as did the natural sepiolite.[22] The micrographs of natural sepiolite sample showed the fibres had needle morphology of 30–50 nm in diameter and 1 μm in length. After surface modification, the needle morphology was maintained but with reduced fibre length. The fibres of the functionalized sample formed bundle-like aggregates.

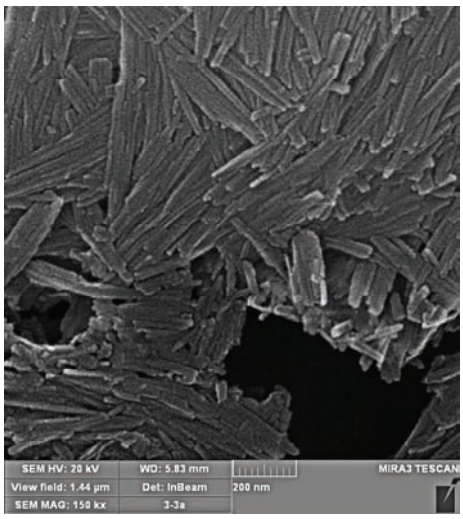

Fig. 2. SEM micrograph of the modified sepiolite.

The FTIR spectrum of the modified sample (Fig. 3) was generally similar to that of natural sepiolite, confirming that the modified material had maintained the basic structure of sepiolite. Three regions indicative for sepiolite[23,24] could be observed in Fig. 3: bands in the 4000–3000 cm^{-1} range corresponding to the vibrations of the Mg–OH group (3690 cm^{-1}), bound water coordinated to magnesium in the octahedral sheet (3570 cm^{-1}) and zeolitic water in the channels (at 3422 cm^{-1}); a band at 1658 cm^{-1} due to the vibration of zeolitic water; bands in

the 1200–400 cm^{-1} range characteristic of silicate: bands centred at 1016 and 467 cm^{-1} due to Si–O–Si vibration; bands at 1215 and 1078 cm^{-1} due to Si–O bonds; a band at 437 cm^{-1} originating from octahedral–tetrahedral bonds (Si–O–Mg bonds) and bands at 690 and 637 cm^{-1} corresponding to vibrations of the Mg–OH bond. The band at 1381 cm^{-1} corresponds to vibrations of C–H of the CH_2 groups. The C–H stretching vibrations of the methoxy ($O–CH_3$) and chain methylene (CH_2) groups could be observed at 2850 and 2930 cm^{-1}, respectively.[9,13] A band, assigned to symmetric COO^- stretching vibrations,[25] could be clearly observed at 1407 cm^{-1}. The detected CH_2 and COOH groups belong to the units of the MSEA, clearly indicating the presence of the organic modifier in the sample.

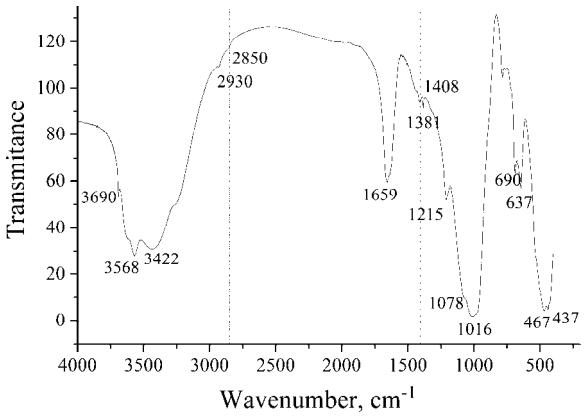

Fig. 3. FT-IR spectrum of the MSEAS sample.

The DTA curve of the modified sepiolite, shown in Fig. 4, revealed the decomposition of the aminocarboxylic group on the surfaces of MSEAS and dehydration of the sepiolite structure. The endothermic peak represents the loss

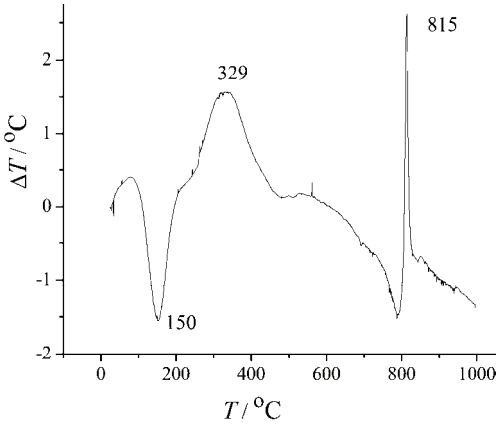

Fig. 4. DTA curve of the MSEAS sample.

of zeolite water (at 150 °C),[26] the exothermic peak at 815 °C represents the dehydratation of the octahedrically coordinated hydroxyl groups, *i.e.*, phase transformation of sepiolite into enstatite ($MgSiO_3$). The broad exothermic peak at ≈329 °C reveals the decomposition of the grafted silane ligand and clearly proves the presence of organic silane molecules on the modified material.

Textural properties of modified sepiolite

Adsorption–desorption isotherms at −196 °C for MSEAS, and the pore volume and pore size distribution are presented in Fig. 5a and b. The MSEAS showsa hysteresis pattern which is associated with the filling and emptying of the mesopores by capillary condensation, but does not show a plateau at high p/p_0 values, which is characteristic of a Type IV isotherm. The hysteresis loop is of Type H3. According to the classification of Rouquerol *et al.*,[18] such a shape of a nitrogen

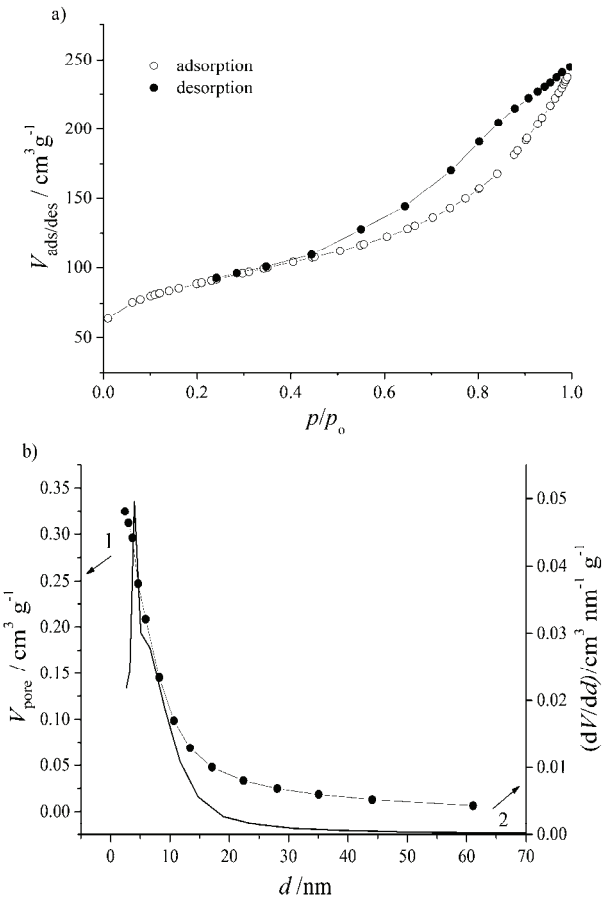

Fig. 5. a) Nitrogen adsorption/desorption isotherms; b) pore volume (1) and pore size distribution (2) of the MSEAS.

isotherm is characteristic for Type IIb indicating that the material contained both mesopores, which are responsible for the hysteresis, and macropores, which results in the absence of the plateau typical for mesoporous Type IV isotherms. The H3 hysteresis pattern indicates the presence of slit-like pores.[27]

From Fig. 5 and the data summarized in Table I (BET surface area, volume of mesopores, $V_{mesopore}$, and micropores, $V_{micropore}$, the overall pore volume, $V_{poretotal}$, and the maximum, d_{max}, and average, d, mesopore diameters) and data obtained for a natural sepiolite,[16] it could be noticed that the modification of the sepiolite with MSEA caused a small change in the specific surface area, an increase in the total pore volume, the micropore volume and the mesopore volume. Increases in the maximum and average mesopore diameters were observed for the modified sepiolite sample. It could be assumed that silane modification occurred almost exclusively on the external sepiolite surface, with only partial entry into the sepiolite channels, *i.e.,* that the pores of the sepiolite were not closed during the functionalization.

TABLE I. The textural properties of the MSEAS

S_{BET} / m^2 g^{-1}	$V_{poretotal}$ / cm^3 g^{-1}	$V_{micropore}$ / cm^3 g^{-1}	$V_{mesopore}$ / cm^3 g^{-1}	d_{max} / nm	d / nm
309.9	0.374	0.054	0.325	4.00	6.51

Determination of the point of zero charge of the modified sepiolite

The point of zero charge (pH_{pzc}) is an important interfacial parameter, extensively used in characterizing the ionization behaviour of a surface. It is very important for the determination of the acid–base characteristics of the surface functional groups and their interactions with ions from aqueous solutions. The surface potential exists as a direct result of the presence of surface charge. The solution pH value at which the surface charge density of the solid phase is equal to zero ($\sigma_0 = 0$, $\psi_0 = 0$), is called the point of zero charge (pH_{pzc}). The solid phase surface is positively charged if $pH < pH_{pzc}$ and negatively if $pH > pH_{pzc}$.

The point of zero charge of MSEAS in KNO_3 solutions of different concentrations, determined by the batch technique from the plateaus, *i.e*., the curve inflexions, from the dependences pH_f *vs*. pH_i, (Fig. 6) was at pH 7.0±0.1. The pH_{pzc} determined in KNO_3 solutions of different concentrations were independent of the ionic strength of the KNO_3 solutions, indicating that KNO_3 was an inert electrolyte, *i.e*., specific sorption of K^+ and NO_3^- did not occur at the surface.

The slight change in the point of zero charge of MSEAS compared with the pH_{pzc} of the natural sepiolite sample (7.4±0.1)[16] indicates an insignificant decrease in the basicity of the sepiolite surface after functionalization.

The dependence of the quantity of Mg^{2+} released into the solution during equilibration of 0.05 g of the MSEAS with 25 cm^3 0.01 mol L^{-1} KNO_3 solution

is also shown in Fig. 6 in order to determine the degree of dissolution of the modified sepiolite powder. In the investigated pH range, the quantity of Mg^{2+} present in the solution as a result of the dissolution of sepiolite was almost constant and equal to 0.05 mmol g^{-1} MSEAS.

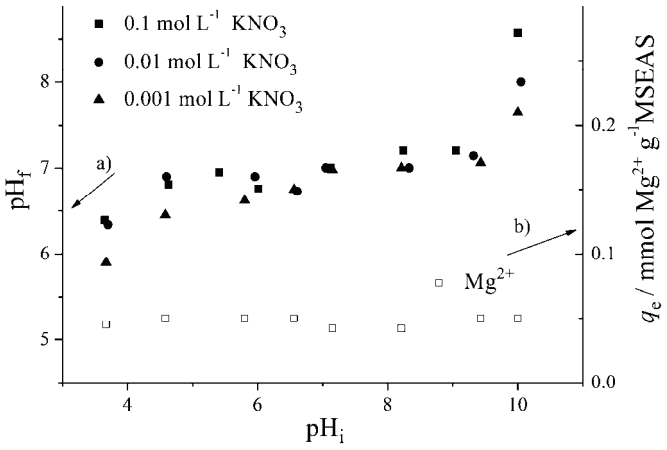

Fig. 6. a) Determination of the pH_{pzc} of MSEAS in KNO_3 solutions of different concentrations; b) dependence of the quantity of Mg^{2+} released into the solution per unit mass of MSEAS on pH_i during equilibration with 0.01 mol L^{-1} KNO_3 solutions.

CONCLUSIONS

The obtained results showed that natural sepiolite from the Andrici deposit could be modified by treating with *N*-[3-(trimethoxysilyl)propyl]ethylenediamine triacetic acid trisodium salt in the presence of an aqueous solution. The surface modification of the sepiolite involved chemical reaction of the silanol groups on the sepiolite surface with the alkoxy groups of the organosilane molecule. The signs of modification of the sepiolite surface were: the presence of new exothermic peaks in the DTA spectrum for modified sepiolite, the detection of carboxylic functional groups present on modified sepiolite by FTIR spectroscopy. The point of zero charge of MSEAS in KNO_3 solutions of different concentrations, determined by the batch technique, was pH 7.0±0.1.

Acknowledgements. Financial support through the Ministry of Education, Science and Technological Development of the Republic of Serbia, Project No. III 45019, and FP7 NANOTECH FTM No. 245916 is gratefully acknowledged.

ИЗВОД

ФУНКЦИОНАЛИЗАЦИЈА СЕПИОЛИТА ПРИМЕНОМ СОЛИ НАТРИЈУМА N-[(3-ТРИМЕТОКСИ)ПРОПИЛ]ЕТИЛЕНДИАМИНТРИАЦЕТАТНЕ КИСЕЛИНЕ. ПРВИ ДЕО: ПРИПРЕМА И КАРАКТЕРИЗАЦИЈА

СЛАВИЦА С. ЛАЗАРЕВИЋ, ИВОНА М. ЈАНКОВИЋ-ЧАСТВАН, БОЈАН М. ЈОКИЋ, ЂОРЂЕ Т. ЈАНАЋКОВИЋ и РАДА Д. ПЕТРОВИЋ

Технолошко-металуршки факултет Универзитета у Београду, Карнегијева 4, 11000 Београд

Природни сепиолит из налазишта Андрићи је функционализован применом соли натријума *N*-[(3-триметокси)пропил]етилендиаминтриацетатне киселине успостављањем ковалентне везе између модификатора и Si–OH површинских група сепиолита. Карактеризација функционализованог узорка означеног са MSEAS извршена је одређивањем морфолошких карактеристика применом скенирајуће електронске микроскопије (SEM), одређивањем фазног састава рендгенско-дифракционом анализом (XRD) и применом инфрацрвене спектроскопске анализе (FT-IR) и диференцијално-термијске анализе (DTA), као и одређивањем специфичне површине и расподеле величина пора BET методом и тачке нултог наелектрисања (pH_{pzc}). Кристална структура сепиолита није битно промењена поступком функционализације. Резултати FT-IR и DTA анализе потврдили су присуство основне сепиолитске структуре у узорку MSEAS, као и присуство карбоксилних група органског модификатора. Тачка нултог наелектрисања узорка MSEAS, одређена у растворима KNO_3 различитих концентрација применом методе уравнотежавања посебних проба, износи 7,0±0,1.

(Примљено 19. фебруара, ревидирано 11. маја, прихваћено 14. маја 2015)

REFERENCES

1. Y. Xie, C. A. S. Hill, Z. Xiao, H. Militz, C. Mai, *Composites, A* **41** (2010) 806
2. R. Celis, M. C. Hermosin, J. Cornejo, *Environ. Sci. Technol.* **34** (2000) 4593
3. I. P. Blitz, J. P. Blitz, V. M. Gunko, D. J. Sheeran, *Colloids Surfaces, A* **307** (2007) 83
4. K. F. Lam, C. M. Fong, K. L. Yeung, G. McKay, *Chem. Eng. J.* **45** (2008) 185
5. A. M. F. Guimaraes, V. S. T. Ciminelli, W. L. Vasconcelos, *Appl. Clay Sci.* **42** (2009) 410
6. A. N. Vasiliev, L. V. Golovko, V. V. Trachevsky, G. S. Hall, J. Khinast, *Micropor. Mesopor. Mat.* **118** (2009) 251
7. X. Liang, Y. Xu, G. Sun, L. Wang, Y. Sun, Y. Sun, X. Qin, *Chem. Eng. J.* **174** (2011) 436
8. X. Liang, Y. Xu, X. Tana, L. Wang, Y. Sun, D. Lin, Y. Sun, X. Qin, Q .Wang, *Colloids Surfaces, A* **426** (2013) 98
9. V. Marjanović, S. Lazarević, I. Janković-Častvan, B. Potkonjak, Dj. Janaćković, R. Petrović, *Chem. Eng. J.* **166** (2011) 198
10. M. Alkan, *Micropor. Mesopor. Mat.* **84** (2005)75
11. O. Demirbas, M. Alkan, M. Dogan, Y. Turhan, H. Namli, P. Turan, *J. Hazard. Mater.* **149** (2007) 650
12. Y. Turhan, P. Turan, M. Dogan, M. Alkan, H. Namli, O. Demirbas, *Ind. Eng. Chem. Res.* **47** (2008) 1883
13. M. Dogan, Y. Turhan, M. Alkan, H. Namli, P. Turan, O. Demirbas, *Desalination* **30** (2008) 248
14. V. Marjanović, S. Lazarević, I. Janković-Častvan, B. Jokić, A. Bjelajac, Dj. Janaćković, R. Petrović, *Hem. Ind.* **67** (2013) 715

15. V. Marjanović, S. Lazarević, I. Janković-Častvan, B. Jokić, Dj. Janaćković, R. Petrović, *Appl. Clay. Sci.* **80**–**81** (2013) 202
16. S. Lazarević, I. Janković-Častvan, D. Jovanović, S. Milonjić, Dj. Janacković, R. Petrović, *Appl. Clay Sci.* **37** (2007) 47
17. J. F. Bringley, Y. J. Lerat, U.S. Pat. Appl. 2005276862
18. F. Rouquerol, J. Rouquerol, K. Sing, *Adsorption by Powders and Porous Solids,* Academic Press, London, 1975
19. E. P. Barrett, L. G. Joyner, P. P. Halenda, *J. Am. Chem. Soc.* **73** (1951) 373
20. B. C. Lippens, J. H. De Boer, *J. Catal.* **4** (1965) 319
21. S. Milonjic, A. Ruvarac, M. Susic, *Thermochim. Acta* **11** (1975) 261
22. S. Lazarević, Ž. Radovanović, Dj. Veljović, A. Onjia, Dj. Janaćković, R. Petrović, *Appl. Clay Sci.* **43** (2009) 41
23. F. R. Cannings, *J. Phys. Chem.* **72** (1968) 1072
24. C. Serna, J. L. Alrichs, J. M. Serratosa, *Clay Clay Miner.* **23** (1992) 452
25. R. De Palma, S. Peeters, M. J. Van Bael, H. Van den Rul, K. Bonroy, W. Laureyn, J. Mullens, G. Borghs, G. Maes, *Chem. Mater.* **19** (2007) 1821
26. A. Singer, W. F. A. Kirsten, C. Buhmann, *S. Afr. J. Geol.* **95** (1992) 165
27. U. Kuila, M. Prasad, *Geophys. Prospect*. **61** (2013) 341.

Journal of the Serbian Chemical Society
JSCS-info@shd.org.rs • www.shd.org.rs/JSCS
J. Serb. Chem. Soc. 80 (9) 1203–1214 (2015)
JSCS–4791
UDC 546.171.1:541.183+549.67:537.872:504.53–035.22
Original scientific paper

The use in grass production of clinoptilolite as an ammonia adsorbent and a nitrogen carrier

JELENA MILOVANOVIĆ[1], SUSANNE EICH-GREATOREX[2], TORE KROGSTAD[2], VESNA RAKIĆ[3] and NEVENKA RAJIĆ[4]*

[1]*Innovation Centre of the Faculty of Technology and Metallurgy, University of Belgrade, Karnegijeva 4, 11120 Belgrade, Serbia,* [2]*Faculty of Environmental Science and Technology, Norwegian University of Life Sciences, 1432 Aas, Norway,* [3]*Faculty of Agriculture, University of Belgrade, Nemanjina 6, 11080 Zemun, Serbia and* [4]*Faculty of Technology and Metallurgy, University of Belgrade, Karnegijeva 4, 11120 Belgrade, Serbia*

(Received 17 March, revised 14 May, accepted 18 May 2015)

Abstract: Clinoptilolite-rich tuff (NZ) from the Zlatokop deposit (Vranjska Banja, Serbia) was studied as a nitrogen carrier for grass production. The mechanism of binding ammonium cations present in aqueous solutions by NZ was examined, as well as the possibility of adsorption of ammonia released in fresh cattle manure during its fermentation. The NH_4^+ binding from solutions proceeded *via* an ion-exchange process that followed pseudo-second-order kinetics. Adsorption isotherms studied at 298–318 K followed the Freundlich isotherm equation. The NZ readily adsorbs ammonia liberated from manure and the addition of 10 wt. % of NZ to manure can preserve up to 90 % of ammonia. The potential benefit of this effect was examined in greenhouse pot experiments with Italian ryegrass (*Lolium multiflorum*, var. Macho) using three different types of soil (silty, clayey and sandy). The zeta potential measurements showed that the stability of their colloidal dispersions differed mutually and that the addition of NZ affected the stability and nitrogen cycling differently. All results indicated that NZ could be applied in grass production.

Keywords: zeolites; manure; Freundlich isotherm; soil; Italian ryegrass.

INTRODUCTION

Nitrogen is an essential nutrient for plant growth that has to be added to the soil to ensure the best growth and yield of crops. However, mineral nitrogen fertilizers have been implicated in various environmental issues. Ammonium and nitrate ions are readily lost from the soil by volatilization, leaching or surface run-off. As a result, different nitrogenous species are frequently present not only in agricultural wastewater, but also in groundwater. This may cause serious envi-

* Corresponding author. E-mail: nena@tmf.bg.ac.rs
doi: 10.2298/JSC150317042M

ronmental problems such as eutrophication of water bodies and deterioration of water sources, also with possible consequences for humans, in particular for the health of small children.[1]

The removal of NH_4^+ from water through adsorption using various available sorbents was studied by many authors.[2–7] Natural zeolites as non-toxic, ecologically advantageous and affordable materials appear to be well suited for binding NH_4^+ from aqueous media due to their ion exchange and adsorption properties.[8–11] Moreover, the use of natural zeolites for agricultural purposes is becoming widespread because zeolites are particularly useful for controlling agricultural soil fertilization and for preventing or retarding leaching and for increasing yields.[12–14]

Clinoptilolite is a very widespread zeolitic mineral in Serbia. The clinoptilolite-rich tuff from the deposit Zlatokop (Vranjska Banja, Serbia) contains more than 70 wt. % of clinoptilolite and was found to exhibit good adsorptive and ion-exchange properties.[15–17] In the present study, the tuff was investigated as a sorbent for ammonium ions and ammonia, and subsequently the ammonium-enriched zeolite was evaluated as a fertilizer.

In particular, the present study examined: 1) the kinetics of binding of NH_4^+ from aqueous solution to NZ; 2) the efficiency of NZ in binding the NH_3 released from fresh cattle manure; 3) whether the addition of ammonium-loaded NZ (AM–NZ) influences the ζ-potential of the soil and accordingly the availability of NH_4^+ for plants; 4) the effect of the use of NZ in herbage grass growth.

EXPERIMENTAL

Materials and methods

The zeolite material (NZ) was obtained from a large sedimentary Zlatokop deposit in Vranjska Banja. The particle size of the samples used was in the range of 0.063–0.1 mm. A detailed X-ray powder diffraction analysis based on quantitative Rietveld refinement showed that the NZ contained 72.6 % clinoptilolite, 14.6 % feldspar plagioclase and 12.8 % quartz.[18]

Chemical analysis of the clinoptilolite phase present in the NZ obtained by scanning electron microscopy and X-ray microanalysis (JEOL JSM-6610LV) gave the following composition expressed by corresponding oxides (wt. %): SiO_2, 65.63; Al_2O_3, 12.97; Fe_2O_3, 1.48; Na_2O, 0.95; K_2O, 1.33; CaO and MgO. 1.41. The loss on ignition at 1073 K, obtained by thermal analysis (TA Instruments, SDT, Q600), was 12.9 wt. %. Furthermore, the porosity of NZ measured by nitrogen adsorption at 77 K (Hiden Isochema HTP1-V Volumetric Analyzer) gave for the BET specific surface area (S_{BET}) and micropore volume (V_{mic}) 42 $m^2\ g^{-1}$ and 0.0032 $cm^3\ g^{-1}$, respectively.

Prior to the experiments, the NZ was washed with deionised water and ethanol to remove soluble amorphous impurities, and then dried to a constant mass at 105 °C.

Adsorption/desorption studies in solution

The adsorption experiments were performed in the batch mode using NH_4Cl solutions of different (initial) strengths, *i.e.*, 5, 10, 25, 50 and 100 mg $NH_4^+\ dm^{-3}$. The study was realized by mixing 1 g of NZ with 100 cm^3 of a solution of the chosen concentration. The suspension

was shaken in a thermostated water bath (Memmert WNB22) for a period from 30 min to 24 h. The solid, ammonia-loaded NZ (AM–NZ) was separated by filtration.

Three parameters were varied in the experiment: initial concentration of NH_4^+ in solution, temperature and contact time. Adsorption isotherms were determined at 298, 308 and 318 K.

The NH_4^+ desorption experiments were conducted at 298 K by treating AM–NZ (containing 1.1 mg NH_4^+ g^{-1}) with the KCl or NaCl solutions varying the salt concentration from 0.1 to 0.001 mol dm^{-3}.

Adsorption study in manure

The capture of ammonia released during fermentation of fresh cattle manure (some of its chemical characteristics are given in Table I) was studied using a modified procedure described by Sharadqah and Al-Dwairi.[19] Glass jars (volume 0.5 dm^3) were filled with fresh cattle manure up to 2/3 their volume and tightly closed. Into four of the jars, a well homogenized mixture of the fresh cattle manure and NZ was added in different 100:*n* weight ratios (*n* = 5, 10, 15 or 20). The fifth jar without NZ served as the system control.

TABLE I. Chemical characteristics of the manure used in the experiments (g kg^{-1})

pH	Dry matter	Loss on ignition	Total C[a]	Total N[a]	NO_3-N[b]	NH_4-N[b]	Total P	Total K
7.60	28.5	713.2	390.0	18.9	0.08	27.01	8.9	67

[a]Measured in dried sample; [b]measured in fresh sample

In each jar, a porcelain crucible containing 10 cm^3 of 0.1 M H_2SO_4 was placed on a tripod. After 24 h, the crucibles were replaced by new ones containing fresh H_2SO_4, and the solutions from the old ones were collected in a volumetric flask. The same process was repeated every day during 10 days, taking care that the jars were held open for the shortest possible time. The experiment was performed in triplicate.

Zeta potential measurements

Zeta (ζ) potentials of the soil samples and mixtures of the soil and AM–NZ suspended in water were measured. Prior to the measurements, a suspension of 5 g of the soil sample (or a homogenized mixture of 5 g of soil and 100 mg of AM–NZ) in 25 cm^3 deionised water was homogenized by a standard procedure[20] for 30 min by horizontal orbital shaking (120 rpm). The suspensions were left to settle overnight, and then a part of the colloid fraction was taken for the measurement. All measurements were performed in triplicate and expressed as mean values of the ζ-potential ± standard deviation.

Pot experiments

A greenhouse pot experiment was conducted under controlled conditions (20 °C, 18 h per day) with three different soil types and the Italian ryegrass (*Lolium multiflorum*, var. Macho) as the test crop. The soil types included a loam, a silt and a sandy soil. The former two were passed through a 5-mm mesh filter prior to being filled into pots of 3 dm^3 volume. Some chemical parameters of the soils are given in Table II.

The following treatments/fertilizers were used in the pots: a) control without any fertilizer, b) mineral fertilization with NH_4NO_3, c) fresh cattle manure, d) fresh cattle manure with the addition of 10 wt. % NZ, and in the silt soil only experiment and e) AM–NZ (containing 1.1 mg NH_4^+ g^{-1}). All treatments were performed in triplicate. In all treatments, except in the control, the amounts of fertilizer corresponded to that typically used in grass production

in Southern Norway (a nitrogen dose at the start of the experiment being equivalent to 120 kg N ha^{-1}). The amount of manure was determined based on the NH_4^+ content in the wet sample and assuming that approximately 10 % of the organically bound N would be available over the experimental period, based on a previous mineralization study (results not shown).

TABLE II. Some properties of the soils used in the pot experiments

Soil	Sand	Silt	Clay	*LOI*[a]	pH	Total C	Total N	P-AL[b]	K-AL[b]
	g kg^{-1}					mg kg^{-1}			
Clay	450	380	170	61.0	5.2	23.1	2.1	58	195
Sand	940	30.0	30.0	13.0	5.1	2.8	0.1	16	10
Silt	20	930	50.0	37.0	6.5	14.5	1.0	49	200

[a]Loss on ignition; [b]ammonium acetate lactate extractable

In addition, an amount phosphorus equivalent to 20 kg ha^{-1} and an amount of potassium equivalent to approximately 100 kg ha^{-1}, as well as all other macro- and micronutrients in appropriate amounts, were added in the case of the mineral fertilizer treatment. After the first cut, in all treatments except the one without nutrients, an additional amount of mineral N, equivalent to 60 kg N ha^{-1}, was added. The pots were sown with 0.3 g of the seeds of Italian ryegrass. The moisture content in the soil was maintained at 60 % of the field capacity by irrigation with deionised water. The grass was cut three times after 5, 9 and 13 weeks of growth.

Analytical methods and instrumentation

The NH_4^+ concentration in the solutions was determined photometrically (Hach DR2800) using the Nessler reagent (Hach Method 8038). The cation concentrations of Na, K, Mg and Ca in solution ere determined by AAS using a Varian Spectra 55B instrument; at least five measurements were performed for each determination.

Fourier transformed infrared (FTIR) spectra of NZ and AM–NZ were recorded in the 4000–400 cm^{-1} range on a Digilab-FTS-80 spectrophotometer, using the KBr pellet technique.

Measurements of the ζ-potential were performed by electrophoresis using the laser Doppler method and a SZ-100 (Horiba Co. Ltd.) instrument in which a cell containing carbon electrodes is employed as a sample holder. The ζ-potential was calculated using the peak values of the mobility distributions detected by the Doppler shift in light scattering – the electrophoretic mobility of the particles was automatically calculated and converted to the ζ-potential using the Smoluchowski equation.[21]

The particle size distribution of the soils was determined by the pipette method.[22] Soil and manure samples were ignited overnight at 823 K in order to determine the loss on ignition. The pH of the soil samples was measured by suspending the soil in H_2O, with a soil to solution ratio of 1:2.5. The pH of the manure was measured directly in a wet sample. For both the soil and manure analyses, the total C content was determined in crushed samples by dry combustion[23] at 1323 K using a Leco CHN-1000 instrument (St. Joseph, MI, USA). The total N content was measured using the same instrument according to the Dumas method.[24] The ammonium and nitrate contents in the manure (NH_4-N, NO_3-N) were measured by flow injecttion analysis (FIA, Tecator FIAstar 5010 Analyzer, Hillerød, Denmark) after extracting a fresh sample with 2 mol dm^{-3} KCl. The plant-available P and K in the soil were estimated by extraction with an ammonium acetate lactate solution (0.1 M ammonium lactate and 0.4 mol dm^{-3} acetic acid, pH 3.75),[25] followed by inductively coupled plasma optical emission spectrometry (ICP-OES, Perkin Elmer Optima 5300 DV, Waltham, MA, USA). The total P and K

in the manure were determined on the same instrument after autoclave digestion in concentrated HNO_3 (0.25 g to 0.3 g sample in 5 cm^3) and subsequent dilution to 50 cm^3.

The effect of different treatments on the yield in the pot experiments was tested statistically by analysis of the variance (General linear model). The Student–Newman–Keuls test was performed to identify the different means. Results with $p < 0.05$ were considered significant. The statistical analysis was realized using SAS 9.3 software (SAS Institute Inc., Cary, NC, USA).

RESULTS AND DISCUSSION

Adsorption study

Adsorption capacity of the NZ increased with the initial NH_4^+ solution concentration and slightly decreased with temperature. At 298 K, it varied from 0.37 mg NH_4^+ g^{-1} (for c_0 = 5 mg NH_4^+ dm^{-3}) to 6.45 mg NH_4^+ g^{-1} (for c_0 = 100 mg NH_4^+ dm^{-3}). A slight decrease in the adsorption capacity was found at 318 K: 0.32 mg NH_4^+ g^{-1} (for c_0 = 5 mg NH_4^+ dm^{-3}) and 6.10 mg NH_4^+ g^{-1} (for c_0 = = 100 mg NH_4^+ dm^{-3}). The results showed that the adsorption of NH_4^+ by NZ is an exothermic process, which agrees with the results obtained for a Turkish and clinoptilolite-rich tuff.[26]

The Langmuir and Freundlich models were used to describe the equilibrium isotherm data.[27]

The Langmuir model can be represented as:

$$q_e = \frac{q_{max} b_L c_e}{1 + b_L c_e} \quad (1)$$

where c_e is the equilibrium concentration of the solute (mg dm^{-3}), q_e is the equilibrium concentration of the adsorbed solute (mg g^{-1}), while q_{max} (mg g^{-1}) and b_L (dm^3 mg^{-1}) are Langmuir constants (q_{max} corresponding to the maximum achievable uptake by a system, and b_L is related to the affinity between the adsorbate and the adsorbent).

The Freundlich model can be represented as:

$$q_e = K_F c_e^n \quad (2)$$

where q_e (mg g^{-1}) is the equilibrium solute uptake, K_F (dm^3 g^{-1}) is the isotherm constant of the Freundlich model, c_e (mg dm^{-3}) is the equilibrium solution concentration, and n is the exponent of the Freundlich model. K_F and n are characteristics of the system and are indicators of the adsorbent capacity (or affinity for the solute) and adsorption intensity, respectively.

For the Langmuir isotherm analysis, the value of the separation factor (R_L) defined as:

$$R_L = \frac{1}{1 + b_L c_0} \quad (3)$$

is of special importance[28] and for the Freundlich isotherm the value of the exponent ($1/n$) is significant. In all the experiments, the values of R_L, which can be calculated using the b_L values from Table III, and the $1/n$ values prove, according to the literature,[16,28] that the adsorption was a favourable process ($0< R_L <1$ and $1/n <1$, Table III), in accord with the fact that NZ readily adsorbs NH_4^+ from aqueous solutions. As can be seen from Table III, the equilibrium adsorption data gave a better fit (higher values of R^2) for the Freundlich than for the Langmuir model.

TABLE III. Isotherm constants for the sorption of NH_4^+ from aqueous solution by NZ

Temperature, K	Langmuir isotherm			Freundlich isotherm		
	q_{max}[a] / mg g^{-1}	b_L[b] / dm^3 mg^{-1}	R^2	K_F[c] / dm^3 mg^{-1}	$1/n$[d]	R^2
298	8.8879	0.0794	0.9943	0.9507	0.5531	0.9663
308	7.6329	0.1115	0.9836	1.2017	0.4663	0.9929
318	9.7514	0.0554	0.9906	0.7724	0.6150	0.9963

[a]Maximal monolayer adsorption capacity; [b]Langmuir constant; [c]Freundlich constant; [d]Freundlich model exponent

The NH_4^+ adsorption kinetics were studied at 298, 308 and 318 K for solutions with c_0 = 5, 10, 25, 50 and 100 mg NH_4^+ dm^{-3}. The experimental data were analyzed by the Lagergren pseudo-first-order model and by the pseudo-second-order kinetics model.[27] A linear dependence was obtained only for the pseudo-second-order model, indicating that the binding of NH_4^+ by NZ occurs by the pseudo-second-order reaction mechanism described by the following equation:[25]

$$\frac{dq_t}{dt} = k_2 \left(q_e - q_t\right)^2 \tag{4}$$

where q_e (mg g^{-1}) is the adsorption capacity at equilibrium and k_2 (g mg^{-1} min^{-1}) is the rate constant of the pseudo-second-order adsorption. Integration between the limits $t = 0$ to $t = t$ and $q = 0$ to $q = q_e$, gives the following expression:

$$\frac{t}{q_t} = \frac{1}{k_2 q_e^2} + \frac{1}{q_e} t \tag{5}$$

The plot of t/q_t *vs.* t is a straight line if the experimental data conform to this kinetic model, and the values of q_e and k_2 are obtained respectively from the slope and intercept of such a plot. As representative, the results obtained at different temperatures for the initial concentration c_0 = 25 mg NH_4^+ dm^{-3} are shown in Fig. 1. The adsorption capacity at equilibrium (q_e) decreases with temperature whereas the rate constant changes irregularly with temperature. This was also observed for the other initial concentrations studied (data not presented). No acceptable explanation could be offered nor found in the literature for this phenomenon.

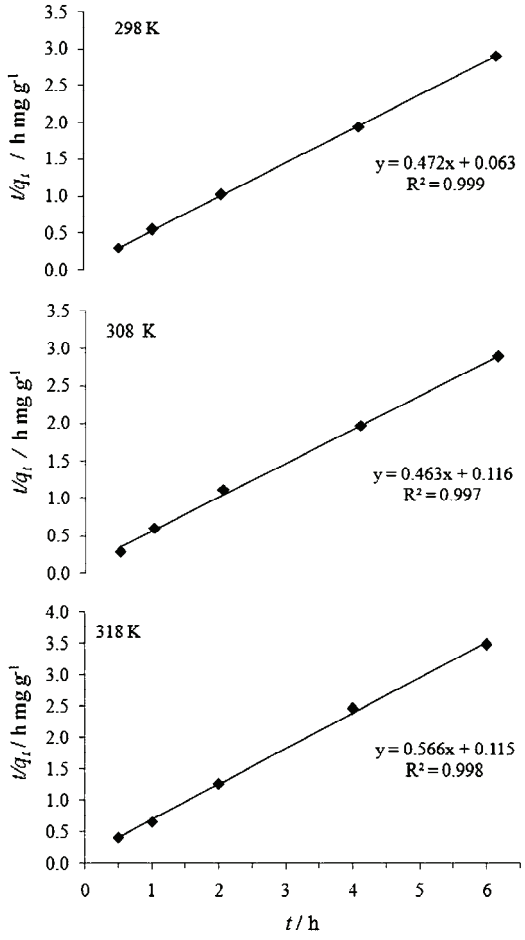

Fig. 1. Kinetic curves at different temperatures obtained by fitting the experimental data to the pseudo-second-order rate model (c_0 = 25 mg NH_4^+ dm^{-3}).

The FTIR spectrum of AM–NZ (not shown) confirmed the presence of NH_4^+ in the sample (vibration band at about 1400 cm^{-1} attributed to NH_4^+, which was not present in the spectrum of NZ), suggesting that the binding of NH_4^+ from aqueous solution by NZ proceeds by an ion-exchange reaction. This was proved further by elemental AAS analysis of the liquid phase after the adsorption studies, *i.e.*, after AM–NZ separation from the suspensions. The concentrations of Na^+, K^+, Ca^{2+} and Mg^{2+} determined in the filtrate entirely corresponded to the amount of NH_4^+ bound by the NZ.

In order to check whether the NH_4^+ in AM–NZ could be desorbed and thus become available as a nutrient in the soil, NH_4^+-desorption experiments were performed by treating AM–NZ with the NaCl or KCl solutions. The obtained results are given in Table IV. It is evident that the percentage of NH_4^+ desorption depended on the initial Na^+/K^+ concentration, showing that the desorption was

also an ion-exchange process. It is interesting to note that desorption was more efficient in the KCl than in the NaCl solution. This could be explained by the fact that the radius of the NH_4^+ (151 pm) is very similar to that of the K^+ (152 pm). Desorption in 0.1 M KCl was completed in 30 min.

TABLE IV. Percentage NH_4^+ desorbed at 298 K from AM–NZ into solutions of NaCl or KCl in dependence on the salt concentration

Concentration of NaCl/KCl, mol dm^{-3}	Released NH_4^+, %	
	in NaCl(aq)	in KCl(aq)
0.100	64	100
0.010	42	50
0.005	24	42
0.001	17	18

It is well known that fresh cattle manure is rich in nitrogen, making it a good fertilizer. Nitrogen is present mainly in the organic matter, the content of which in the fresh manure being about 50 wt. %. However, during fermentation, manure looses significant amounts of nitrogen. Thus, the loss in four days may reach up to 90 % due to the extensive liberation of ammonia.[29] In order to mitigate this loss, investigations were performed to determine: a) whether the addition of NZ to fresh cattle manure could retain the liberated NH_3, and b) the optimal amount of NZ that has to be used for NH_3 capture.

Addition of the NZ to fresh manure conserved the NH_3 released during fermentation, and the percentage of the captured NH_3 ranged between 67 and 98 % depending on the applied amount of NZ (5–20 wt. %). Since about 90 % of NH_3 was captured on addition of 10 wt. % NZ in comparison to the control, this amount of NZ was chosen as the optimal amount for the pot experiments (*vide infra*).

ζ-potential values

The zeta potential is an important parameter for soil/zeolite suspensions in water since it could be interpreted as an indicator of the stability of the suspended colloidal dispersions with respect to particle aggregation.[30] For most soils, the ζ potential has a negative value because the ground surface is usually negatively charged. Moreover, the soil stability is a qualitative indicator of biological activity, energy flow and nutrient cycling. A dispersion is regarded as stable, when the ζ-potential is < –30 mV.[31] The results of the ζ-potential measurements are listed in Table V. It is evident that the clayey soil showed the lowest value of ζ, which could be explained by the strong electronegativity of the clays present in the soil sample. The sandy soil also showed a very low ζ-potential, which could be attributed to the presence of organic matter in which carboxyl groups are ionized.[31] The silty soil exhibited the highest ζ-potential, implying a lower sta-

bility. The addition of AM–NZ influenced the ζ-potential of all three types of soil but the changes were most pronounced for the clayey and sandy soils. The stability of clayey soil decreased on addition of AM–NZ in contrast to sandy soil in which the colloidal fraction became more stable.

TABLE V. The values of ζ-potentials, mV

Soil sample	System	
	Soil/water	Soil+AM–NZ/water
Clay	–45.0±0.7	–38.0±0.8
Silt	–23.6±1.1	–22.3±1.6
Sand	–37.0±0.9	–40.6±0.7

Pot experiments

To obtain an insight into a possible use of NZ in grass production, pot experiments were performed with Italian ryegrass, *Lolium multiflorum*, var. Macho. Italian ryegrass was used because it is fast-growing and responds to high N fertilization by yielding an abundance of vegetative matter.

The results for the three cuts in the pot experiment are given in Fig. 2, expressed as tones of dry matter (DM) per hectare.

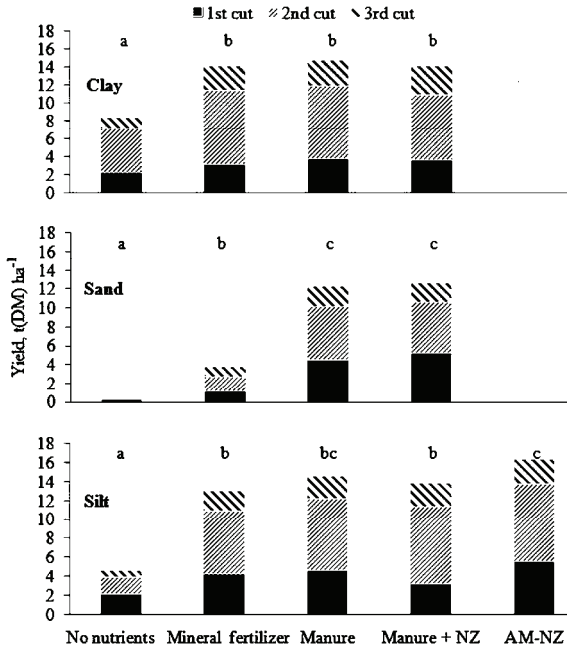

Fig. 2. Yields of ryegrass for different treatments and different types of soil. Statistically significant differences are indicated by different letters ($p < 0.001$).

Figure 2 reveals similar overall yields for the mineral fertilizer, the manure and the manure+NZ treatments, with the exception of the sandy soil where con-

siderably less biomass was produced in the control than in the other two treatments. In general, there was little difference between the amounts of biomass harvested at different cuts for these three treatments. A slight but significant difference (statistics for the separate cuts are not shown) was found in the silt, with a somewhat lower biomass in the first cut in the manure+NZ treatment compared to mineral fertilizer and manure alone. However, this slower growth at the beginning was compensated for by a good yield in the second cut.

It seems that NZ added to the silt binds NH_4^+ strongly at least in the initial phase of the growing period. This could, at least partly, have been due to the relatively high pH value of the silty soil (6.5), at which value cations are strongly adsorbed and hence less available than in the clayey and sandy soils. This suggestion is in accordance with the zeta potential measurement, which showed that the stability of colloidal fractions of the silty soil is not influenced by the addition of zeolite.

The yields in the treatments without fertilizer are, as expected, much smaller than in the other treatments, especially in the sandy soil, which contained the smallest amount of nutrients. Even when the sandy soil was treated with the mineral fertilizer, the plants grew poorly – most likely due to the low original pH of the soil (*i.e.*, 5.1, Table II). Treatments including both manure and manure+NZ improved the growing conditions in the sandy soil, which was reflected in the much higher yields.

In the silty soil, the treatment with AM–NZ resulted in slightly higher overall yields than in the manure+NZ and the mineral fertilizer treatment but not compared to the manure alone. The may be explained by the fact that the AM–NZ was obtained by the ion-exchange reaction using a NH_4^+-solution of well-defined strength as opposed to the NZ exposed to manure. In the latter case, less NH_4^+ was bound by NZ because the manure used possessed not only NH_4^+ present in the liquid phase, but also organically bound N. It should be stressed that the available N from manure cannot be determined accurately in comparison to the available N in AM–NZ. Accordingly, the resulting differences are likely to have caused the small differences in growth between the different treatments in the silty soil.

CONCLUSIONS

This study evaluated the adsorption ability of zeolitic tuff from the Zlatokop deposit towards NH_4^+ present in liquid medium and towards NH_3 liberated in manure, as well as its capability to be a nitrogen reservoir for plant growth.

The adsorption studies show that the process proceeded *via* an ion-exchange mechanism, which followed the pseudo-second-order kinetic model ($R^2 > 0.99$). The adsorption isotherms studied at 25–45 °C followed the Freundlich isotherm model.

The addition of 10 wt. % of the tuff to fresh cattle manure conserved about 90 % of ammonia and preserved its nutritive value. Greenhouse pot experiments with Italian ryegrass suggested that the plants utilize the NH_4^+ bound by the tuff in a similar manner to the NH_4^+ in easily soluble mineral fertilizers. Further work will be directed towards exploitation of the tuff in odour control as well as towards its potential use in the reduction of the nitrogen oxide emission during manure application in agriculture. The results of such work could be expected to significantly contribute not only to a less odoriferous, but also to a healthier environment.

Acknowledgements. This research was supported by the Norwegian Programme in Higher Education, Research and Development HERD (Project "The use of natural zeolite (clinoptilolite) for the treatment of farm slurry and as a fertilizer carrier") and by the Ministry of Education, Science and Technological Development of the Republic of Serbia (Project No. 172018).

И З В О Д

ПРИМЕНА КЛИНОПТИЛОЛИТА КАО АДСОРБЕНТА АМОНИЈАКА И НОСАЧА АЗОТА ЗА ПРИМЕНУ У УЗГОЈУ ТРАВЊАКА

ЈЕЛЕНА МИЛОВАНОВИЋ[1], SUSANNE EICH-GREATOREX[2], TORE KROGSTAD[2], ВЕСНА РАКИЋ[3] и НЕВЕНКА РАЈИЋ[4]

[1]Иновациони центар Технолошко–металуршког факултета,Универзитет у Београду, Карнегијева 4, 11000 Београд, [2]Faculty of Environmental Science and Technology, Norwegian University of Life Sciences, 1432 Aas, Norway, [3]Пољопривредни факултет, Универзитет у Београду, Немањина 6, 11080 Земун и [4]Технолошко-металуршки факултет, Универзитет у Београду, Карнегијева 4, 11000 Београд

Зеолитски туф (NZ) са великим садржајем клиноптиолита из рудника Златокоп (Врањска Бања) испитиван је као носач азота за потребе гајења траве. Проучен је механизам и кинетика везивања амонијум-јона из водених раствора за NZ као и могућност везивања амонијака који настаје ферментацијом свежег стајњака. Везивање амонијум-јона је реакција јонске измене која следи кинетику псеудо-другог реда. Адсорпционе изотерме испитане на 298–318 K следе Фројндлихову једначину. NZ лако везује амонијак који се ослобађа у стајњаку и додатак 10 мас. % NZ може да сачува 90 % амонијака. Потенцијална корист овог ефекта испитивана је праћењем раста Италијанског љуља (Italian ryegrass, *Lolium multiflorum*, var. Macho) у саксијама у стакленој башти применом три различите врсте земљишта (прашина, глина, песак). Мерењем цета потенцијала утврђено је да се стабилност колоидних дисперзија земљишта међусобно разликује и да додатак NZ утиче различито на стабилност, а тиме и на кружење азота у земљишту. На основу укупних резултата закључено је да се NZ може користити при узгоју травњака.

(Примљено 17. марта, ревидирано 14. маја, прихваћено 18. маја 2015)

REFERENCES

1. K. G. Cassman, A. Dobermann, D. T. Walters, *AMBIO* **31** (2002) 132
2. H. Liu, Y. Dong, H. Wang, Y. Liu, *Desalination* **263** (2010) 70
3. M. Khan, N. Yoshida, *Bioresource Technol.* **99** (2008) 575
4. P. Vassileva, P. Tzvetkova, R. Nickolov, *Fuel* **88** (2009) 387

5. P. Vassileva, D. Voikova, *J. Hazard. Mater.* **170** (2009) 948
6. T. C. Jogensen, L. R. Weatherley, *Water. Res.* **37** (2003) 1723
7. W. M. Rostron, D. Stuckey, A. A. Young, *Water Res.* **35** (2001) 1169
8. M. Reháková, S. Cuvanová, M. Dyivák, J. Rimár, Z. Gaval'ová, *Solid State Mater. Sci.* **8** (2004) 397
9. P. J. Leggo, B. Ledésert, G. Christie, *Sci. Total Environ.* **363** (2006) 1
10. S. Leung, S. Barringtin, Y. Wan, X. Zhao, B. El-Husseini, *Bioresource Technol.* **98** (2007) 3309
11. J. Venglovsky, N. Sasakova, M. Vargova, Z. Pacajova, I. Placha, M. Petrovsky, D. Harichova, *Bioresource Technol.* **96** (2005) 181
12. A. C. de Campos Bernardi, P. P. Anchão Oliviera, M. B. de Melo Monte, F. Souza-Barros, *Micropor. Mesopor. Mater.* **167** (2013) 16
13. H. V. Der Stok, T. Sofyan, DE and WO2013119108 A1 (2013)
14. S. Belboom, A. Leonard, in *Plant Sciences Reviews*, D. Hemming, Ed., CABI, Wallingford, 2011, p. 52
15. Dj. Stojakovic, J. Milenkovic, N. Daneu, N. Rajic, *Clay Clay Miner.* **59** (2012) 277
16. Dj. Stojakovic, J. Hrenovic, M. Mazaj, N. Rajic, *J. Hazard. Mater.* **185** (2011) 408
17. N. Rajic, Dj. Stojakovic, M. Jovanovic, N. Z. Logar, M. Mazaj, V. Kaucic, *Appl. Surf. Sci.* **257** (2010) 1524
18. Š. Cerjan Stefanović, N. Zabukovec Logar, K. Margeta, N. Novak Tušar, I. Arčon, K. Maver, J. Kovač, V. Kaučič, *Micropor. Mesopor. Mater.* **105** (2007) 251
19. S. I. Sharadqah, R. A. Al-Dwairi, *Jordan J. Civ. Eng.* **4** (2010) 378
20. M. W. I. Schmidt, C. Rumpel, I. Kogel-Knabner, *Eur. J. Soil Sci.* **50** (1999) 87
21. R. J. Hunter, *Zeta Potential in Colloidal Science: Principles and Applications*, Academic Press, London, 1981
22. P. Elonen, *Acta Agralia Fenn.* **122** (1971) 1
23. D. W. Nelson, L. E. Sommers, in *Methods of Soil Analysis Part 2*, A. L. Page, R. H. Miller, D. R. Keeney, Eds., American Society of Agronomy Inc., Soil Science Society of America Inc., Madison, WI, 1982, pp. 539–579
24. J. M. Bremner, C. S. Mulvaney, in *Methods of Soil Analysis Part 2*, A. L. Page, R. H, Miller, Eds., Vol. 9 of Agronomy Monograph, American Society of Agronomy, Madison, WI, 1982, pp. 595–624
25. H. Egnér, H. Riehm, W. R. Domingo, *Lantbrukshögskolans Annaler* **26** (1960) 199
26. A. Mishra, J. H. Clark, G. A. Kraus, P. R. Seidl, A. Stankiewicz, Y. Kou, *Green Materials for Sustainable Water Remediation and Treatment*, The Royal Society of Chemistry, Cambridge, 2013, p. 93
27. S. Sen Gupta, K. G. Bhattacharyya, *Adv. Colloid Interface Sci.* **162** (2011) 39
28. A. M. Yusof, L. K. Keat, Z. Ibrahim, Z. A. Majid, N. A. Nizam, *J. Hazard. Mater.* **174** (2010) 380
29. K. A. Rabai, O. H. Ahmed, S. Kasim, *Afr. J. Biotechnol.* **11** (2012) 12825
30. Y. Yukselen, A. Kaya, *Water Air Soil Poll.* **145** (2003) 155
31. J. P. Mendez, F. P. Garcia, O. A. A. Sandoval, M. A. M. Marzo, *Acta Montan. Slovaca* **18** (2013) 17.

Journal of the Serbian Chemical Society
JSCS-info@shd.org.rs • www.shd.org.rs/JSCS

J. Serb. Chem. Soc. 80 (9) 1215 (2015)

Errata (printed version only)

1. Vol. 75, issues No. 3 and 4 (2010):

– First seven characters of the doi numbers of all articles should read: 10.2298

2. Vol. 80, issue No. 8 (2015), article No. *JSCS-4782*, page 1097:

– The following paragraph is to be added before the paragraph "*Acknowledgements.*":

SUPPLEMENTARY MATERIAL

Description of area and sampling location, as well as contents of heavy metals and several major components in sediment samples from ZLT-2 borehole, reference standard values and weathering indices are available electronically from http://www.shd.org.rs/JSCS/, or from the corresponding author on request.